(2)

CSD 2060 FR

OSCILLATORY INTERNAL FLOW FIELDS STUDIES

FINAL TECHNICAL REPORT

August 30, 1992

Prepared for

DIRECTOR OF AEROSPACE SCIENCES
AIR FORCE OFFICE OF SCIENTIFIC RESEARCH
BOLLING AIR FORCE BASE
DISTRICT OF COLUMBIA 20332

by
C. W. Shaeffer and R. S. Brown

by
UNITED TECHNOLOGIES CHEMICAL SYSTEMS

DISCLAIMER NOTICE

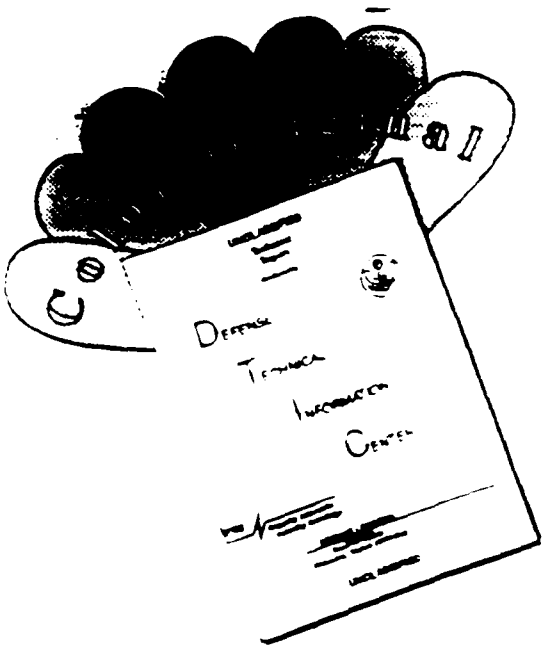

THIS DOCUMENT IS BEST QUALITY AVAILABLE. THE COPY FURNISHED TO DTIC CONTAINED A SIGNIFICANT NUMBER OF COLOR PAGES WHICH DO NOT REPRODUCE LEGIBLY ON BLACK AND WHITE MICROFICHE.

CONTENTS

ILLUSTRATIONS

ILLUSTRATIONS (Continued)

ILLUSTRATIONS (Continued)

1.0 INTRODUCTION

The Chemical Systems Division of United Technologies Corporation is conducting a collaborative program to study the basic and unique mechanisms by which acoustic waves interact with the mean gas flow in the combustion chamber of solid propellant rocket motors. These flows differ significantly from the traditional boundary layer concepts which dominate the interpretation of fluid mechanics. Thus, basic mechanistic research is required to understand and characterize these flows, and thereby provide the basic knowledge required to solve applied problems involving the internal ballistics in rocket motors. This specific CSD program proposes the experimental studies in the combined analytical and experimental research program; the analytical studies are being conducted concurrently by Professor G. A. Flandro of the Georgia Institute of Technology, and more recently of the University of Tennessee Space Institute (UTSI).

Recent measurements and analyses of the mean and oscillatory flow fields in simulated solid propellant rocket motors have demonstrated the unique behavior of the basic fluid mechanics. Radial velocity and turbulence profiles of the mean flow field show the evolution of gas from the propellant surface causes the flow to be dominated by pressure and inertial forces, and not by viscous forces. Thus, the flow is rotational because of inertial effects and the time average vorticity results from the forces required to turn and accelerate the flow from the side wall to the axial direction. Interpreting these flows by analogy to growing and/or fully developed turbulent boundary layers is, therefore, not only invalid, but is also very misleading. In fact, the concept of a boundary layer is not valid for these flows because the velocity gradients extend a substantial distance across the flow channel. Furthermore, turbulence is important only towards the aft end of the motor, not all along the motor, as is usually assumed. Neither the rotational nature of the flow nor the turbulence effects are included in standard flow models use to interpret motor behavior.

When acoustic waves are imposed on this steady rotational flow, two phenomena are observed which differ significantly from the irrotational behavior assumed to characterize these waves. First, the measured magnitudes of the waves differ significantly from the expected plane wave behavior. Specifically, the radial gradients of the oscillatory velocity magnitude extend well into the core of the flow channel and the classical irrotational behavior is limited to approximately 1/3 of the flow area near the core region. In addition, the limited measurements which resolved the vector direction of these waves indicate that the oscillatory (in time) vorticity is substantial and is also spatially periodic. Not only is the wave motion rotational, but the gradients have characteristic distances that significantly exceed the thickness of the acoustic boundary layer. Therefore, an acoustic boundary layer approach is

not valid for interpreting the effect of wall blowing on the wave motion. It would appear that understanding this behavior is essential to interpreting the overall wave behavior and developing improved stability prediction methods.

Second, a substantial interaction is observed between the turbulence in the mean flow and the wave motion. This interaction destroys the wave motion in the near wall region and prevents the coupling between the wave motion in the core flow with the oscillatory surface heat transfer driving "velocity coupling." In effect, the turbulence appears to destroy the wave motion near the wall and thereby appears to add an additional source of acoustic damping to the chamber. This apparent additional damping is also not considered in the standard stability predictions.

Including both the mean and oscillatory vorticity provides a physically realistic basis for resolving the basic differences between the multi-dimensional and one-dimensional acoustic stability models. Specifically, the multi-dimensional stability model assumes both the mean and oscillatory flows to be irrotational. On the other hand, the one-dimensional model contains a simplified and unique rotational behavior for the mean flow (infinite in magnitude over zero spatial distance), and irrotational behavior of the wave motion. This rotational mean flow gives rise to the "flow turning" term in the one-dimensional model, which does not arise in the multi-dimensional model. To date, this fundamental difference between the models has not been resolved.

Adding both the mean and oscillatory vorticity in the multi-dimensional acoustic stability model, however, suggests how this difference can be resolved. Adding the vorticity to the model results in two additional terms. One term accounts for the energy required to turn and accelerate the mean side wall flow to the axial wave motion, and thus is analogous to the flow turning term in the one-dimensional model. The second term represents the energy required to turn and accelerate the oscillatory wall flow to the mean flow velocity. In effect, this second term corrects the surface admittance for side wall blowing effects, much as the Flandro "boundary layer" correction term. Thus, including both the mean and oscillatory vorticity appears to explain qualitatively the discrepancy between the acoustic stability models.

The oscillatory vorticity in the wave motion also provides a basis for resolving the basic inconsistency between the rotational mean flow and the supposed irrotational oscillatory flow. This inconsistency arises as the frequency of the wave motion approaches zero. At low frequency, the wave motion must eventually become quasi-steady, that is, rotational. This

rotational behavior is not permitted by the current irrotational model. Adding vorticity effects, however, would eliminate this inconsistency.

The quantitative analysis of these two additional terms requires detailed data on the radial profiles of the oscillatory velocity vector. These data are needed to define the wave behavior as a function of mean flow conditions, frequency, oscillatory surface flow behavior, and axial position. These data must then be correlated quantitatively to provide the predictive basis for acoustic stability analyses. This document reports the experimental portion of the collaborative program, which emphasizes measuring and correlating the data required to fully characterize the vorticity contributions to the wave motions and acoustic stability behavior. The concurrent analytical program is being conducted separately through the Georgia Institute of Technology and UTSI.

2.0 TECHNICAL BACKGROUND

Pressure oscillations in rocket combustors have caused significant design and operational problems. Low amplitude oscillations can couple with the motor case and other system components to generate substantial acceleration loads on critical motor components. Large changes in the mean chamber pressure can also be produced which can cause mechanical failures and alter the thrust-time characteristics of the motor. Hence, potential effects of oscillatory pressures must be considered in the design and qualification of motors.

The stability of the oscillatory chamber pressure is determined by a delicate balance between the sources and sinks of acoustic energy. Based on this approach, methods have been developed for estimating the stability of the combustion pressure in realistic motor geometries.[1,2,3,4] These methods have been applied to a wide variety of solid propellant rocket motor designs with some, but not complete, success. Unfortunately, a number of motors that were predicted to be stable were, in fact, found to generate oscillatory chamber pressures spontaneously. In other cases, motors that were predicted to be unstable were found to be stable after much testing and expense. Obviously, either erroneous prediction can have a significant detrimental impact on the motor development schedule and cost, as well as the credibility of the technology community.

Brown[5] compared the predicted stability of several generic motor designs with their observed stability to obtain further insight into the mechanisms responsible for these discrepancies. The processes contributing to the overall stability were divided into three categories: those which are believed to be well understood, those where the level of understanding is partially known but subject to large uncertainty, and those known to be poorly understood. Well understood contributions include:

- The acoustic frequency and mode structure predictions using NASTRAN or other finite element methods.
- Pressure-coupled response functions based on laboratory measurement methods. It should be noted that the Flandro acoustic boundary layer correction term is often ignored.
- Nozzle damping, which assumes quasi-steady flow in a short nozzle. The effect of temperature fluctuations entering the nozzle (the famous entropy wave issue) is circumvented by assuming an oscillatory isentropic flow enters the nozzle.

Contributions where the predictive accuracy is uncertain include:

- The potential mean flow model is known to be erroneous. From subsequent research, this flow is known to be rotational and, under some conditions, turbulent. The ability to include this effect in stability predictions, however, has not been developed.
- Particle damping predictions are valid for irrotational flow situations where the particle size distributions are known, usually from experimental measurements. Significant corrections from rotational flow effects, however, cause significant uncertainty.
- Periodic vortex shedding is qualitatively understood and well established. Quantitative predictions, however, are another matter.

Contributions which are known to be poorly characterized include:

- Velocity coupling models have been the subject of much study, debate, contradictory information and controversy.
- Flow turning predictions are included based on the one-dimensional or multi-dimension models. Experimental verification of these predictions has been attempted but has been difficult.
- Distributed combustion is often ignored because of the poor understanding and lack of supportive evidence. Current research by Beckstead[6] is addressing this issue.
- Acoustic/turbulence interactions are never considered because all the models are based on non-turbulent flows. Recent studies by Beddini[7] and by Yang[8] have started to address this issue.

Some of the motor discrepancies can be attributed to uncertainties in the propellant combustion properties, such as the response function or alumina particle size distributions. In a number of motors, however, the erroneous predictions cannot be explained on this basis. This result suggests either that additional sources of acoustic energy may be significant, or that the analytical methods for characterizing previously identified contributions are not correct. The summary above notes that three of the four least understood aspects of these predictions relate to the steady and unsteady flow behavior.

Concurrent research has verified that the flow-related models in the stability methods are inaccurate. This research has concentrated on the flow aspects of the interior ballistics and, in particular, the coupling between the flow and the acoustic waves. Based primarily on experimental results obtained in cold flow simulators, these studies have suggested significantly increased understanding of the mean flow environment and the contributions of flow-related mechanisms to the overall acoustic energy balance. The following sections summarize the analytical and experimental background, describe the unresolved technical

issues and indicate how their resolution will enhance the technical basis for improved stability predictions by this collaborative research program.

2.1 THE MECHANISTIC PROBLEM — ANALYTICAL PERSPECTIVE

Analytical models for the acoustic stability of rocket combustion chambers have shown qualitatively that the detailed mechanisms are extremely important. Unfortunately, these models do not agree quantitatively. One basic issue is resolving the details of how the flow from the burning surface interacts with wave motions parallel to that surface. The acoustic energy effects of this interaction can be significant in the overall acoustic energy balance and hence have an important effect on the predicted stability. The following paragraphs summarize the major analytical elements in this problem.

Hart, Bird, and McClure[1] conducted the first analytical study of the acoustic stability of solid propellant rocket combustion chambers. Assuming potential flow behavior (i.e., irrotational flow) for both the steady state and acoustic waves, they developed a multi-dimensional model for the stability of low amplitude acoustic waves based on the surface admittances of the chamber. While valid for waves that are normal to the surface, their work did not address the issue of wave motions parallel to the burning surface. In fact, this model allows a "slip" flow component of velocity at the burning surface parallel to the surface.

Later, Culick,[2,3] and Flandro[9] both recognized this analytical problem and attempted to eliminate this deficiency. Culick basically conducted two analytical studies. The first was motivated by the T-burner geometry and assumed both the mean and acoustic motion to be one-dimensional. He argued that the gas flow from burning surfaces is normal to the surface based on molecular viscosity. Hence, this flow has no momentum parallel to the surface. However, this gas flow mixes with the acoustic waves and acquires the momentum of the wave motion, which extracts energy from the waves. The effect was labeled the "flow turning loss" and resulted in an additional term in the acoustic energy balance equation. In his other study, Culick repeated Hart's analysis and concluded that the flow turning term must be added to the multi-dimensional model. He justified this correction by noting that the Hart model did not include these viscous effects which prevent the "slip" flow velocity component.

About the same time, Flandro also recognized this problem with the Hart model, but took an acoustic boundary layer approach to solving the problem. He argued that an acoustic boundary layer would be generated in the wave motion parallel to the burning surface by viscous forces. The boundary layer could also change the amplitude and phase of the wave motion. Hence, the acoustic waves impinging on the surface differ from the waves in the

core of the combustion chamber. Flandro's model resulted in an admittance correction term which differs in functional form from the "flow turning" term.

Recently, Flandro[10,11,12] and Brown[13] have collaborated on analytical studies to determine the relative magnitudes of the inertial and viscous forces in defining the acoustic wave behavior in the presence of side-wall blowing. The objective of these studies was to develop a model for these observed shear waves, which are convected away from the surface. A basic concern in these studies is the relative magnitude of the inertial forces compared to viscous forces. Initial results for one set of conditions are shown in figure 2-1. Comparing the predicted behavior against experimental data suggests that inertial forces dominate near the wall, but viscous forces are important in damping the shear waves as they approach the centerline of the chamber. Figure 2-2 shows the corresponding predicted phase angle between the local axial velocity component and the head-end acoustic pressure. According to the acoustic models, this phase angle should be -90 deg across the entire chamber radius. Obviously significant differences are both predicted and observed. These differences, however, extend from the wall much farther into the chamber than predicted by the acoustic boundary layer type models.

More recently, deJong and Baum[14] have predicted the oscillatory wave and vorticity structure in a simulated cylindrical port using a Navier-Stokes approach. Their predictions clearly demonstrate the oscillatory rotational behavior of these flows and the large penetration of nonplanar oscillatory motions into the chamber. Concurrently, Vuillot and Avalon[15] have conducted similar predictions for two-dimensional chambers to model experimental studies being conducted by Avalon and Comas.[16] They also observed large predicted penetrations of the oscillatory vorticity into the mean flow and concluded that neglect of these effects is a serious weakness of stability predictions. Yang[8] also predicted significant axial velocity overshoot from the classical potential acoustic waves, but not the spatial oscillations predicted by Frandro's early analyses shown in figures 2-1 and 2-2. Kassoy[17] has approached the analytical problem in a somewhat different manner. Unfortunately, these studies have assumed the oscillatory flow field to be independent of the mean flow, thus making their results inapplicable to this problem under study.

Brown[5,13] noted that both the mean flow and wave motions are highly rotational. The resulting vorticity results, which appear as shear waves, are not confined to the near wall region of the flow. Hence, boundary layer approaches are not valid for these flows. He then extended the multi-dimensional to include the interaction between the mean flow vorticity and the acoustic waves, as well as the interaction between the vorticity of the waves and the mean flow. This model results in two additional terms to the basic Hart model, one similar to the flow turning term and the other similar to the admittance correction term. Quantitative

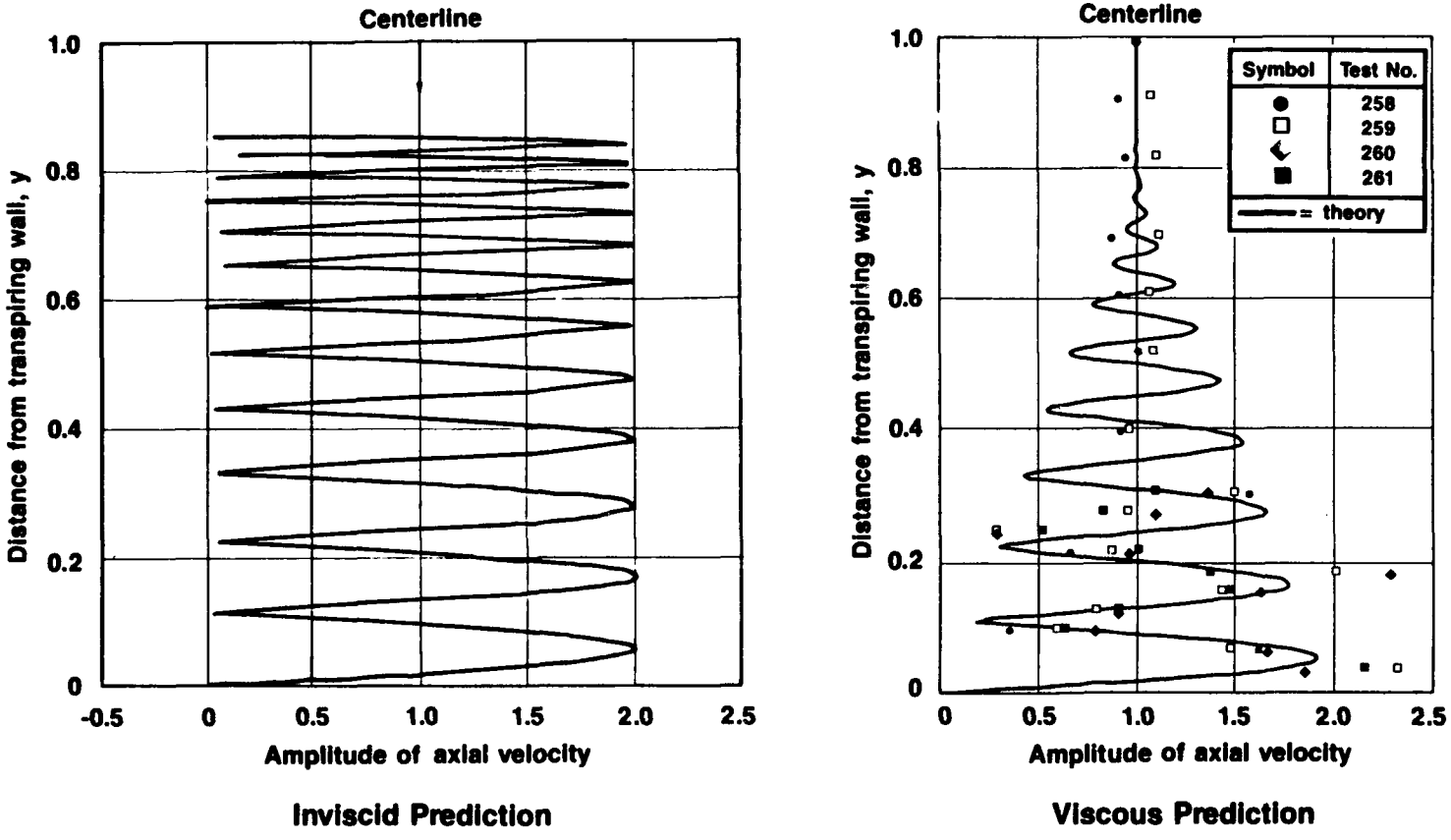

Figure 2-1. Vortical Flow Analysis by Flandro

CSD-V-52172

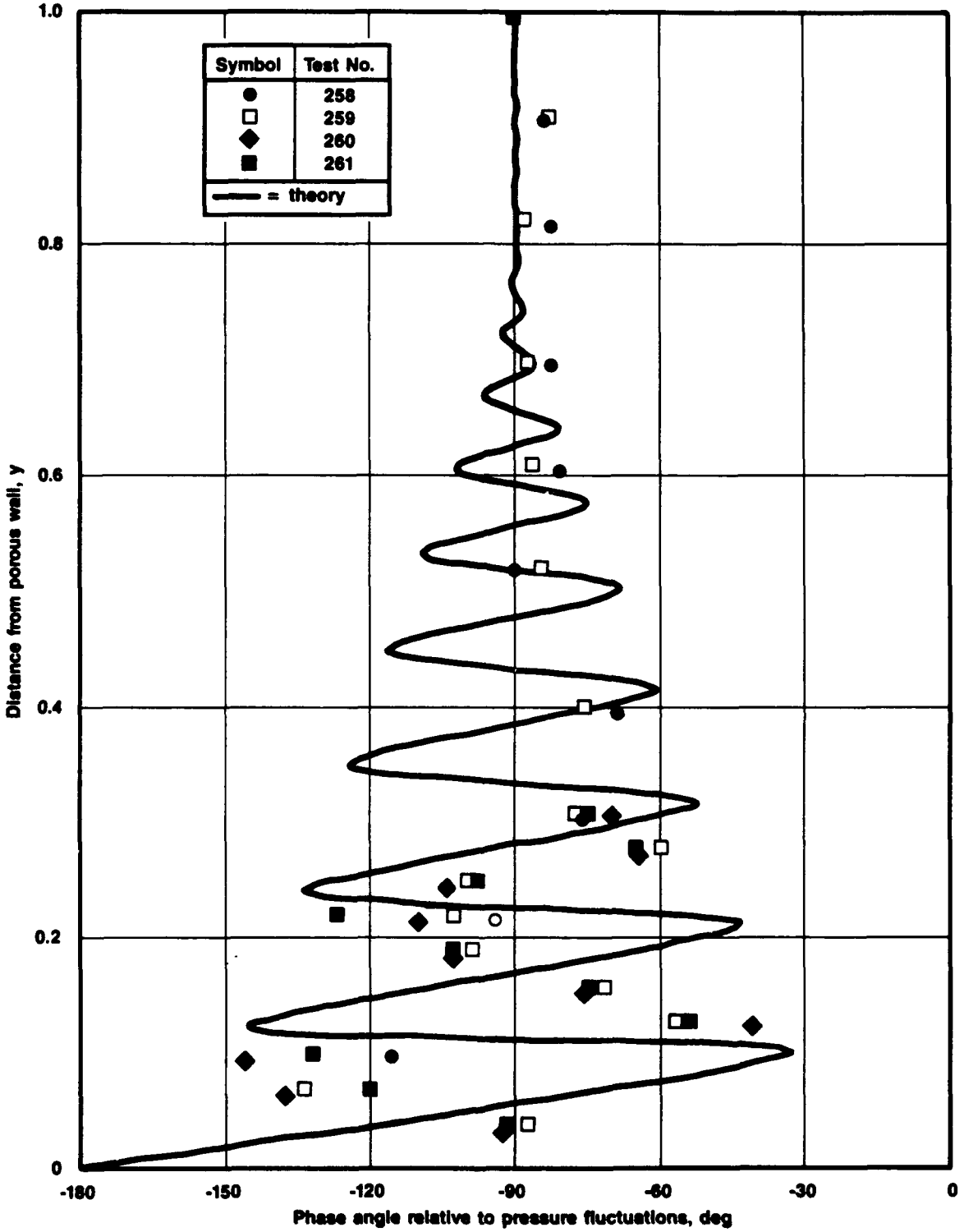

Figure 2-2. Comparison of Numerical Solution with 84 Hz Cold Flow Data

47372

evaluation of these two terms, however, requires quantitative predictions for the vorticity of the waves motions.

In summary, the analytical interpretation of this problem is incomplete. The current model for the wave motions parallel to a burning surface, which is incorporated in acoustic stability prediction methods, is inappropriate for stability predictions. Approaches to significantly improving these models have been defined by Professor Flandro in his concurrent analytical studies of this problem and appear to offer a high probability of being correct.

2.2 THE MECHANISTIC PROBLEM — EXPERIMENTAL PERSPECTIVE

A number of experimental studies have been conducted to define both the mean and oscillatory flow field in solid propellant rockets.[18,19,20,21,22] These studies have demonstrated that the mean flow follows the rotational inviscid model, which is controlled by inertial forces. The wave motion is also rotational with significant deviations from irrotational behavior extending well into the combustion chamber. Turbulence effects become important in both the mean flow and wave motions about 7 to 8 diameters downstream. Figure 2-3 summarizes the current conceptual model for these flows. The following paragraphs describe the experimental studies in more detail.

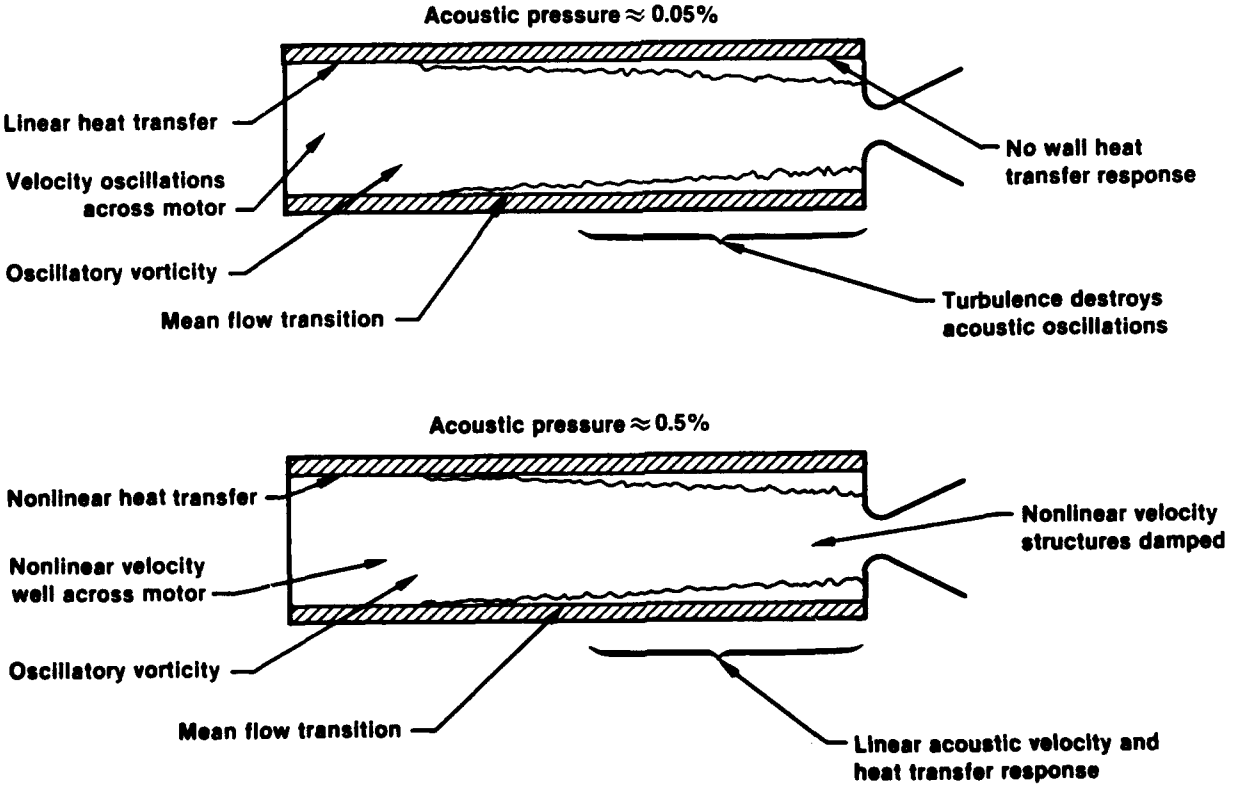

Figure 2-3. Conceptual Flow Field Model

37485

A number of experimental studies have been conducted specifically to define the velocity and turbulence characteristics of mean flow field resulting from side wall injection. Dunlap et al.[18] and Yogodkin[22] measured profiles of the magnitude of the velocity and the turbulence in cold flow simulators using hot wire anemometers. Excellent agreement was found with rotational inviscid flow models first proposed by Taylor[23] and Culick.[24] These tests showed the boundary layer approach to modeling these flows to be invalid because the profiles extend half way from the chamber wall to the centerline.

In a later study, Dunlap and co-workers[20] made more detailed measurements of the mean and fluctuating velocity vectors and the turbulent shear stresses in the principal coordinate directions. Spectral and length scale data were also determined for selected conditions. Mean velocity and turbulence profiles are compared to predictions from Beddini's[25] model in figure 2-4. The measured and predicted mean velocity profiles prior to transition show good agreement and are consistent with those derived independently by Taylor[23] and Culick[24] for a rotational inviscid flow.

In addition, Dunlap's data and Beddini's model both show that at some critical length to diameter ratio, which was predicted to be approximately 5 to 7, the turbulence levels increases in the near wall region and propagates towards the centerline as the fluid travels downstream. The corresponding turbulence data in figure 2-4 show the predicted development. It is important to note that both the measured scale of the turbulence and the scale required to predict the turbulence from the model are approximately half the scale associated with turbulent pipe flow.

Measurements have also been made to investigate the characteristics of the wave motion in these mean flows in this same cold flow simulation apparatus.[19] Both single element hot wire anemometer and split film anemometer measurements were conducted. The single element anemometer data show the magnitude and phase of the wave motions deviate significantly from the plane wave behavior predicted by the potential flow acoustics model. These deviations extend up to 40% of the distance from the wall to the chamber centerline. Thus, the acoustic boundary layer corrections to the wave models do not provide a realistic representation of the wave behavior.

The experimental measurements of the acoustic velocity vector provide even more basic insight into the wave behavior. The specially fabricated split film probe, which Dunlap et al.[20] designed and calibrated to measure the mean flow velocity vector, was traversed radially at Z/D = 1.8. The velocity vector data were reduced to obtain the magnitude and phase angle of the axial and radial velocity components with respect to the head end acoustic pressure.

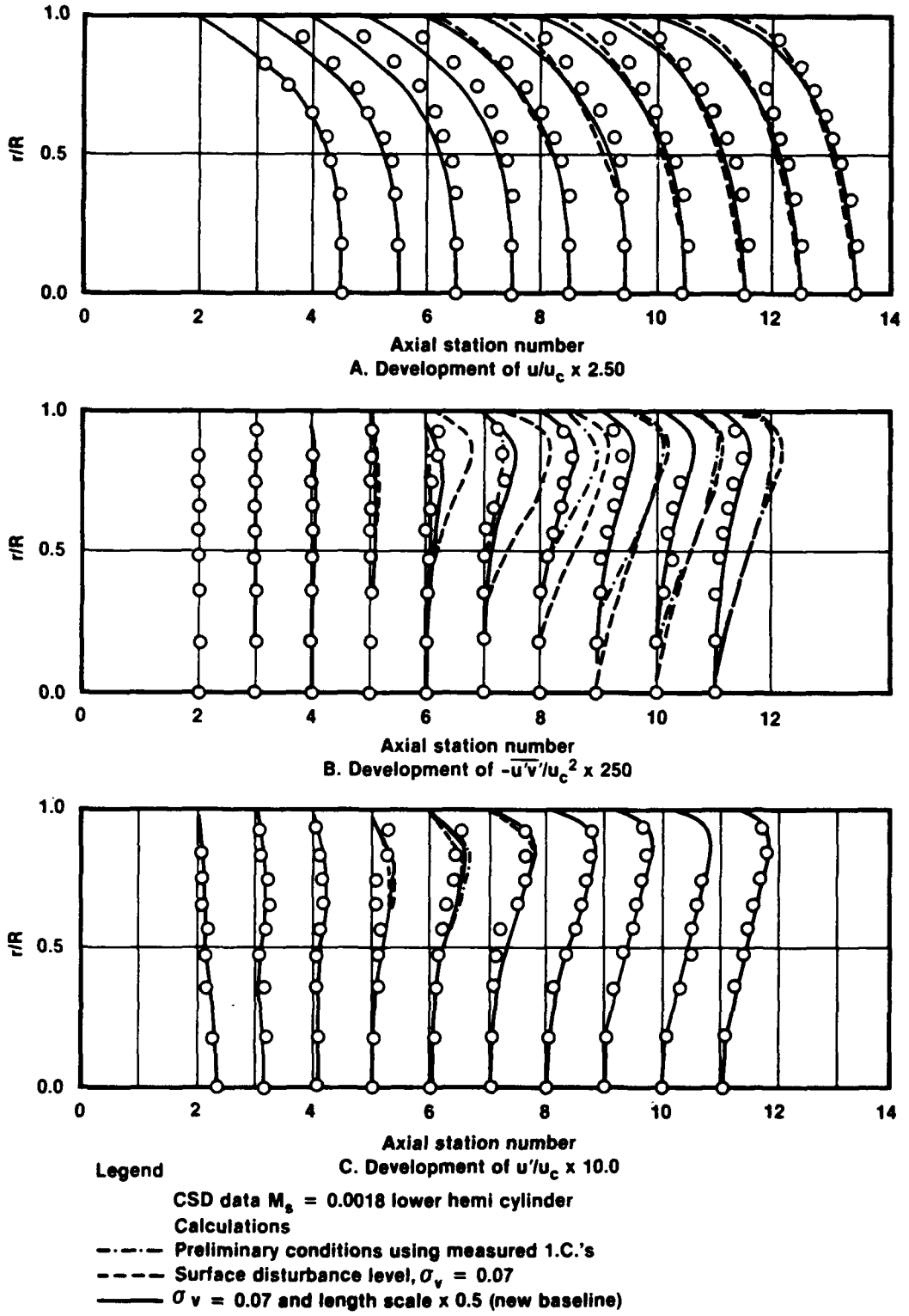

Figure 2-4. Mean and Oscillatory Velocity Profiles
(Sheet 1 of 2)

37293

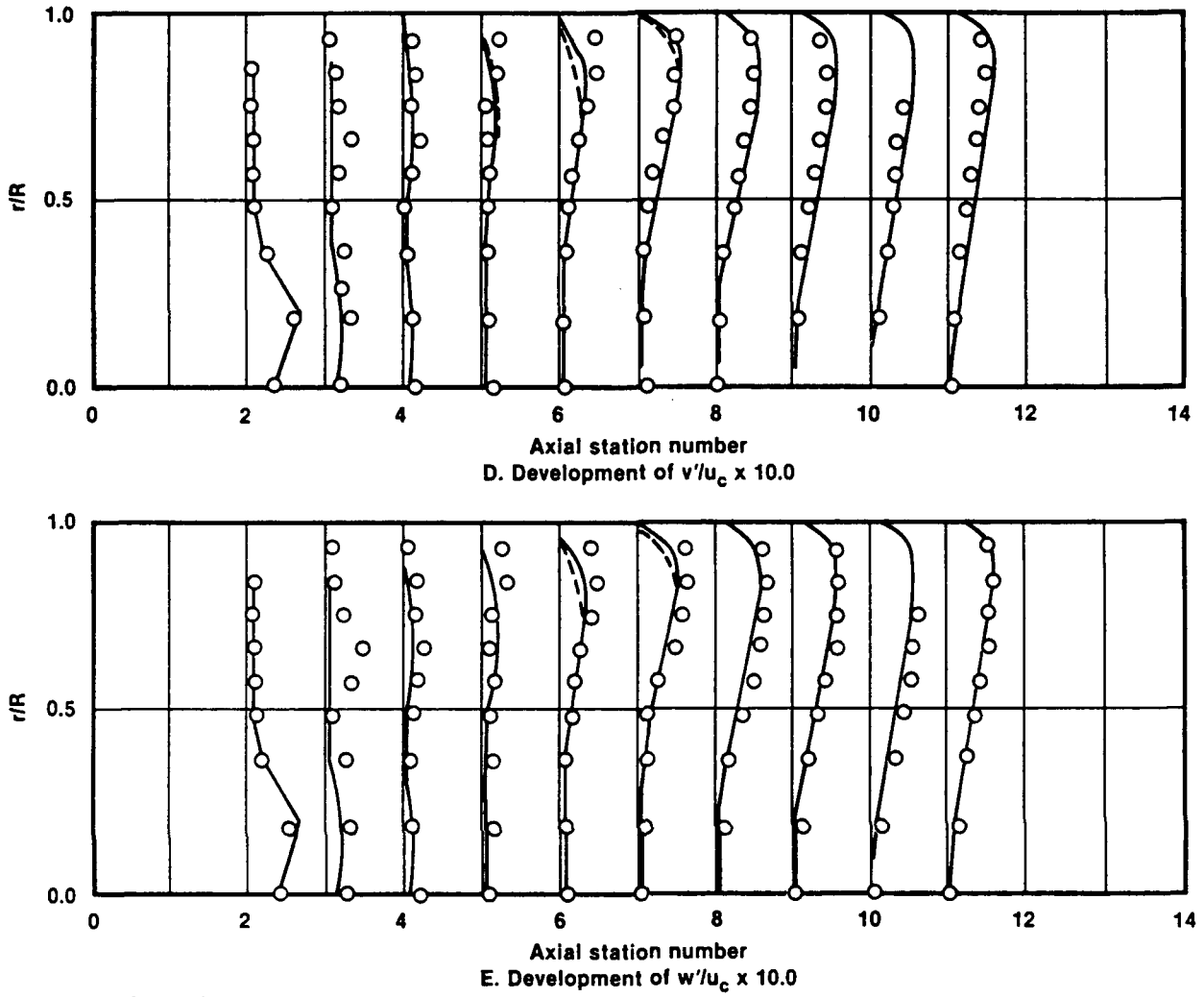

Figure 2-4. Mean and Oscillatory Velocity Profiles
(Sheet 2 of 2)

37293

Figures 2-5 through 2-8 show how the magnitude and vector direction of the oscillatory velocity at Z/D = 1.8 behave during one cycle of the acoustic pressure at several radial stations. The terms "upstream" and "downstream" refer to the direction of the axial component, while "into the wall" and "away from wall" refer to the radial component direction. Figure 2-5 shows the results obtained on the centerline. Here, the radial component is zero, so the wave direction changes instantaneously between the upstream and

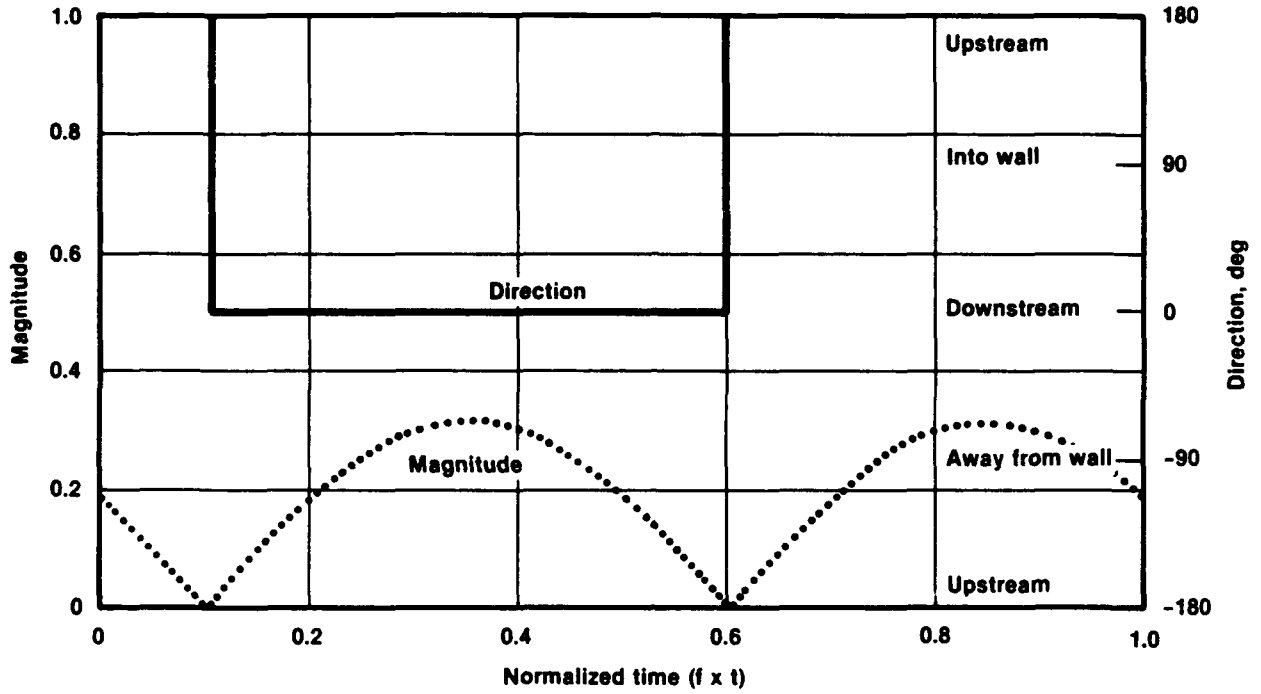

Figure 2-5. Acoustic Velocity Vector
($r/r_w = 0$, $Z/D = 1.8$, $M_s = 0.0018$, $\hat{P}/\gamma\bar{P} = 0.05\%$)

37373

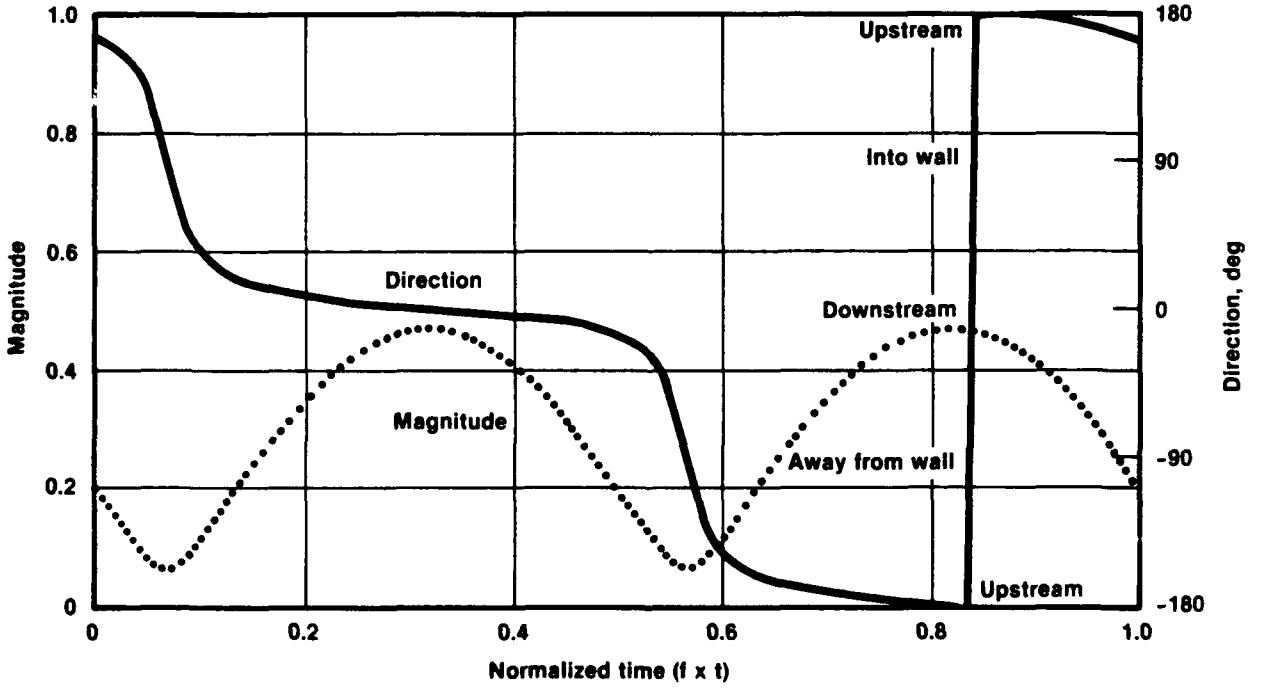

Figure 2-6. Acoustic Velocity Vector
($r/r_w = 0.69$, $Z/D = 1.8$, $M_s = 0.0018$, $\hat{P}/\gamma\bar{P} = 0.05\%$)

37372

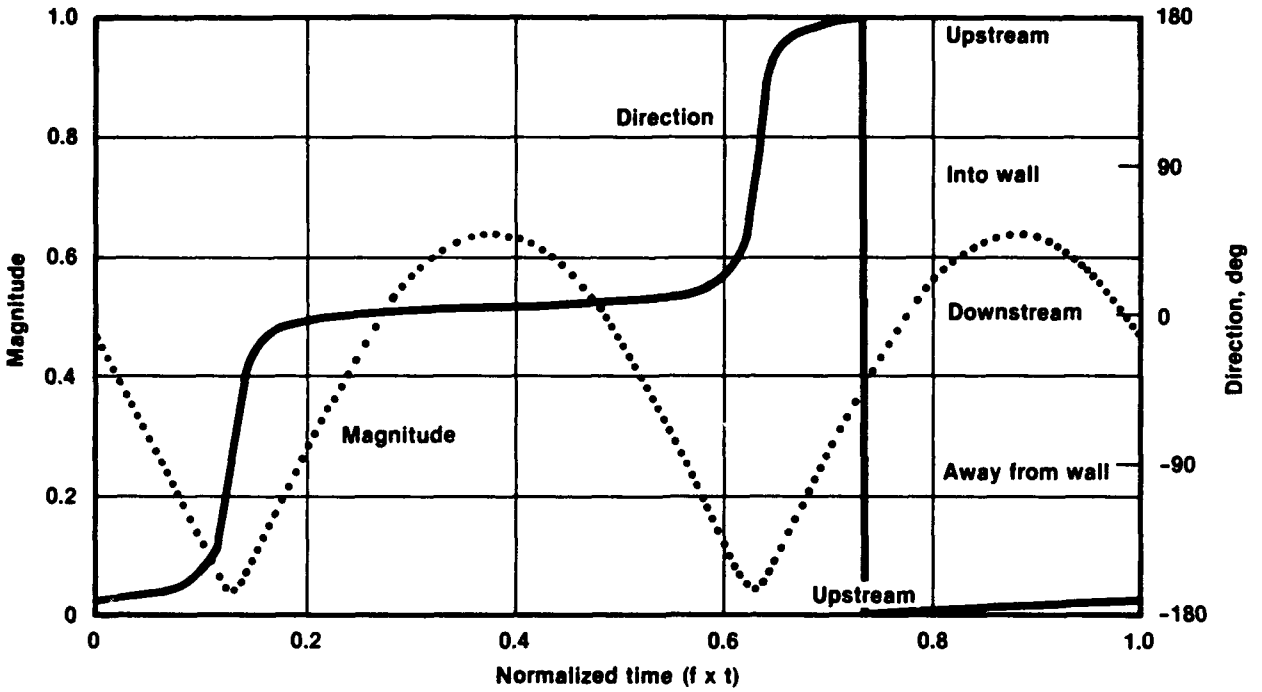

Figure 2-7. Acoustic Velocity Vector
(r/r_w = 0.81, Z/D = 1.8, M_s = 0.0018, $\hat{P}/\gamma\bar{P}$ = 0.05%)

37369

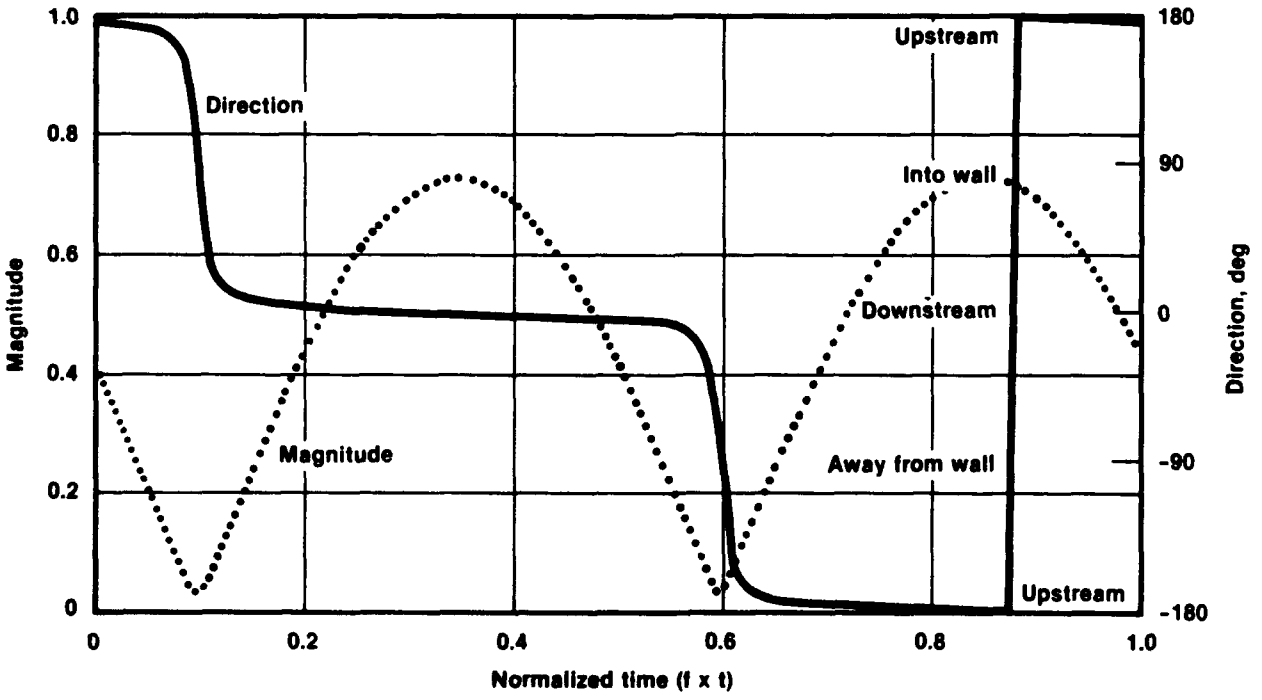

Figure 2-8. Acoustic Velocity Vector
(r/r_w = 0.96, Z/D = 1.8, M_s = 0.0018, $\hat{P}/\gamma\bar{P}$ = 0.05%)

37367

downstream directions as the magnitude goes through zero. This behavior is typical of classical irrotational standing acoustic waves, which are usually assumed to characterize the entire wave behavior.

Figure 2-6 shows the behavior of the oscillatory velocity vector at $r/r_w = 0.69$ for the same test conditions. Here, the radial velocity is not zero, which is expected as the wall is approached because the porous tubing has an acoustic admittance of approximately 0.02. Note the magnitude of the velocity is never zero, even as the direction of the acoustic velocity changes rapidly from the upstream to downstream direction. During this direction change, the velocity rotates into the wall as the wave changes axial direction. Later in the cycle the velocity rotates away from the wall as the vector reverses direction once again. This behavior suggests an oscillatory vortical motion in the flow.

At $r/r_w = 0.81$ (figure 2-7), however, this directional sequence is reversed; it becomes "upstream", then away from the wall, then "downstream", then into the wall, and then finally upstream again. At $r/r_w = 0.96$ (figure 2-8), the station closest to the wall, the directional sequence has again reversed and become equivalent to the sequence for $r/r_w < 0.81$.

Cold flow experiments in a two-dimensional chamber have also been reported recently by Avalon and Comas[16] and Ma et al.[26] Both investigations demonstrated qualitatively similar results with the cylindrical port results described above.

Based on these data, a qualitative picture of the wave motion can be formulated. This picture, which is presented in figure 2-9, shows regions of counter-rotating oscillatory fluid motion extending from the wall into the core region. The magnitude of the velocity in these fluid cells decreases from the wall and merges into the potential (acoustic) wave motion in the core. The size of these cells in both the radial and axial directions is unknown at this time and requires further experimental studies to define.

These variations result from the velocity field adjusting from potential wave behavior in the core to the purely radial velocity oscillations which must exist at the wall. Therefore, an acoustic boundary layer approach, which is based on viscous forces dominating the flow, has been used in these analyses. However, the observed adjustment region extends much farther into the core than the predicted boundary layer thickness. While at first startling, it should be noted that the mean flow is highly rotational.

Thus, it is reasonable to expect the oscillatory flow field might also have significant oscillatory vorticity. Additional data are needed to assess these models and to provide insight

into the relative contributions of inertial and viscous forces in determining the oscillatory flow behavior. Acquisition of these data over a range of surface Mach Numbers, mean pressures, and axial stations is the primary objective of these studies.

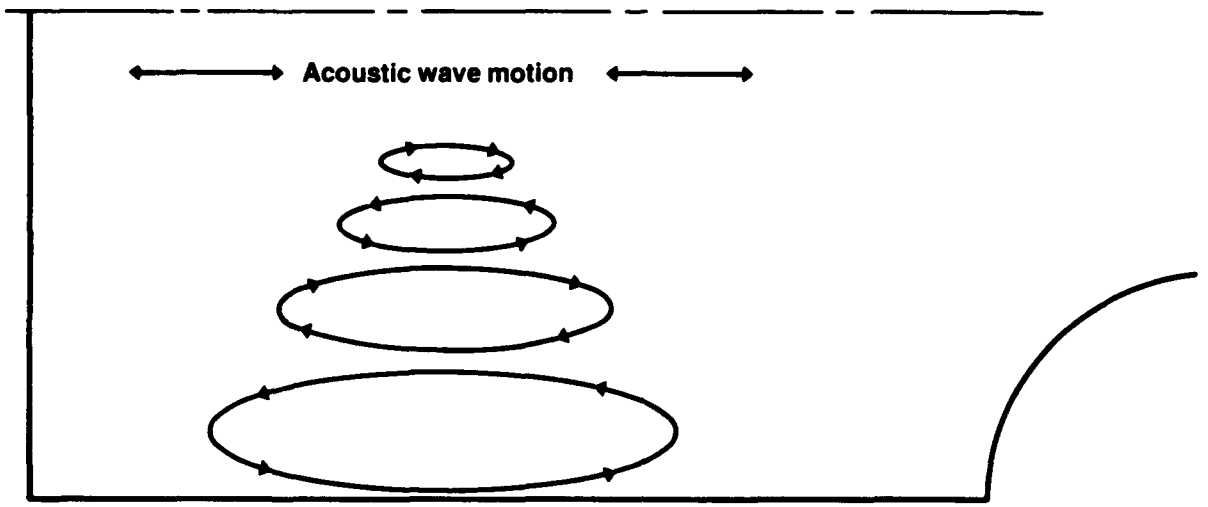

Figure 2-9. Rotational Wave Structure, Vortical Flow Structures

CSD-V-48637

3.0 EXPERIMENTAL STUDIES

This program is experimentally investigating the behavior of the acoustic velocity vector as a function of flow and acoustic conditions. Cold flow tests were conducted with high spatial resolution to measure the oscillatory velocity and vorticity behavior of the waves. Tests were conducted over a range of frequencies, surface Mach Nos. and chamber pressures. Close collaboration is being maintained with concurrent analytical studies proposed by Professor G. A. Flandro of the Georgia Institute of Technology and more recently the University of Tennessee Space Institute. The following paragraphs describe the results of the 24-month experimental study.

3.1 DESCRIPTION OF THE EXPERIMENTAL APPARATUS

Measurements of the mean flow velocity, turbulence, and wave behavior have been an essential aspect of this recent research. To obtain these data, the cold flow apparatus shown schematically in figure 3-1 was constructed and is operational. Nitrogen flows through porous cylindrical bronze tubes to simulate the gas evolution by the propellant combustion and generated a realistic internal flow field. Considerable care was taken to ensure the surface Mach number is constant over the entire simulated burning surface. A flow distribution tube equalizes the flow circumferentially around the 10-cm-diameter porous tube. This basic technique has been used successfully in a number of programs to investigate the steady and oscillatory properties of the flow.[14,16,20,21,25]

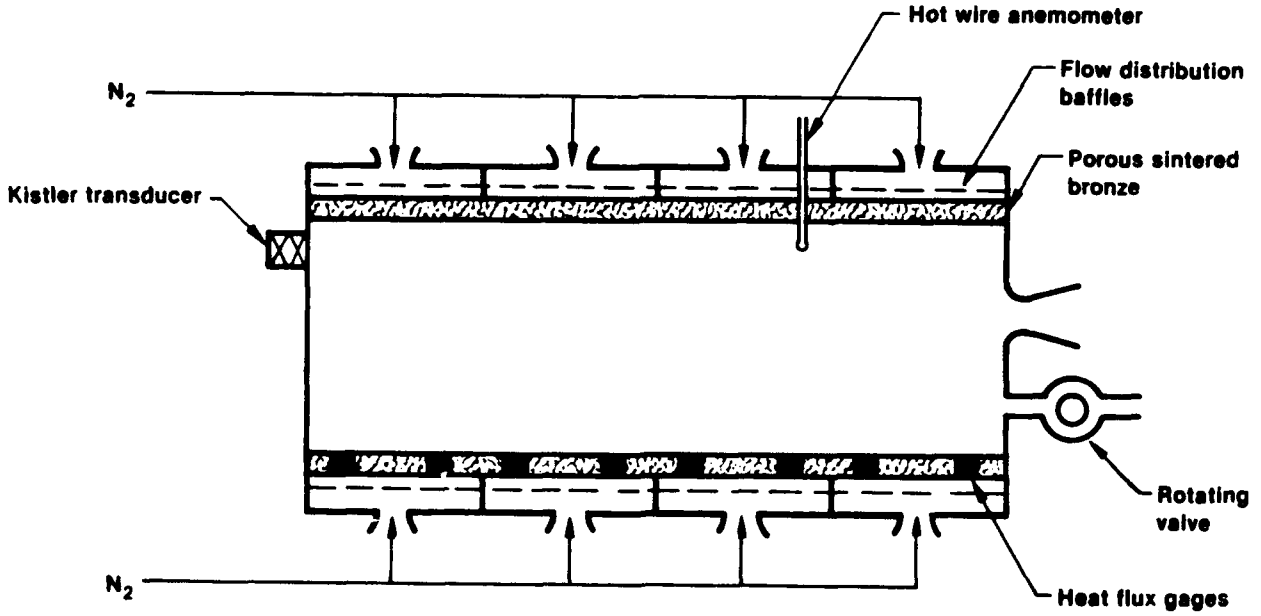

Figure 3-1. Cold Flow Apparatus

37287

One particular version of this apparatus was constructed in seven sections that join together to form a continuous cylindrical surface having an overall length of 17 diameters. The nitrogen flow into each of these sections was choked to further equalize the flow. Figure 3-2 shows an exploded view of one section while an end view is shown in figure 3-3. Each section had two ports for heat flux gages (shown installed in figure 3-3) or for hot wire or split film

Figure 3-2. Exploded View of Segment

37288

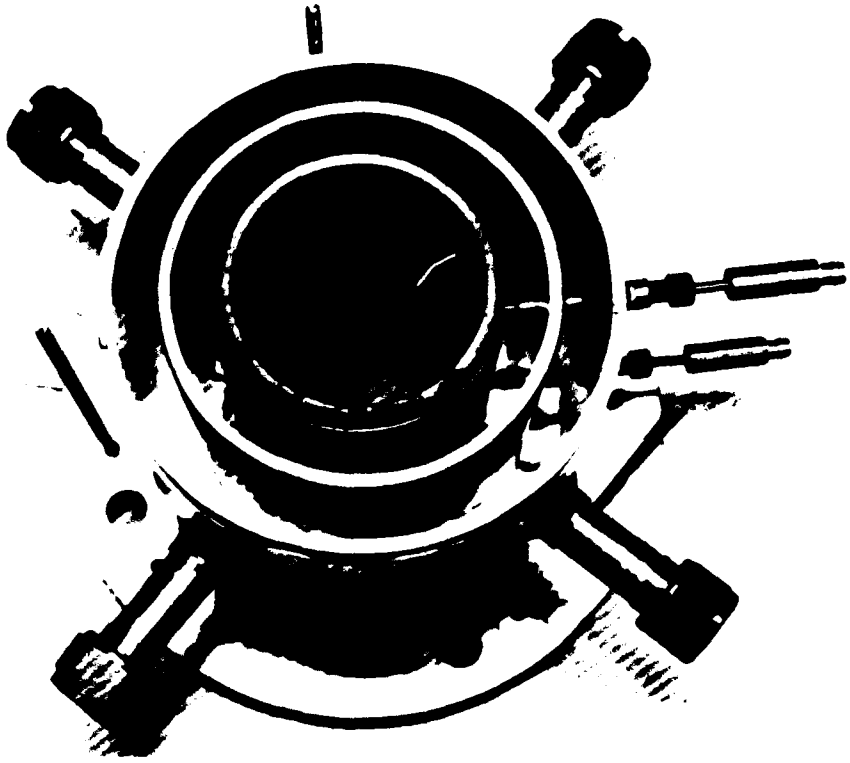

Figure 3-3. End View of Segment

37289

anemometers. The anemometers, or heat flux gages, are connected to signal conditioners which operate the sensors in the constant temperature mode. Hence, the power to the gage measures the gas velocity, or the surface heat transfer, directly with a frequency response of 10 Khz. Figure 3-4 shows the detailed installation of the hot wire anemometers through the side walls. Pressure taps are also located on the simulated propellent surface to measure the mean pressure at the surface throughout the apparatus. Kistler pressure transducers are mounted at both ends of the apparatus to measure the oscillatory pressure behavior. The apparatus was mounted vertically with the exhaust nozzle down.

Flow oscillations are generated by a rotating valve at the aft end. A specially designed aft-end section was fabricated to mount a fixed-diameter sonic exhaust nozzle on the centerline and to minimize the radial distortion of the velocity oscillations entering the port from the rotating valve. A variable speed drive electric motor connected to the rotating valve controls the frequency of the acoustic oscillations. The hole/slot geometry in the rotating

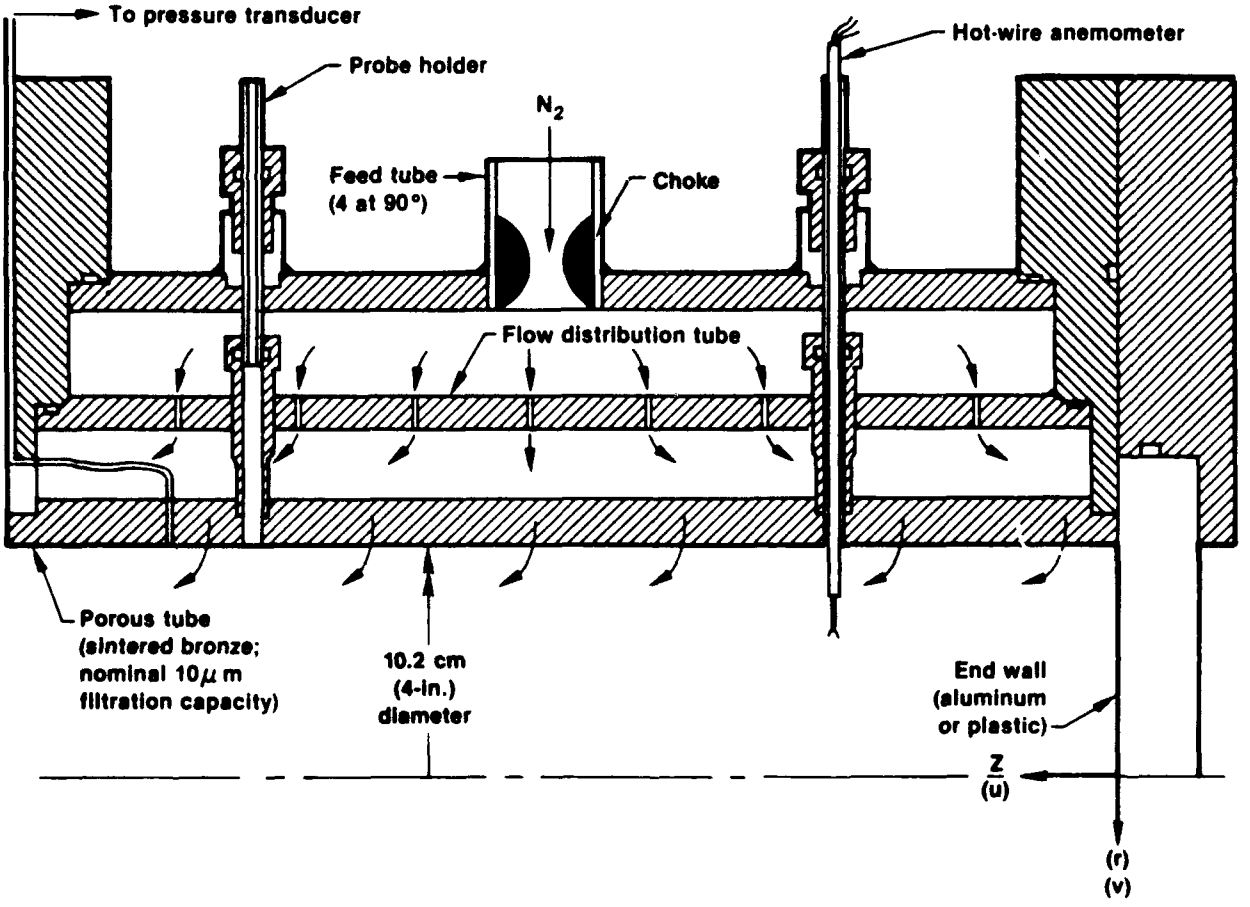

Figure 3-4. Instrumentation Mounting Details

34378

valve produced nearly pure sine wave oscillations: 91% at the driving frequency, 4.5% at the third harmonic, and 4.5% at the higher odd harmonics.[28]

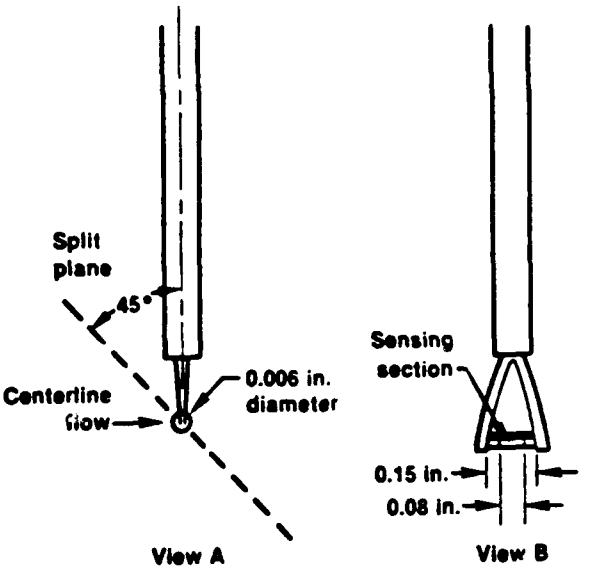

Figure 3-5. Schematic of Split Film Probe

The primary measurement of interest in these tests was the mean and oscillating directional components of the velocity. These data were obtained using the specially designed split film probe used by Dunlap.[20] This probe was constructed by TSI as a modification of their Model 1288 anemometer. The basic sensing element consisted of a quartz core covered with a thin film of platinum etched along the split line. The sensor element was 0.006 in. in diameter and 0.08 in. in lenght. The modification consisted of moving the split plane 45° relative to the axis of the probe, as shown in figure 3-5, to maximize the senitivity to both the axial and radial flow components.

This anemometer was calibrated over flow angles from -10° to +53° relative to the flow direction (which corresponds to -55° to +8° relative to the split plane). The Mach number as varied from 0.001 to 0.2 to cover the range expected in this program. These calibrations were run is a specially designed wind tunnel to provide a well characterized flow, both in magnitude and direction.

The basic approach in correlating the calibration data was to relate the magnitude of the flow to the sum of the power loss from the two films to the gas. The flow direction was then related to the ratio of the power loss from each film. Specifically, the mass flow is defined as:

$$X_o = (\sqrt{P \times M / 30}) \times (T_{gas}/273)^{-0.59} \qquad (3\text{-}1)$$

and the heat flux from each film to the gas becomes

$$F_i = \frac{100 \times (R_i^{set} - R_i^{internal}) \times E_i^2}{(R_i^{set} - R_i^g) \times (40 + R_i^{coax} + R_i^{set})^2} \quad (3\text{-}2)$$

where P is the absolute pressure, M is the Mach number, T_{gas} is the nitrogen temperature, E_i is the film voltage measured on the TSI Model 1050 anemometer, F_i is the heat flux from the film divided by the temperature difference between the film (usually 250°C) and the flowing nitrogen (expressed in film resistance units, R^{set}-R^g), R^{coax} is the cable resistance, and R^{set}-$R^{internal}$ is the film resistance. The heat flux from both films were then combined to form the parameter, Y_o, given by equation 3-3.

$$Y_o = (F_1 + F_2) \times (T_{gas}/273)^{-0.59} \quad (3\text{-}3)$$

Figure 3-6 shows a plot of Y_o vs X_o over a range of flow angles. Note that the total flux is essentially independent of flow angle. Correspondingly, the ratio of the two fluxes, F_1/F_2 is a function of both the flow magnitude and angle, as shown in figure 3-7. Thus, an iterative numerical process is required to derive the instantaneous flow magnitude and angle from the film voltage measurements.

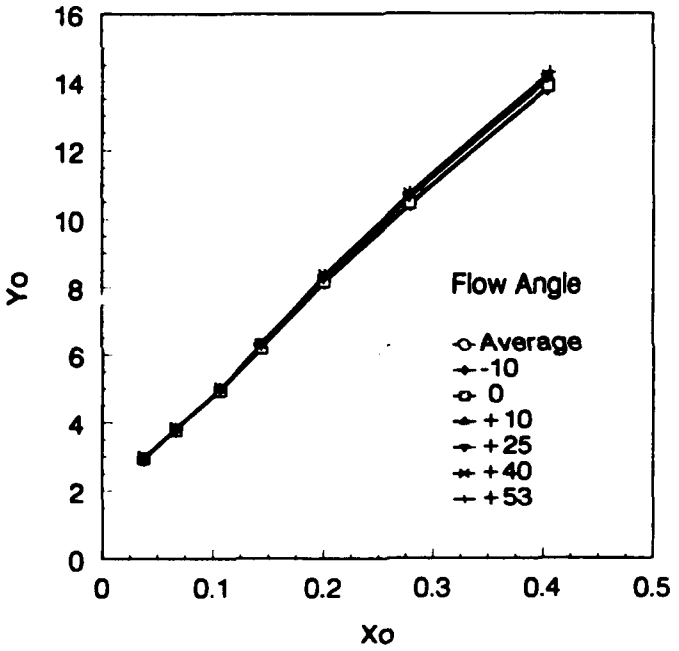

Figure 3-6. Anemometer Total Flux Calibration

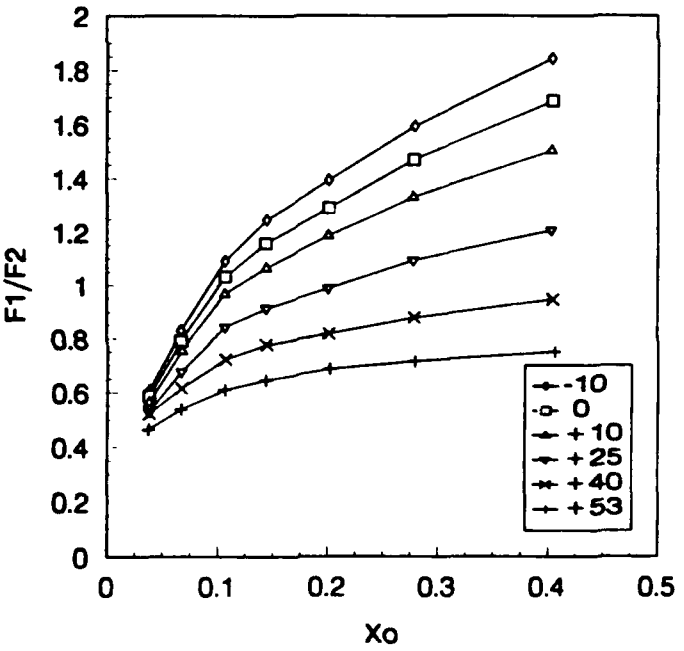

Figure 3-7. Flow Direction Calibration

All the sensor voltages were recorded on a digital data recording system. In addition to the total voltages, the oscillating component of the anemometer voltage was high pass filtered, amplified, and recorded on high sampling rates channels. The Kistler signals were also recorded on the high speed system. All the signals were initially recorded on FM tape. They were subsequently transferred to a MicroVax II based data logging system for subsequent processing and reduction in one tape pass. The data reduction code first derived the mean parameters of interest. Next, the oscillating components were reduced using FFT methods to define the driving frequency, oscillatory pressure and film voltages, the oscillating directional components of the flow velocity normalized to the oscillating head-end oscillating pressure, the coherence between the oscillating directional velocity components and pressure, and the individual bispectral behavior of the film voltages and oscillating pressure.

The entire experiment was controlled by a multistep sequencer which managed the voltage calibrations for each test and stepped the anemometer across the port diameter. In this way, data at multiple radius positions could be obtained from one test using the sequencer to step and hold the anemometer at each radial position. Sufficient times were allowed to acquire and average twenty ensembles of data at each radial position.

Considerable effort and care were taken to ensure the accuracy of this data reduction process. For example, once the anemometer was calibrated, the resulting voltages were treated as input to the data reduction process and the derived flow magnitude and directions compared to the known input values. Excellent agreement was obtained. Several spot checks were run using direct digital meters and manual data reduction to completely bypass the computer system. Again, excellent agreement with the code was observed. The impact of variations in the time average voltages on the derived oscillating components was also investigated. These variations were found to have minimal impact on the derived oscillating components, as tabulated in Appendix A, indicating the system was robust in TQM terms!

The ratio of the oscillatory velocity components to the head-end oscillatory pressure are the primary oscillatory data of interest. Therefore, significant attention was directed to defining a statistical approach to defining confidence intervals for these components. It can be shown that the power in the oscillating velocity components and in the oscillating pressure are χ^2 distributed.[29] Thus, when the oscillating velocity is normalized to the oscillating pressure (i.e., the transfer functions), the result follows the classical F distribution.

Hence,

$$\frac{|\hat{H}(f)-H(f)|^2}{|\hat{H}(f)|^2} > \left[\frac{2}{n-2}\right]\left[\frac{1-\gamma^2}{\gamma^2}\right] F_{2,n-2,\alpha} \qquad (3\text{-}4)$$

defines the radius of a circle of the confidence. Here, H(f) is the ratio of the oscillatory velocity component to the head-end oscillatory pressure, ^ refers to the estimated value, γ^2 is the coherence, F is the probability distribution of n degrees of freedom (20 for this study since 20 ensembles were averaged together) and α is the probability the magnitude will exceed the confidence limit.

Equation 3-4 reveals a number of important effects. First, the estimated coherence is extremely important in defining the radius of the confidence circle. Assuming a confidence limit of 95% (i.e., $\alpha = 0.05$), the standard averaging of 20 ensembles used in the data reduction, F = 3.5549. When the coherence is 0.95, equation 3-4 shows the confidence circle has a radius of 14.4% of the measured amplitude, and when the coherence is 0.99, the radius is 6.30%.

Similarly, equation 3-4 provides a basis for deciding when the radial oscillatory velocity component is zero. When the coherence is 0.282, this leads to a confidence circle having a radius of unity, which means a true amplitude ratio of zero is possible. This condition also implies the confidence interval for the phase angle is ± 90°. Coherences below 0.282 imply that all phase angles are possible since the origin of the coordinate system lies within the confidence circle. This condition therefore defines a reasonable basis for concluding a measured velocity component could be zero.

This statistical analysis also justifies the averaging of 20 ensembles. For example, using 30 ensembles would decrease F to 3.3404 and the critical coherence to 0.192. The impact on the conclusions drawn from the data would not change significantly, while the duration of each test would have increased significantly. Thus, 20 ensembles were selected as a reasonable compromise between data accuracy and the cost of running the tests.

3.2 EXPERIMENTAL RESULTS

Measurements of the oscillatory internal flow field were conducted at axial stations 1.8, 3.04, 4.22 and 5.46 diameters from the head end. The surface Mach numbers of 0.00108, 0.00197 and 0.00327 were tested at a chamber pressure of 30 psia. The two lower Mach numbers were also tested at 90 psia to assess the effect of the kinematic viscosity on the wave behavior. The radial stations were varied to provide the desired spatial resolution.

The pressure-coupled response function for the porous side walls at 92 Hz was estimated using the method described in reference 19. The table below gives these values for the conditions tested in this program. Note that these response functions are relatively large compared to typical solid propellants. Furthermore, they indicate that the porous tubing is a strong damper of the oscillations, rather than a source of acoustic energy, which is the case with solid propellants. Finally note that the magnitude decreases with increasing surface Mach number while the pressure influences both the magnitude and the phase angle.

Porous Surface Response Functions

Surface Mach No.	Pressure, psia	Response Magnitude	Function Phase	Function Real	Function Im
0.00108	30	14.02	-152	-12.4	-6.6
0.00197	30	7.47	-151	-6.53	-3.62
0.00327	30	4.38	-148	-3.71	-2.32
0.00108	90	26.15	-126	15.37	-2.12
0.00197	90	14.32	-126	-8.42	-11.2

3.3 MEAN FLOW VELOCITY

The axial component of the mean flow velocity was compared to the cosine law which was validated in several previous investigations.[19,20,21] These comparisons are shown in figures 3-8, 3-9, 3-10, and 3-11.

Two interesting features are apparent in these data. First, the scatter in the data is significantly higher at a L/D of 1.8 compared to the data at 3.04, 4.22, and 5.46. This scatter is also significantly higher than the previously reported data at this same axial station.[18,19,20] However, it should be noted that these tests were conducted with the exhaust nozzle aimed downwards. As noted by Dunlap,[20] differences were observed between velocity profiles were obtained in the nozzle upwards and horizontal orientations at an L/D of 1.8. These differences were attributed to natural convection effects resulting from the thermal lag in cooling the head end by the apparatus and the flowing gases. Furthermore, these natural convection effects disappeared by the time the flow reached an L/D of 3, just as they appear to do in these data as well. Thus, natural convection effects, which have never been investigated in this orientation, may account for this scatter.

Second, the data at L/Ds of 3.04, 4.22, and 5.46 show excellent consistency with the cosine profile, although the data at 3.04 and 4.22 are offset slightly from the expected cosine profile. This deviation suggests there was an offset in the radial alignment of the anemometer since the previously reported data at these same axial stations showed excellent agreement with the

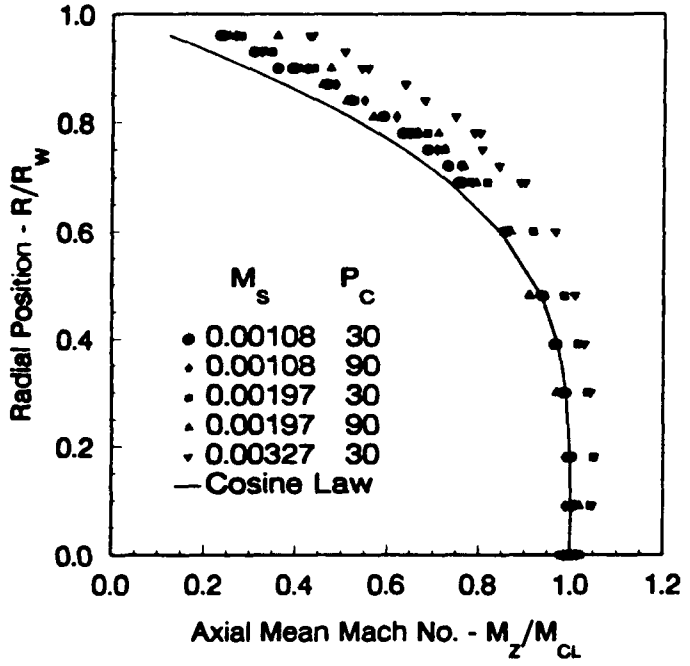

Figure 3-8. Axial Mean Velocity at L/D = 1.8

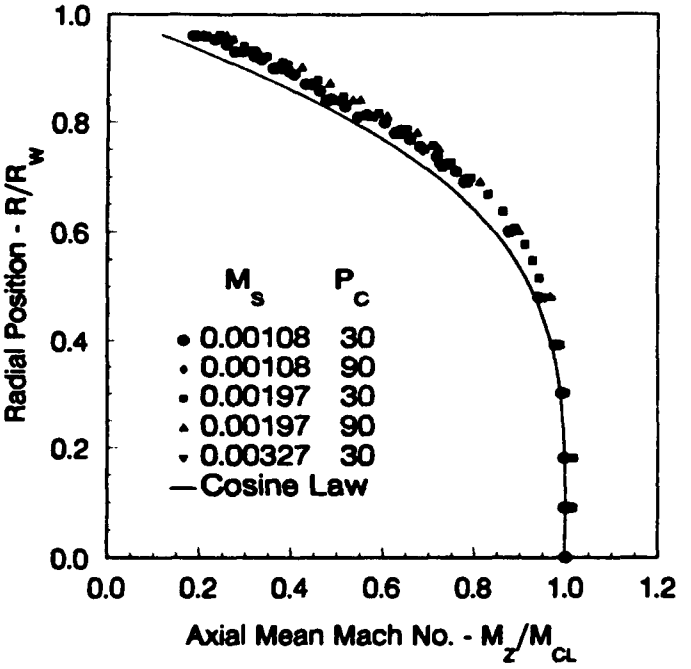

Figure 3-9. Axial Mean Velocity at L/D = 3.04

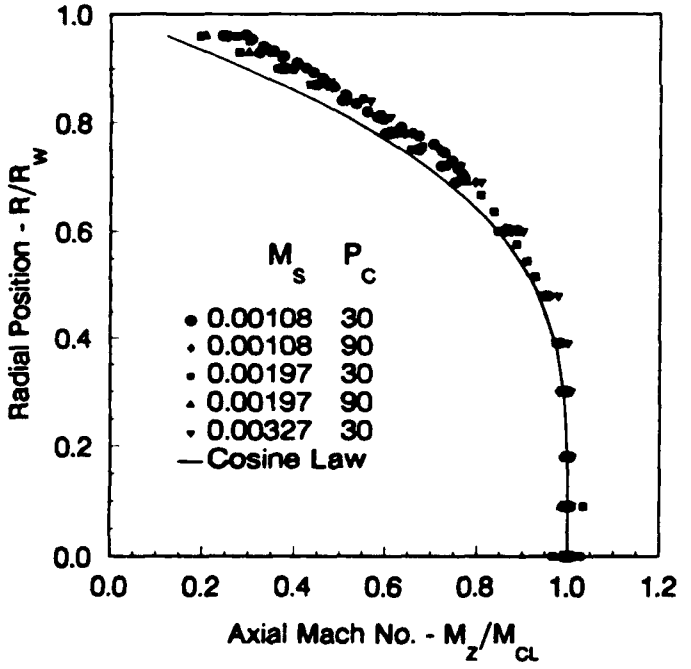

Figure 3-10. Axial Mean Velocity at L/D = 4.22

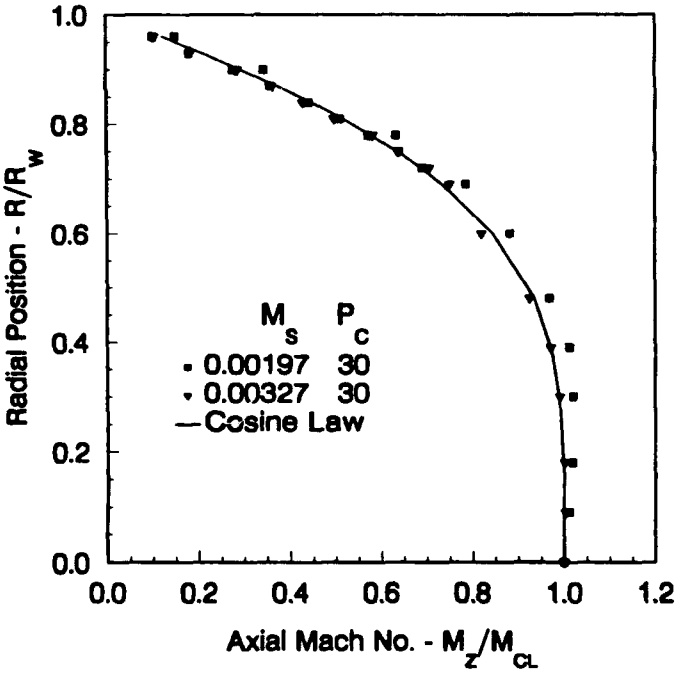

Figure 3-11. Axial Mean Velocity at L/D = 5.46

cosine profile. The data at all three axial stations were then shifted, the offset being r/r_w=0.02 at L/Ds of 1.8 and 4.22 and 0.015 at an L/D = 3.04. Figures 3-12, 3-13, and 3-14 show significantly improved agreement at L/Ds of 3.04 and 4.22, and somewhat better agreement at an L/D of 1.8. The scatter at this upstream location is obviously still apparent.

Several checks of the anemometer alignment procedure were made early in the test program and the traversing mechanism operated satisfactorily. After these tests were completed, a final check was made with the anemometer at an L/D of 4.22. An offset of 0.02 was noted

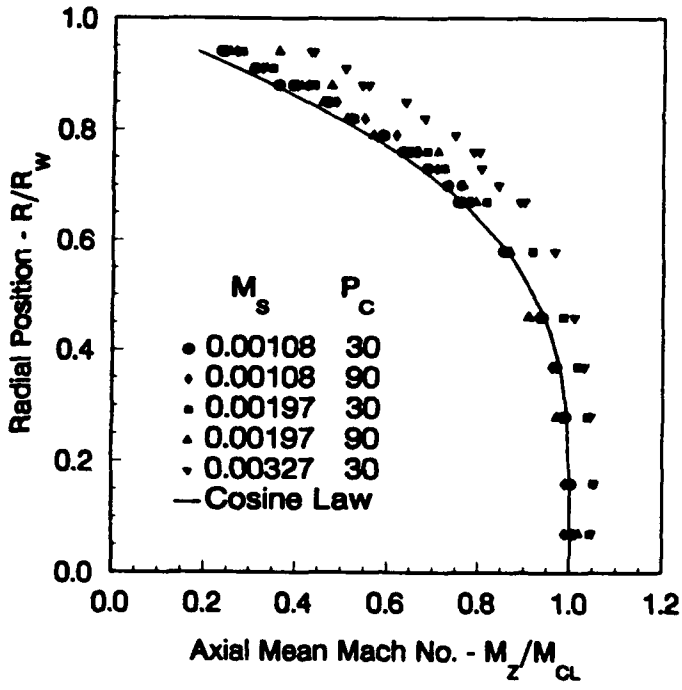

Figure 3-12. Adjusted Axial Mean Velocity at L/D = 1.80

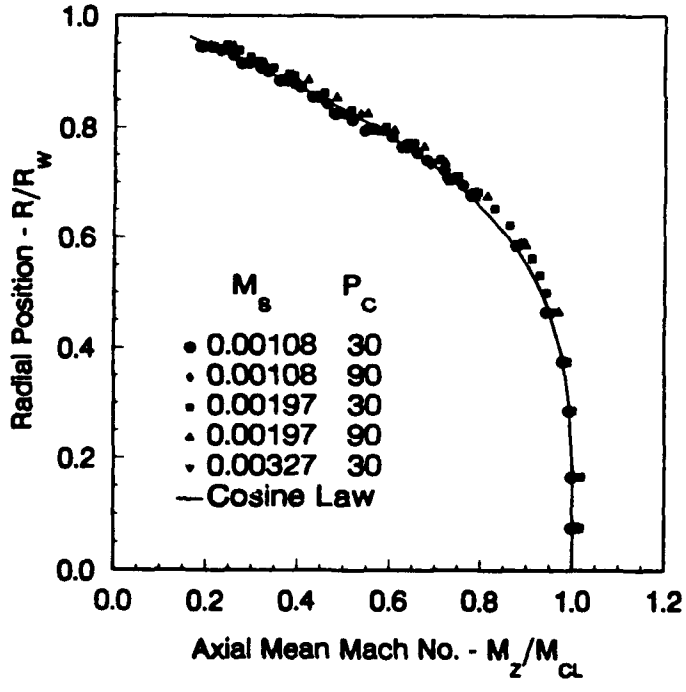

Figure 3-13. Adjusted Axial Mean Velocity at L/D = 3.04

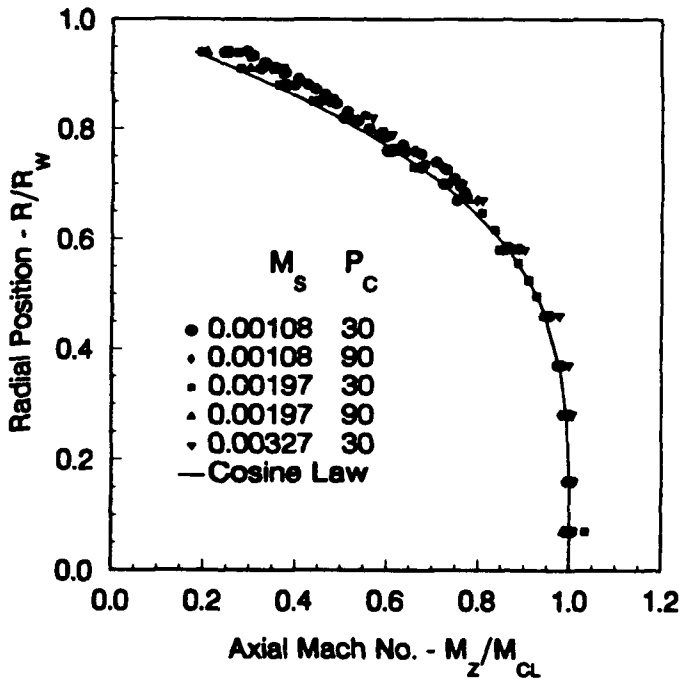

Figure 3-14. Adjusted Axial Mean Velocity at L/D = 4.22

which supports the shifting of the data in figures 3-12, 3-13, and 3-14. It should be noted, however, that shifting the data at L/Ds of 1.8 and 3.04 would be justified only by the improved agreement with the cosine profile. Therefore, in the subsequent presentation of the oscillatory data, these offsets in radial position were not included. These adjustments could, of course, be included by subsequent investigators since the uncorrected mean and oscillatory data are included in the appendices A and B.

3.4 OSCILLATORY BEHAVIOR AT L/D = 1.8

The oscillatory behavior at each set of test conditions was analyzed in two basic ways. First, the magnitude of the axial oscillatory component (normalized to the head-end oscillatory pressure) was plotted as a function of time during one cycle and radial position for each flow condition. Figure 3-15 illustrates the results of this calculation at an L/D of 1.8, 30 psi pressure and a surface Mach No. of 0.00108. Contours of constant axial oscillatory velocity were then derived at velocity intervals of 0.1 and plotted on the "floor" of the three dimensional plots, as shown in figure 3-15.

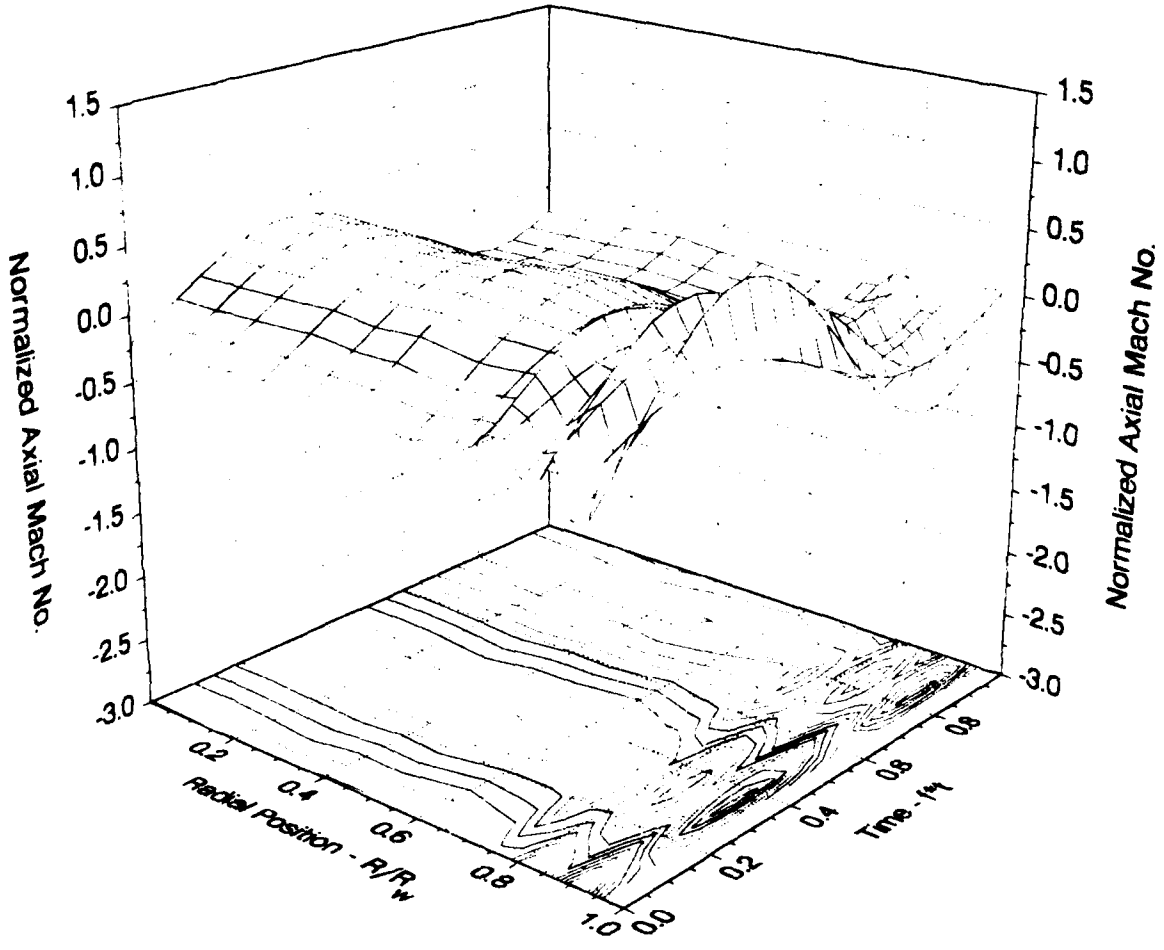

Figure 3-15. Axial Oscillatory Component at L/D = 1.8 (30 psia, M_s = 0.00108)

Note that between the centerline and a radius of 0.75, the axial velocity is essentially independent of the ratios. This behavior is consistent with the behavior expected from classical longitudinal waves. Between 0.75 and the wall, however, the magnitude of the velocity varies significantly and slight phase shifts can also be observed. This behavior, which occupies about 50% of the chamber volume, has been noted previously by Vuillot[15] and Brown.[19]

Next, the direction of the flow over one cycle of oscillation was derived from the amplitudes and phase angles of the radial and axial velocity components. Specifically, the flow angle, θ, is related to the radial and axial velocity components by

$$\tan \theta(t) = \frac{\tilde{v}(t)}{\tilde{u}(t)} \qquad (3\text{-}5)$$

Thus, the flow direction varies throughout the cycle. In this calculation, radial velocities where the coherence with the head-end oscillatory pressure is less than 0.282 were considered to be zero. The flow angle was defined from the basic coordinate signs of the velocity components, i.e., a positive axial velocity flows downstream and a positive radial velocity flows into the wall. The resulting angles were then plotted as a function of time in radial cylindrical coordinates, time being the radius and the angle being the flow direction. Figure 3-16 shows a plot for the flow conditions shown in figure 3-15.

Near the centerline, the flow angle follows the horizontal axis, indicating the flow is either in the upstream or downstream direction. This behavior is characteristic of classical potential longitudinal acoustic waves where the flow changes direction when the magnitude is zero and there is no radial component. At radii between 0.39 and 0.75, the flow rotation is clockwise, while from 0.78 to 0.81, the rotation is counterclockwise. The direction change then reverses again as the wall is approached. This behavior indicates the flow is rotational, as opposed to the classical irrotational models which have been assumed for these flows.

To simplify the interpretation of these complex flow rotation behaviors, composite plots of flow contours and flow directions were constructed for each flow condition. Only the direction of the flow rotation has been shown to simplify the figure and to show the relationship between the magnitude and direction. Figure 3-17 is an example of such a plot for the flow conditions illustrated above. Note that the direction of the flow rotation changes at radial positions where the magnitude is a minimum.

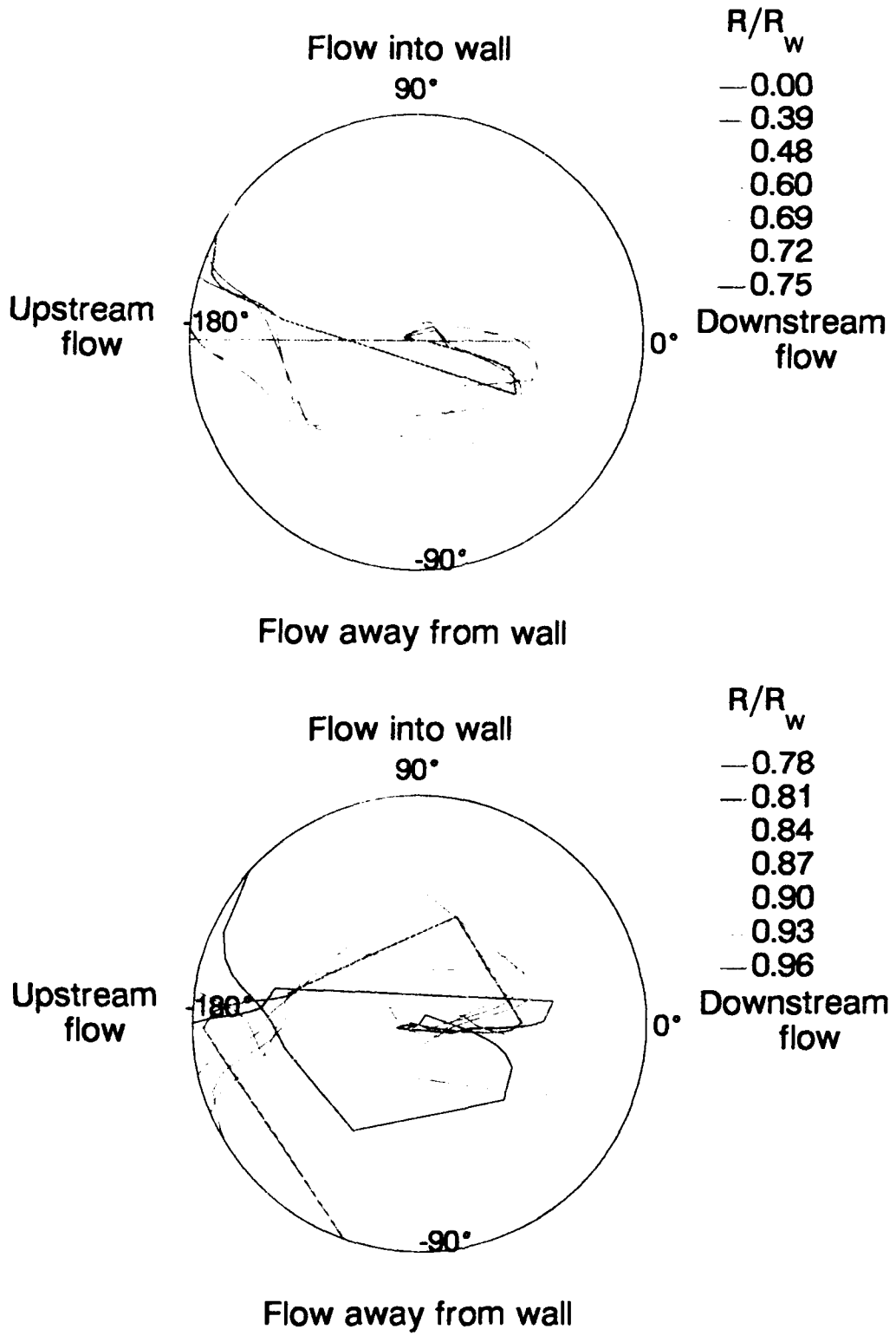

Figure 3-16. Flow Direction During One Cycle (L/D = 1.8, 30 psia, M_s = 0.00108)

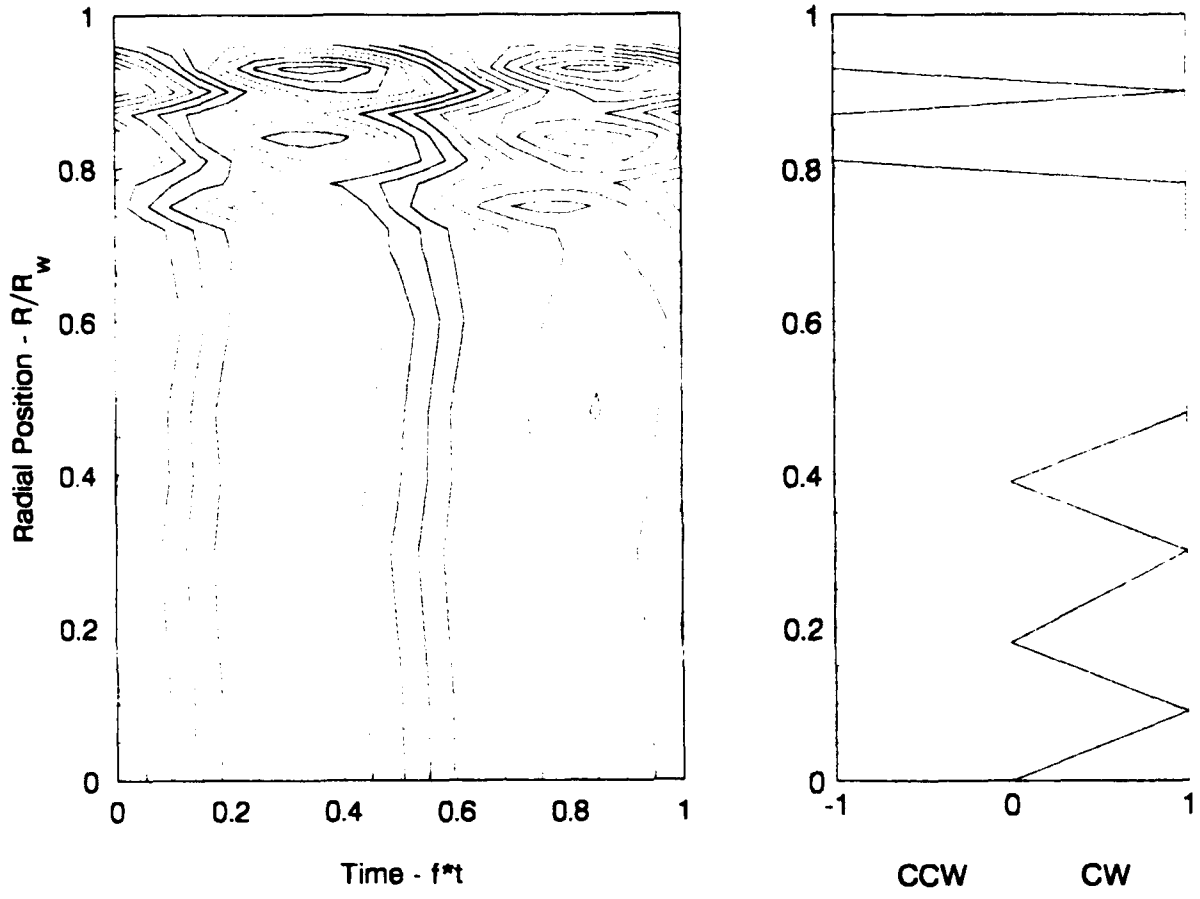

Figure 3-17. Contour and Flow Direction (L/D = 1.8, 30 psia, M_s = 0.00108)

Figures 3-18, 3-19, 3-20 and 3-21 show combinations of figures 3-15 and 3-17 for the other flow conditions at this axial station. Several observations can be made from these data. First, the amplitude of the centerline oscillations for all these flow conditions agrees reasonably well with the levels expected from classical acoustic theory for standing waves at resonance. This apparatus has an overall length of 17 diameters; thus at L/D = 1.8, one would expect the normalized centerline velocity to be 0.33. The measurements at 30 psia (figures 3-15, 3-17 and 3-21) show good agreement with this estimate. The agreement with the results at 90 psia (figures 3-18 and 3-20) is not as good, however, as the measurements are slightly higher than their expected levels estimates. As noted previously, the response function of the porous wall also decreases with increasing mean pressure. Since these tests were run close to the longitudinal mode frequency, the pressure effect may reflect secondary damping and off-resonance contributions.

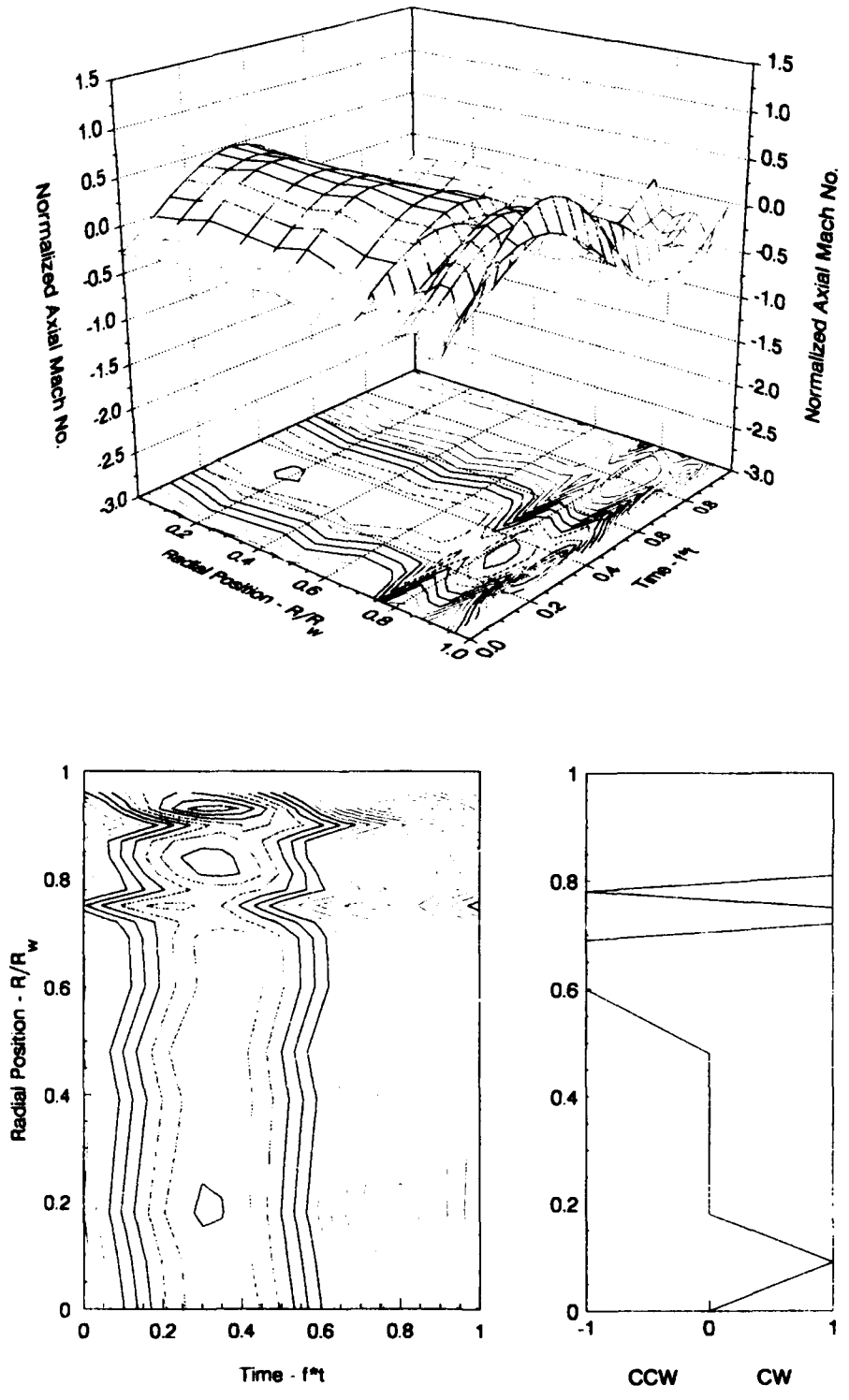

Figure 3-18. Axial Oscillatory Velocity at L/D = 1.8 (90 psia, M_s = 0.00108)

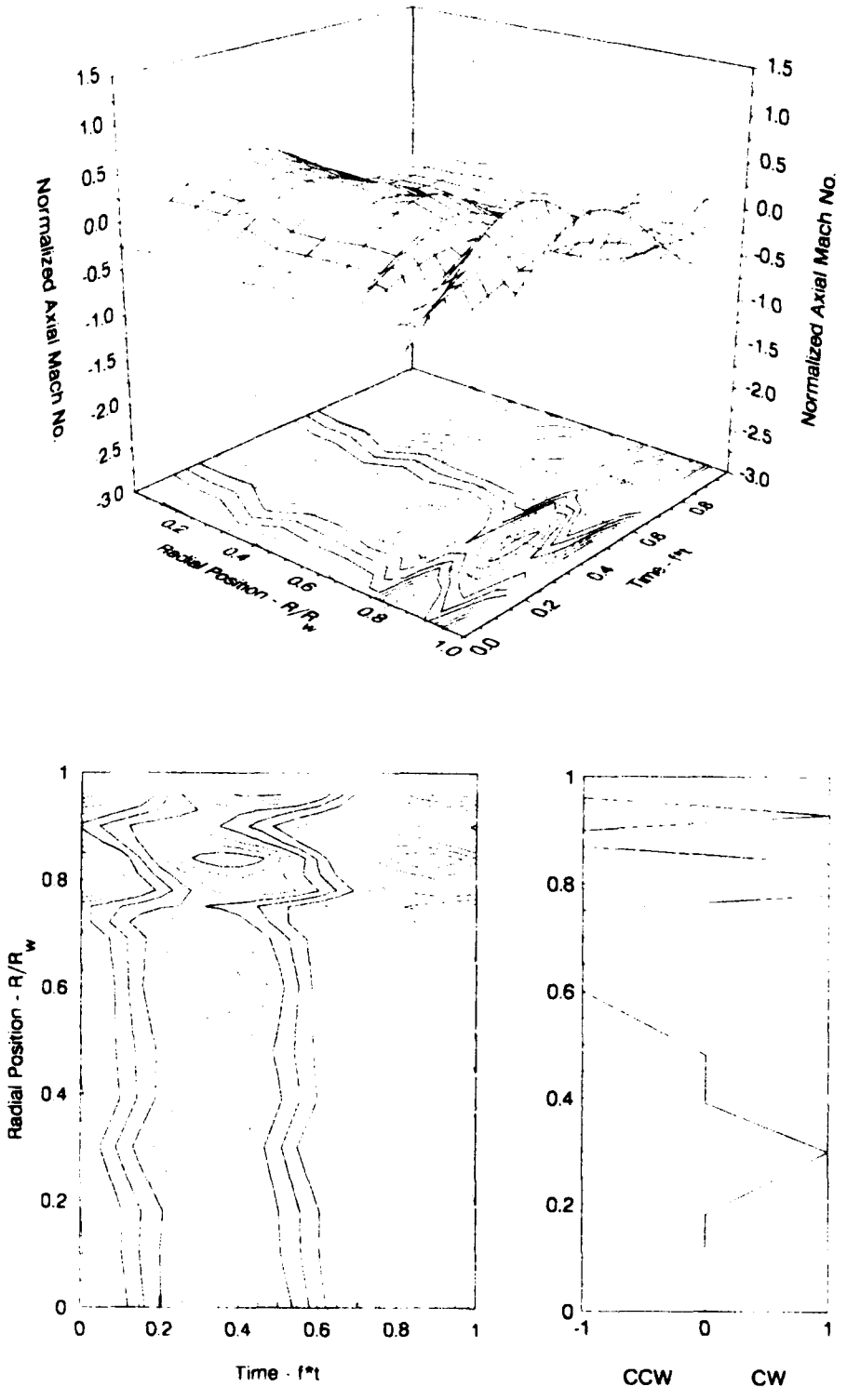

Figure 3-19. Axial Oscillatory Velocity at L/D = 1.8 (30 psia, M_s = 0.00197)

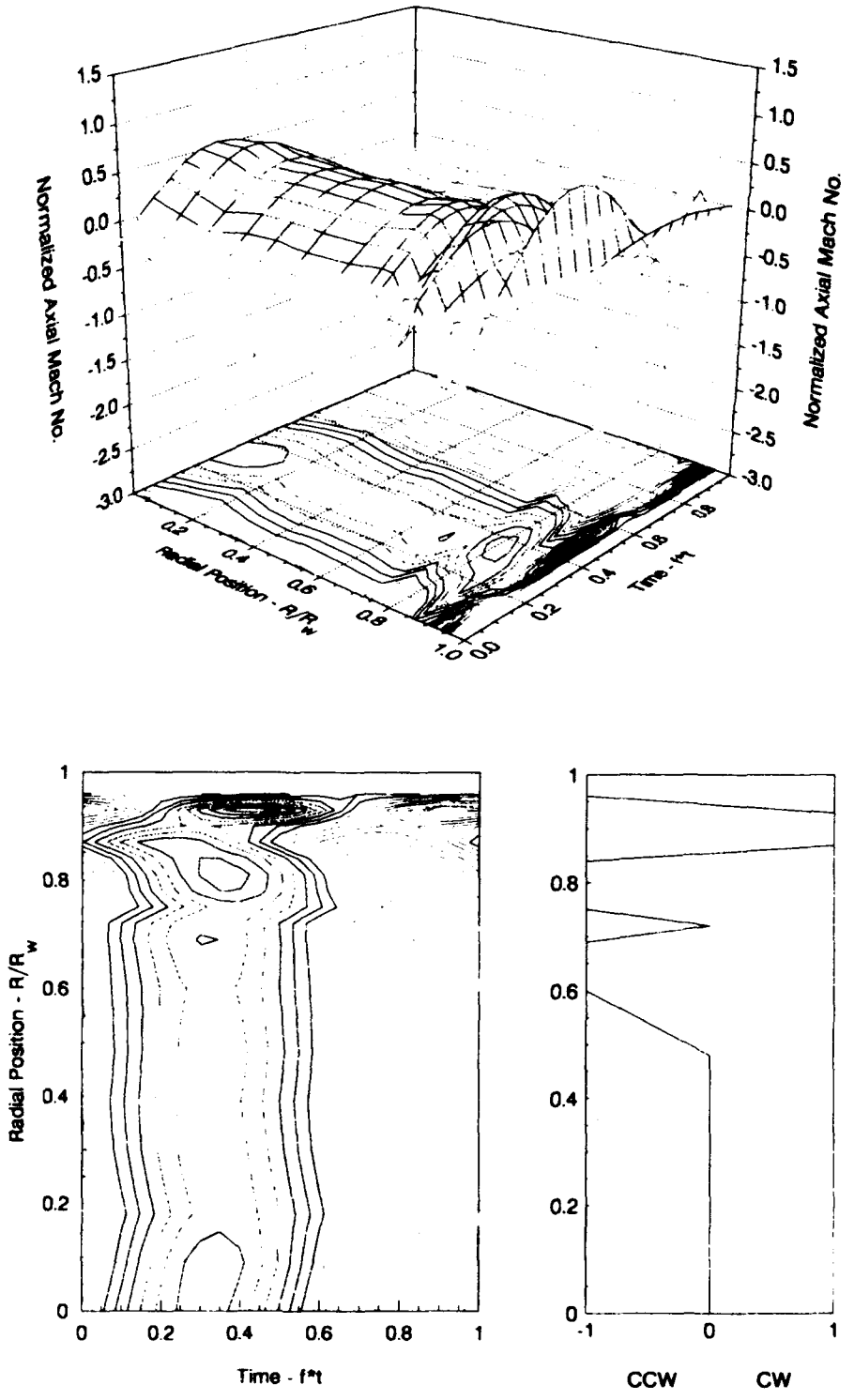

Figure 3-20. Axial Oscillatory Velocity at L/D = 1.8 (90 psia, M_s = 0.00197)

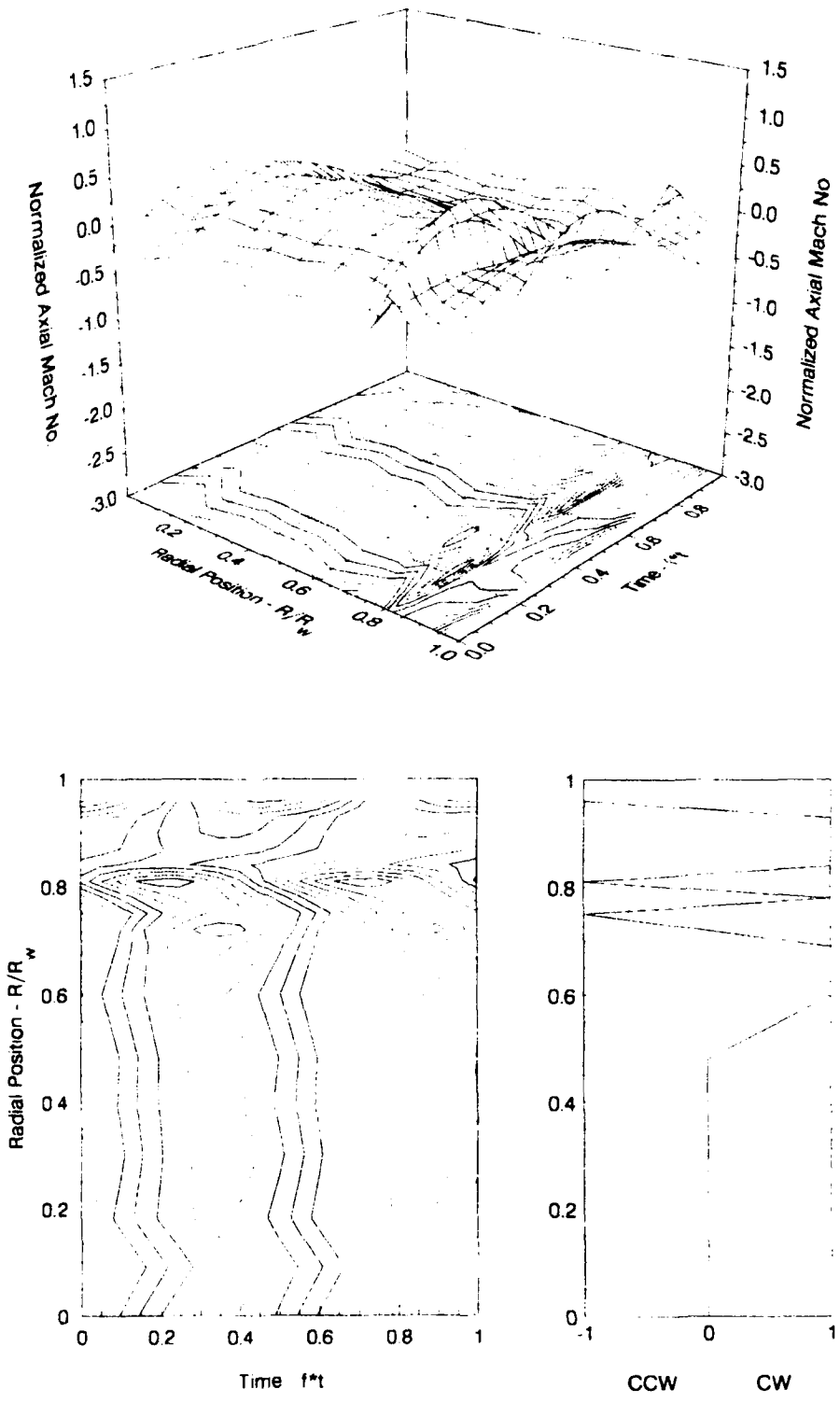

Figure 3-21. Axial Oscillatory Velocity at L/D = 1.8 (30 psia, M_s = 0.00327)

Second, it is apparent that significant deviations from the classical wave motions are observed near the wall in the oscillatory velocity at all the flow conditions. It is also apparent that the surface Mach number has a strong influence on these deviations, particularly on the distance between peak amplitudes. An approximate solution of the radial momentum equation, neglecting radial pressure gradients,[13] suggests that the amplitude of the radial oscillations varies with radial position according to the equation

$$R(r) = \exp\left[\left(\frac{2ifr_w}{a}\right)\times\left(\ln\left[\tan\left\{\frac{\pi}{4}\times\left(\frac{r}{r_w}\right)^2\right\}\right]\right)\right] \qquad (3\text{-}6)$$

Roots of equation 3-6 when R(r) = 2nπ for the various surface Mach numbers are tabulated below:

Roots of Radial Momentum Equation

M_s	n1	n2	n3
0.00108	0.923	0.843	0.764
0.00197	0.857	0.714	0.585
0.00327	0.762	0.547	0.386

Note the radial positions of the peaks in figures 3-18 through 3-21 show reasonable agreement with the predictions in this table.

This agreement suggests that radial momentum effects are important in defining the wave behavior in situations where there is substantial gas evolution from the side walls. The multi-dimensional models include the irrotational contributions of radial momentum across the entire chamber cross section. The one-dimensional model, on the other hand, considers radial momentum effects to be important only in the infinitely small region at the wall. Obviously neither model satisfactorily includes the rotational radial momentum behavior observed in these data. Comparison of the data with analysis is being conducted in a separate effort by by Professor G. A. Flandro.

Comparing figures 3-17 and 3-19 with figure 3-18 and figure 3-19 with 3-20 shows that the mean pressure has a small effect on these radial variations. The principal effect of mean pressure could result from its effect on the kinematic viscosity or the surface response. These results suggest that viscous forces have only a small influence on the wave motions in the chamber. Viscosity does, however, play an important role very near (of the order of several mean free paths for molecular collision) the blowing surface. It is this region of near wall,

viscous forces that cause the gas flow leaving the surface to be normal to the surface. Beyond this important contribution, however, viscous forces appear to have only a secondary influence. Thus, the pressure and inertial forces are paramount in defining the oscillatory flow behavior.

The relationship between the peak magnitudes in the axial velocity and the rotational direction, as noted in figure 3-17, can also be found in these data as well. The direction of the rotation depends on the sign of the sine of the difference phase angles of the two velocity components referenced to the head-end oscillatory pressure. Thus, small errors in these phase angles can have a significant effect on the predicted flow direction. Furthermore, the uncertainty in each phase angle can be estimated from equation 3-4. For example, the phase angle measurement has an uncertainty of ± 30 deg when the coherence is 0.6, which is typical in the core region of the flow. When the coherence is 0.975, the uncertainty in each phase angle reduces to ± 6 deg. Thus, the derived flow directions are reasonably valid near the wall and are highly suspect in the core region.

The time at which the oscillatory velocities peak near the wall (i.e., the phase angle with respect to the head-end oscillatory pressure) is consistent with the predicted phase angles for the wall response functions. The peaks at the mean pressure of 30 psia occur at a cycle time (f*t) of approximately 0.4 to 0.45, which translates two phase lags of 144 to 160 deg. The corresponding phase lag of the response is 150 deg. At the higher mean pressure of 90 psia, the velocity data show a phase lag of 110 to 140 deg, while the response has a predicted phase lag of 122 deg. Thus, in both conditions, reasonable agreement is observed.

Finally, the amplitudes of the radial velocity at $r/r_w = 0.96$ were compared to the amplitudes expected from the response functions tabulated in the table on page 3-8, i.e., $\gamma M_s R$. These comparisons are shown in the table below.

Surface Mach No.	Pressure	Expected Radial Velocity	Observed Radial Velocity
0.00108	30	0.0212	0.044
0.00197	30	0.0206	0.113
0.00327	30	0.0200	0.037
0.00108	90	0.0395	0.128
0.00197	90	0.0394	0.106

It is apparent that significant differences exist between the expected and observed values. Recalling that the observed values were measured at $r/r_w = 0.96$, the most likely explanation

for this divergence is that measurements closer to the wall are required to recover the expected levels. Making such measurements, however, entailed substantial risk that the probe would contact the wall and destroy the anemometer. Substantial cost and manpower expenditures would be required to replace the probe, so the risk for increased accuracy was judged to be unacceptable.

3.5 OSCILLATORY BEHAVIOR AT L/D = 3.04

The oscillatory velocity behavior at an L/D = 3.04 are shown in figures 3-22 through 3-26. The axial velocity components continue to follow the classical acoustic wave behavior from the centerline out to an r/r_w of approximately 0.7. Significantly larger amplitudes are then observed in the near wall region and again they continue to occupy about 50% of the chamber volume. At the mean pressure of 30 psia, the centerline amplitudes agree reasonably well with the amplitudes of the classical acoustic waves at this axial station (approximately 0.6 to 0.7 vs 0.53). Again as noted at L/D = 1.8, the velocity amplitudes increase with slightly increasing mean pressure. Since both viscous effects and the surface responses change with pressure, the mechanistic cause of this behavior is not easily defined.

These results also show some pronounced differences from the results obtained at the 1.8 L/D. First, the radial distribution of axial magnitudes and the flow direction are not as well defined as at the upstream location. This is particularly true for the two lower surface Mach numbers. At a M_s of 0.00327, however, the radial distribution of the axial magnitude is still relatively well defined. Undoubtedly these changes result from the effect of the increased axial mean velocity on the rotational flow structures. (Recall that in the inviscid rotational flow, the mean radial velocity does not vary with axial position, while the axial velocities increase linearly with axial position.) This result, therefore, supports the conclusion from all the analytical studies that mean flow effects have an important effect on the wave motion, and hence their stability. These data are the first solid direct experimental evidence which substantiates this weakness in these analyses. The fact that the organization of the wave flow is preserved at the highest surface Mach number also suggests that convection of radial momentum is an important factor to be considered in the analysis of these flows.

Another significant difference in the wave motion, compared to that upstream, is the shifting phase angles with radial position. These shifts, which are observed at all the flow conditions, are more pronounced at the lower mean pressure. Since the phase angle of the oscillatory velocity (with respect to the oscillatory pressure) can have a critical impact on the stability of the wave motion, this behavior is particularly significant in determining the particle damping and flow turning contributions. This smearing effect of the mean axial flow also makes phase comparisons with the wall response impossible.

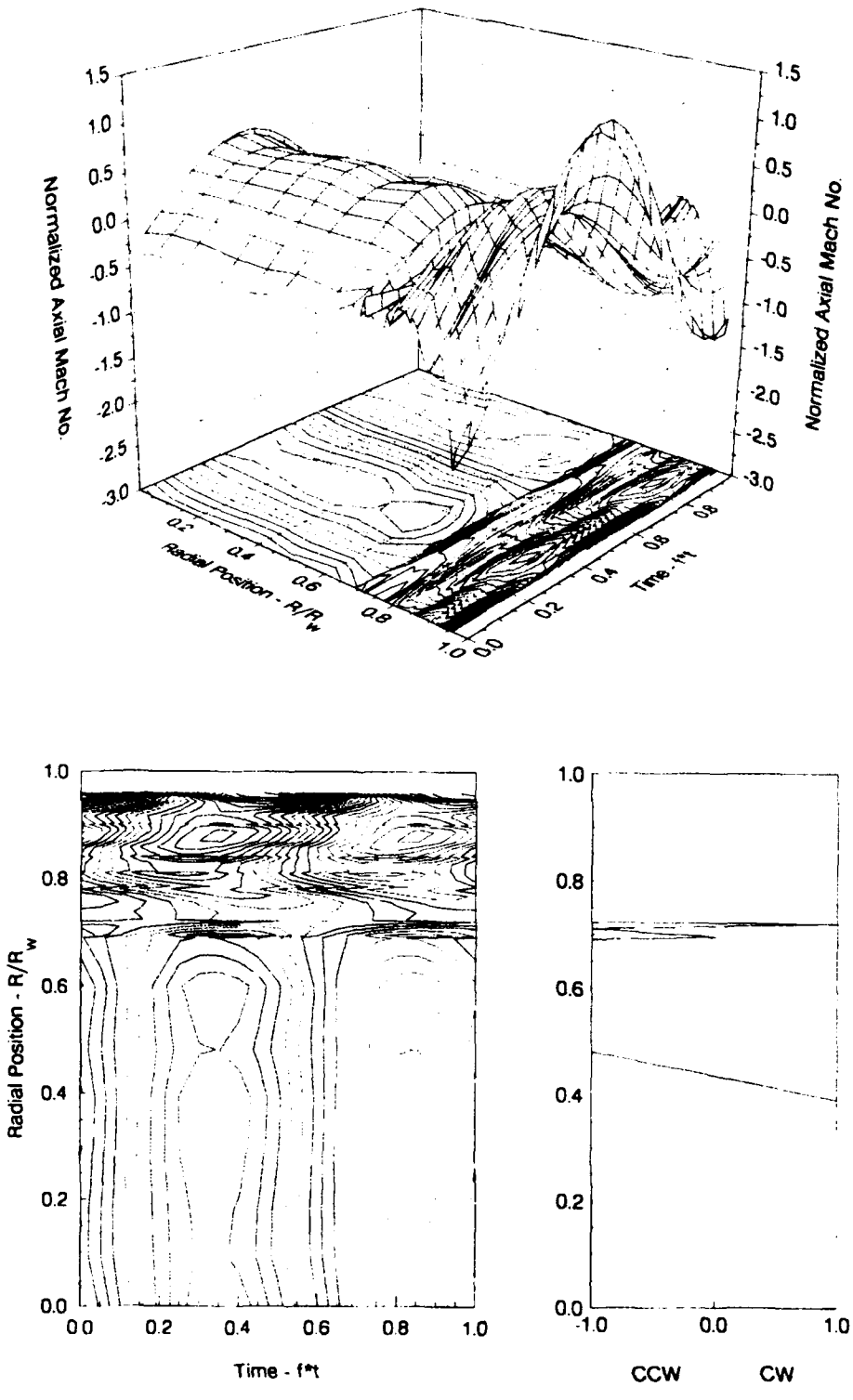

Figure 3-22. Axial Oscillatory Velocity at L/D = 3.04 (30 psia, M_s = 0.00108)

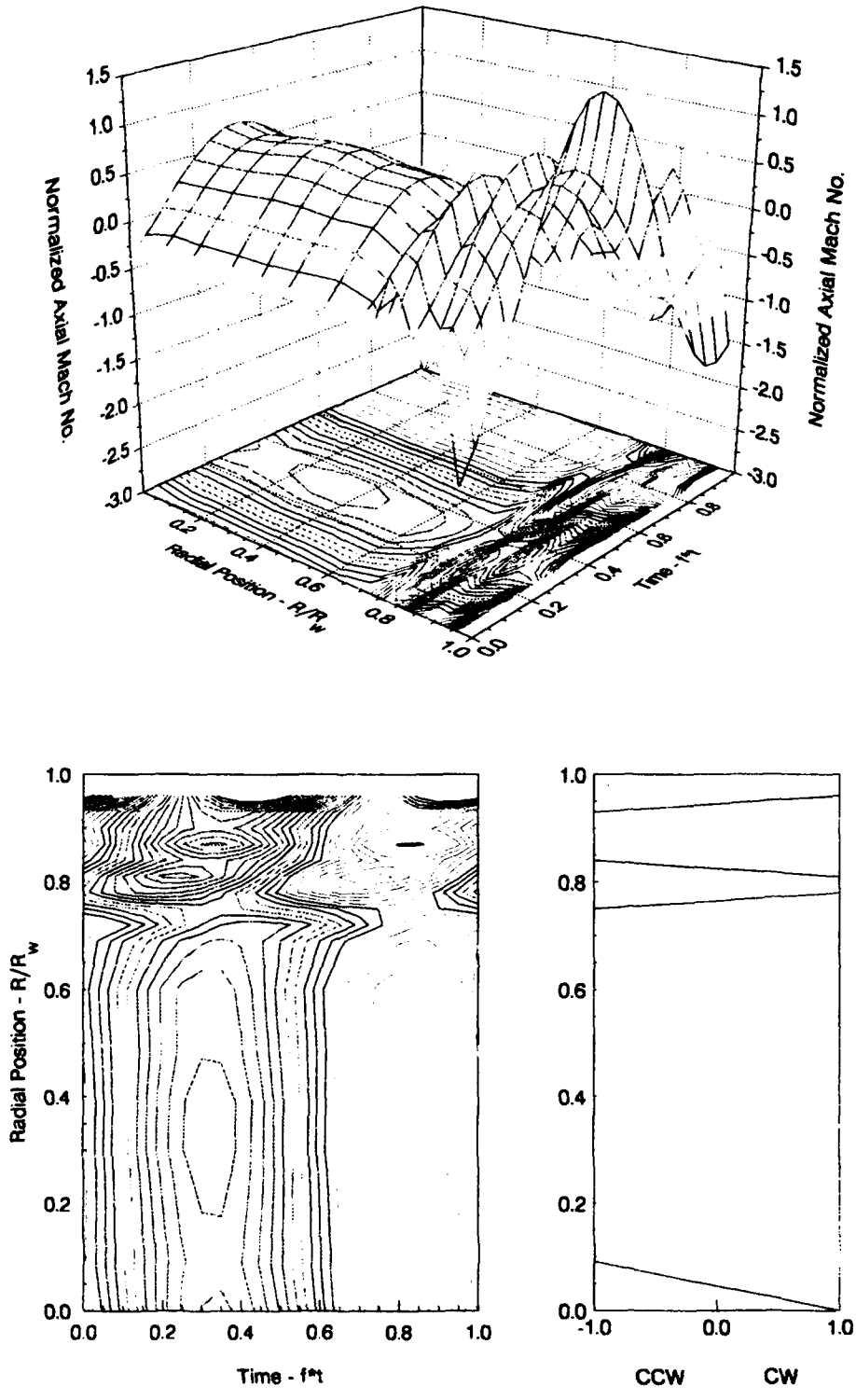

Figure 3-23. Axial Oscillatory Velocity at L/D = 3.04 (90 psia, M_s = 0.00108)

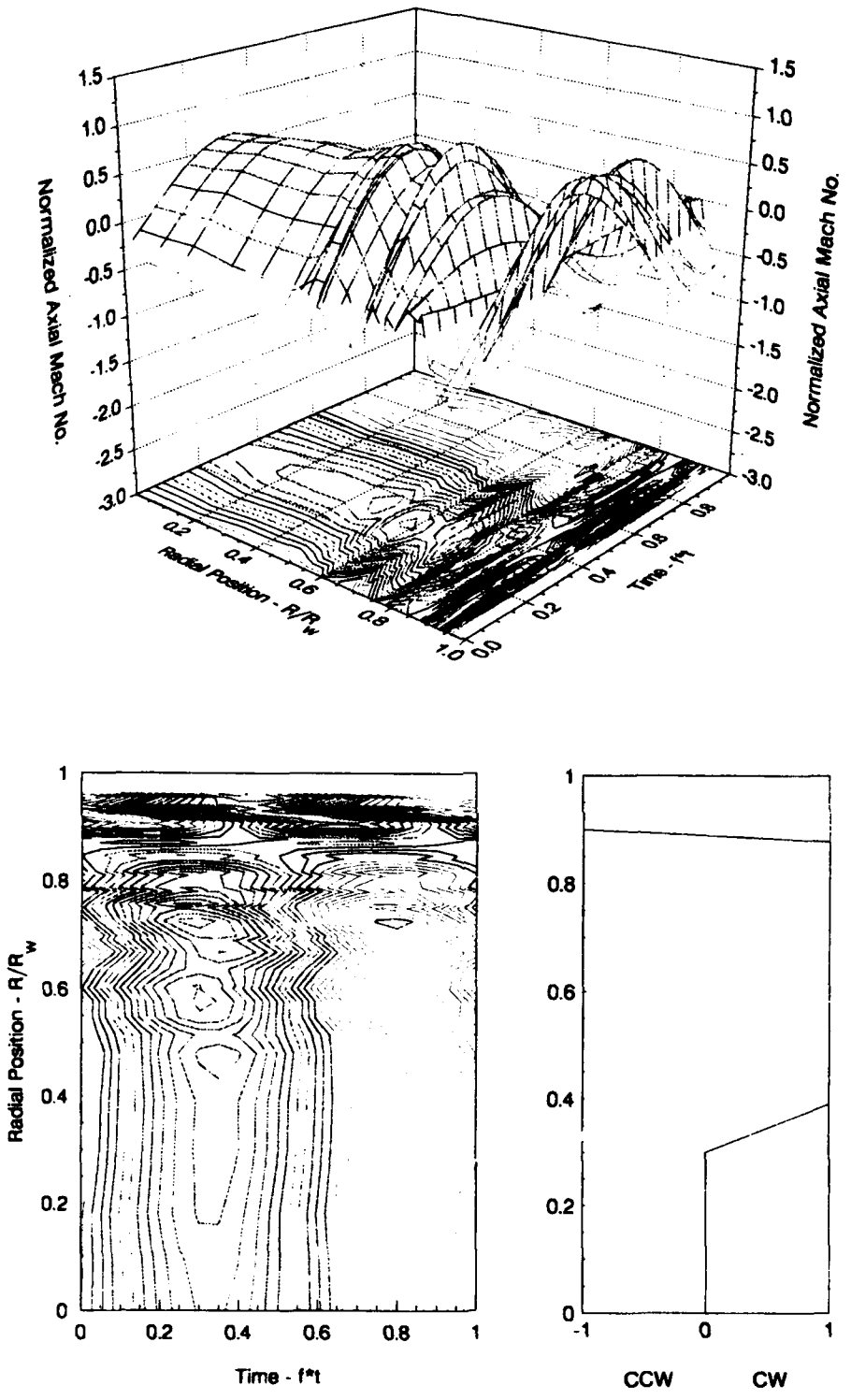

Figure 3-24. Axial Oscillatory Velocity at L/D = 3.04 (30 psia, M_s = 0.00197)

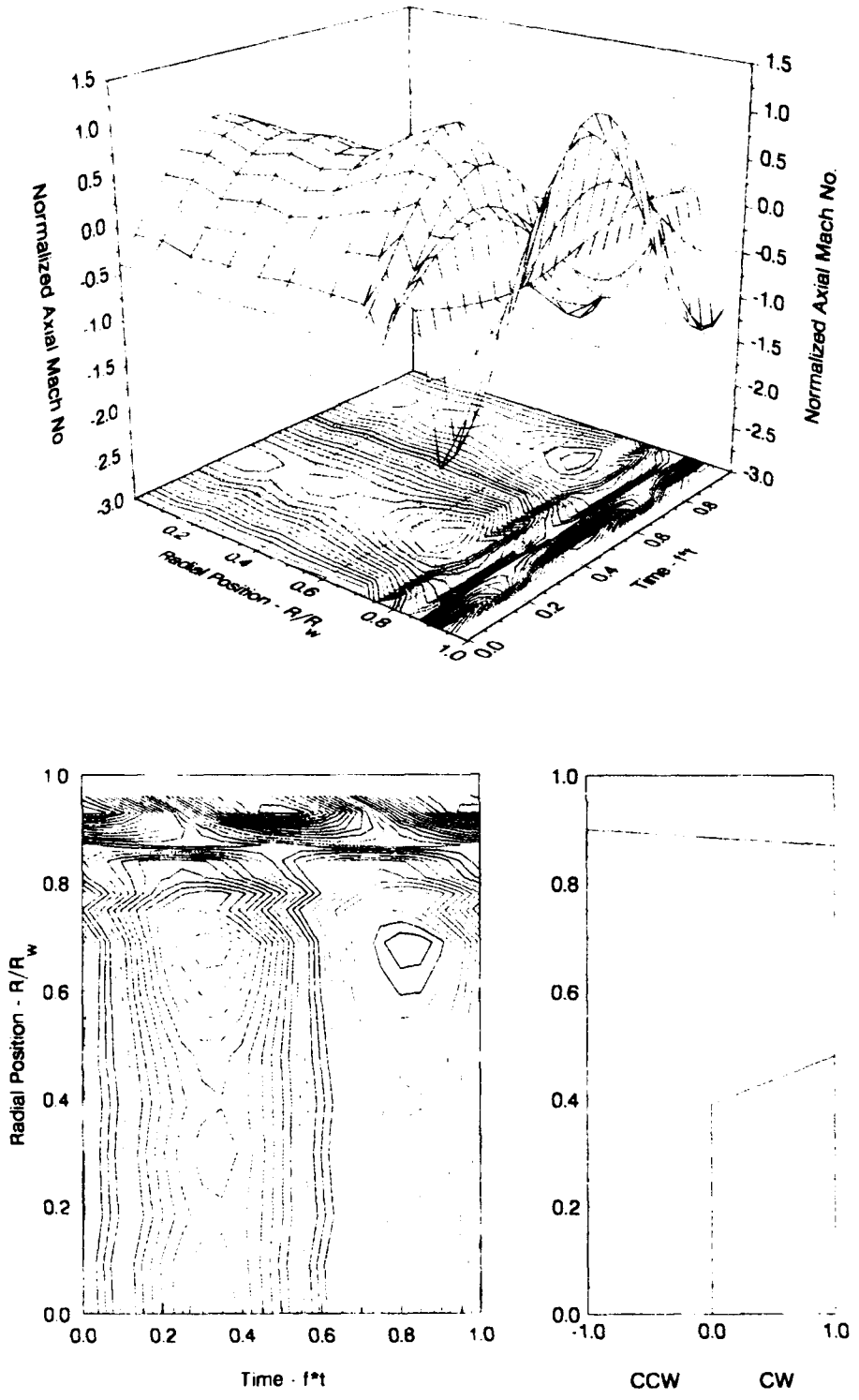

Figure 3-25. Axial Oscillatory Velocity at L/D = 3.04 (90 psia, M_s = 0.00197)

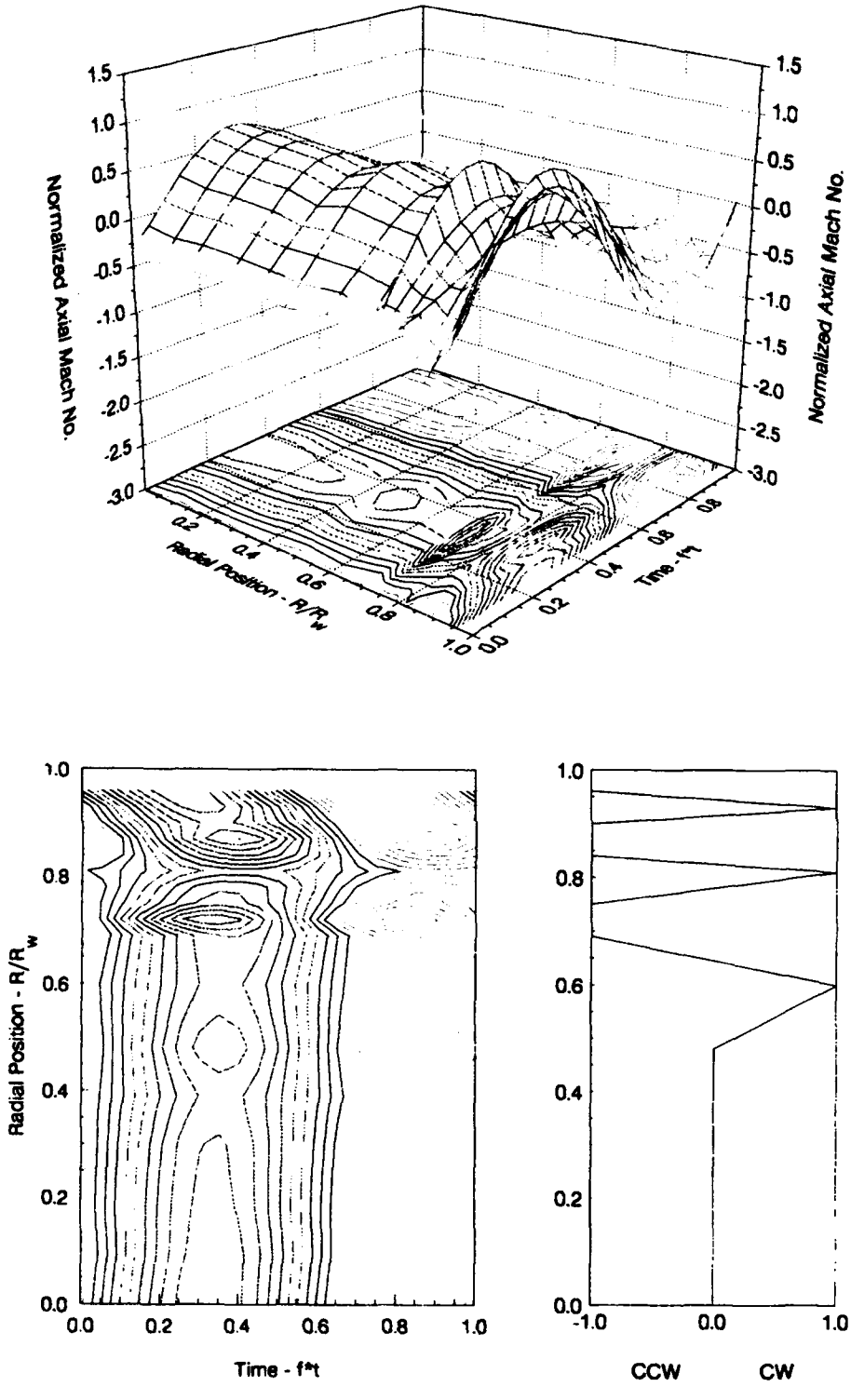

Figure 3-26. Axial Oscillatory Velocity at L/D = 3.04 (30 psia, M_s = 0.00327)

3.6 OSCILLATORY BEHAVIOR AT L/D = 4.22 AND 5.46

The data obtained further downstream at an L/D of 4.22 are shown in figures 3-27 through 3-31. Figures 3-32 and 3-33 show the data obtained at the L/D of 5.46. Many of the same comments and observations noted above for the L/D of 3.04 are also appropriate for this station as well. Particularly evident is the increase in phase shifting with radial position, compared to the behavior at L/D of 3.04.

There is one major difference of particular note in the behavior at a M_s of 0.00197, as shown in figures 3-29, 3-30 and 3-32. Here, the magnitudes of the wave motion in the core are substantially larger (peak amplitudes of 1.8 to 2 at the L/D of 4.22 and 2.5 to 3 at the L/D of 5.46) than the corresponding levels at the other two surface Mach numbers (where peak amplitudes are 0.8 to 1 and are consistent with classical acoustic motions). Furthermore, these surprisingly high magnitudes extend from the centerline to a radius of approximately 0.6. They then basically decrease as the wall is approached. In all the other results, the largest magnitudes all occur close to the wall and not near the centerline. As noted previously, the cause of this behavior is not obvious since the previous measurements close to these conditions did not show this behavior. Unfortunately, project resources did not permit further investigation of this issue.

Comparing figures 3-21, 3-26, 3-31, and 3-32 shows how these flow structures change with axial position. At the highest surface Mach No., which is typical of many solid propellants, the radial momentum sustains the oscillatory flow structures at all four axial stations. It appears, however, that the surface response still determines the near wall phase behavior of the axial velocities. The axial stretching of the oscillatory flow structures, or zones, is also apparent. As these stretched structures move out into the core flow, they adjust to the centerline oscillatory motion. Thus, these regions are complex, involve both axial and radial momentum, and require a detailed theoretical analysis to interpret.

3.7 NONLINEAR BEHAVIOR

During these tests, significant distortions in the wave oscillatory behavior were observed near the wall. Therefore, the data reduction routine was modified to derive the bispectral coherence of each anemometer film voltage oscillation and the head-end oscillatory pressure. Cross bispectral coherences were not considered since the number of combinations to consider would have been rather large and the resulting data reduction routine extremely slow. Figures 3-34, 3-35 and 3-36 shows the resulting bispectral behavior of the film No. 1 voltage at L/D of 3.04, 4.22 and 5.46, respectively, at the driving frequency and twice the driving frequency. At the two upstream locations, the results are shown for the three surface Mach numbers while the last figure shows data for only the two surface Mach numbers investigated.

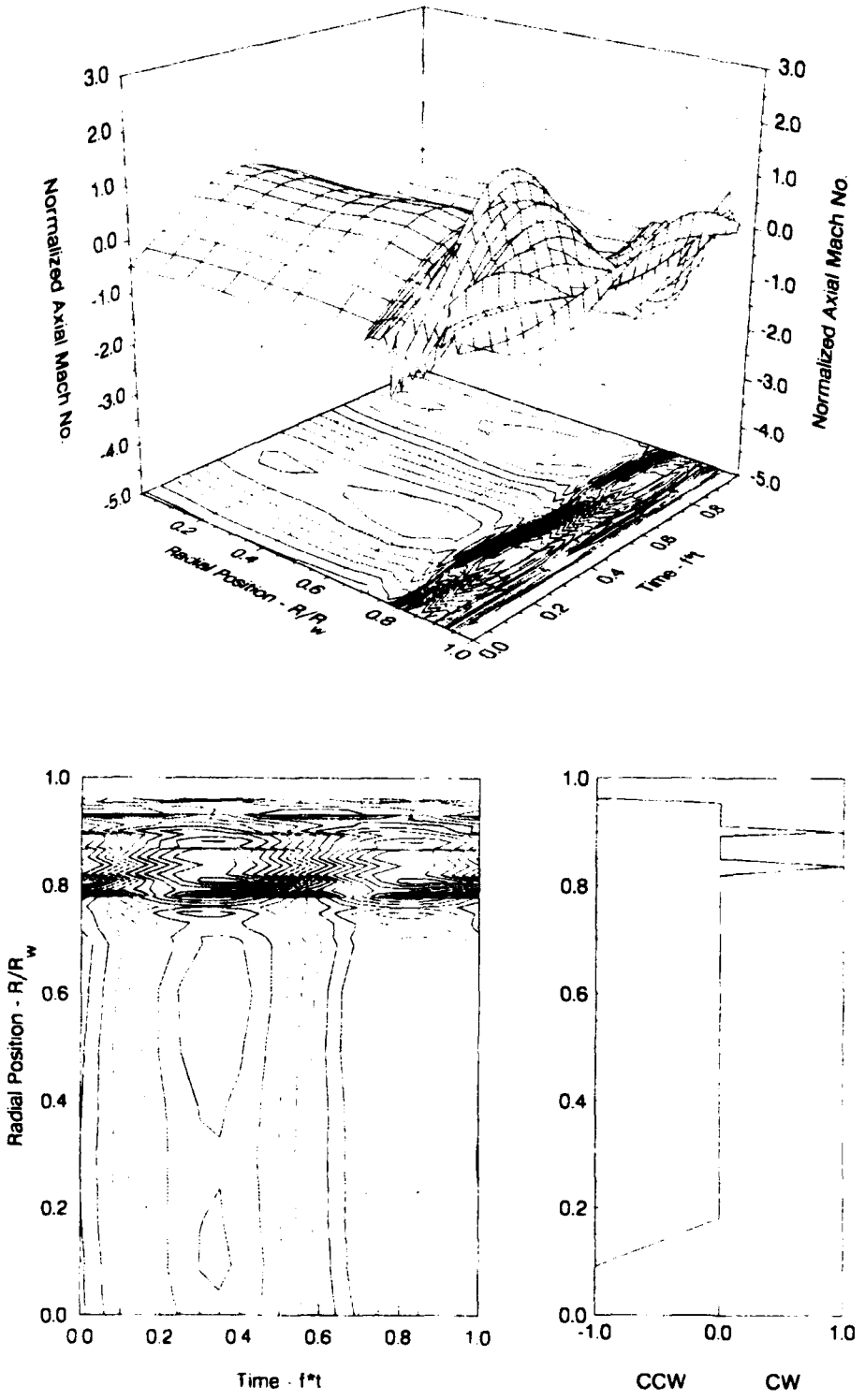

Figure 3-27. Axial Oscillatory Velocity at L/D = 4.22 (30 psia, M_s = 0.00108)

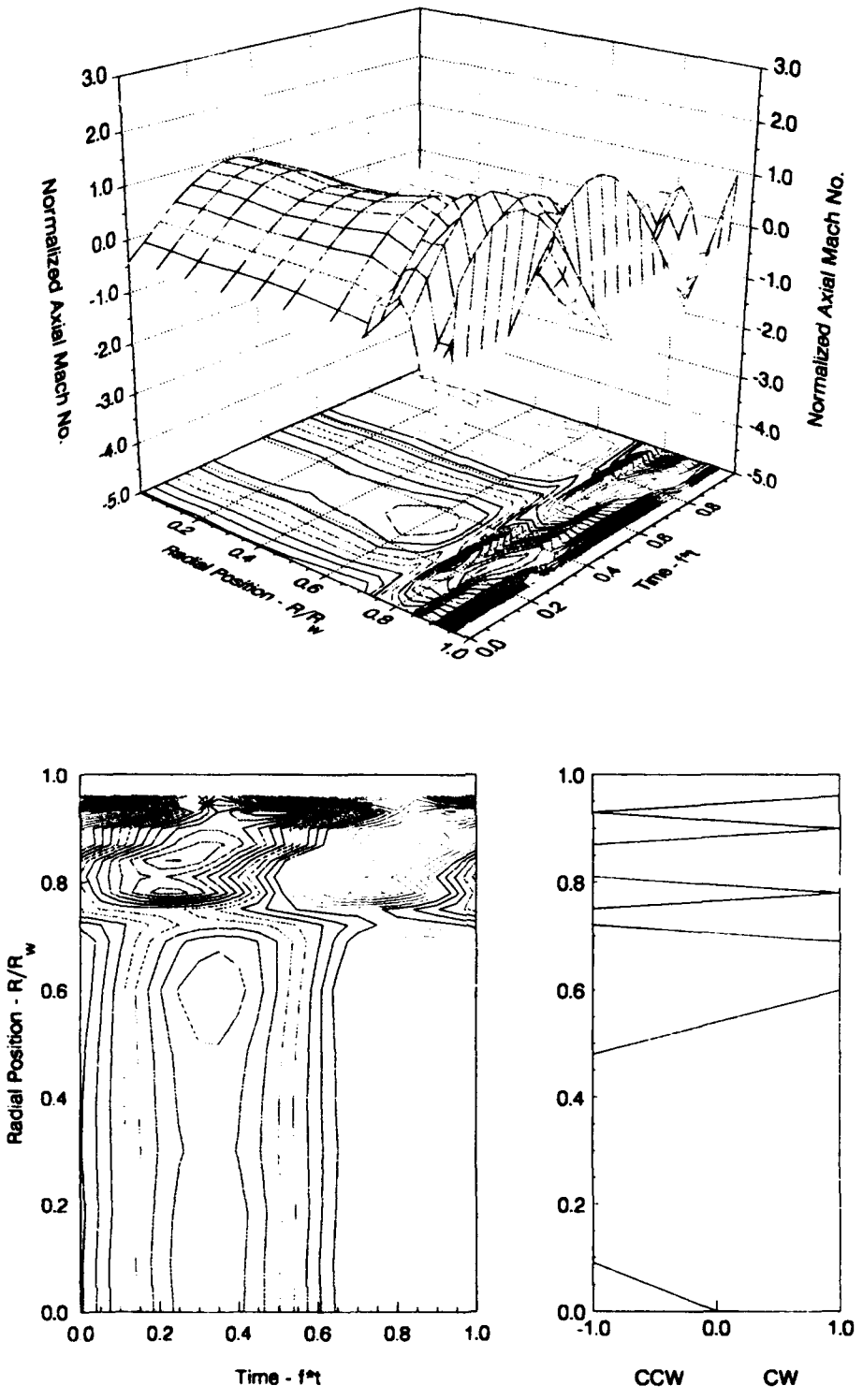

Figure 3-28. Axial Oscillatory Velocity at L/D = 4.22 (90 psia, M_s = 0.00108)

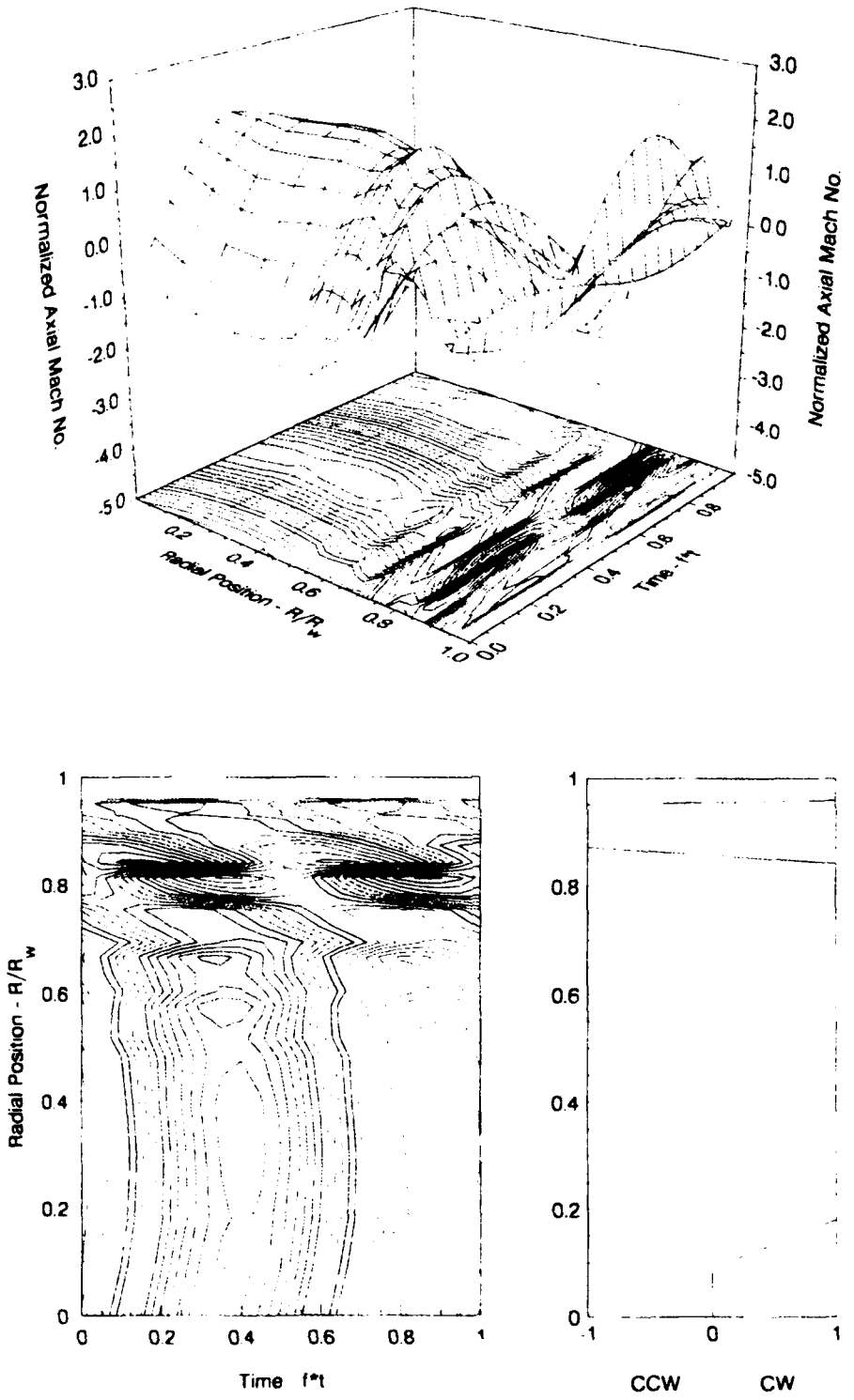

Figure 3-29. Axial Oscillatory Velocity at L/D = 4.22 (30 psia, M_s = 0.00197)

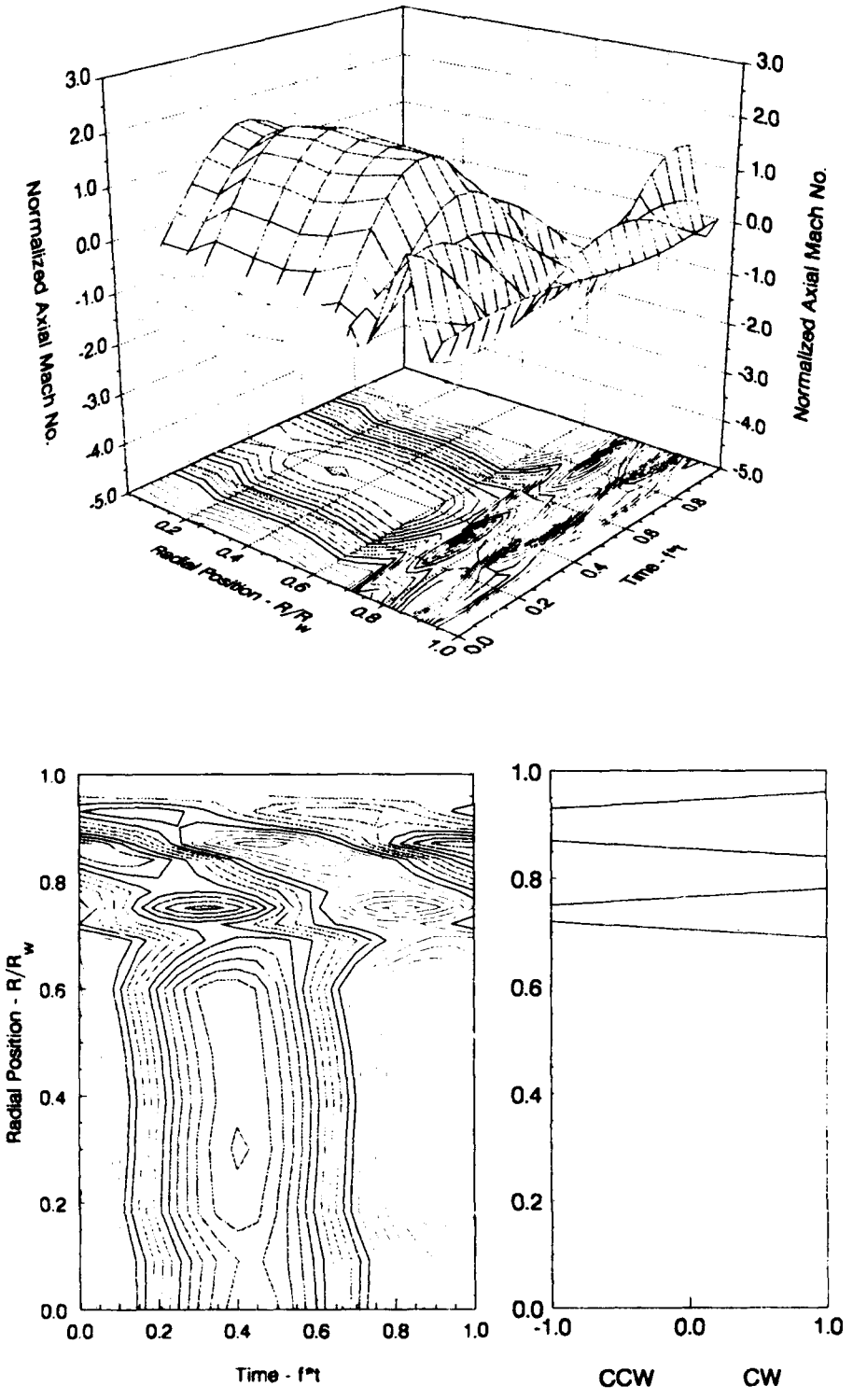

Figure 3-30. Axial Oscillatory Velocity at L/D = 4.22 (90 psia, M_s = 0.00197)

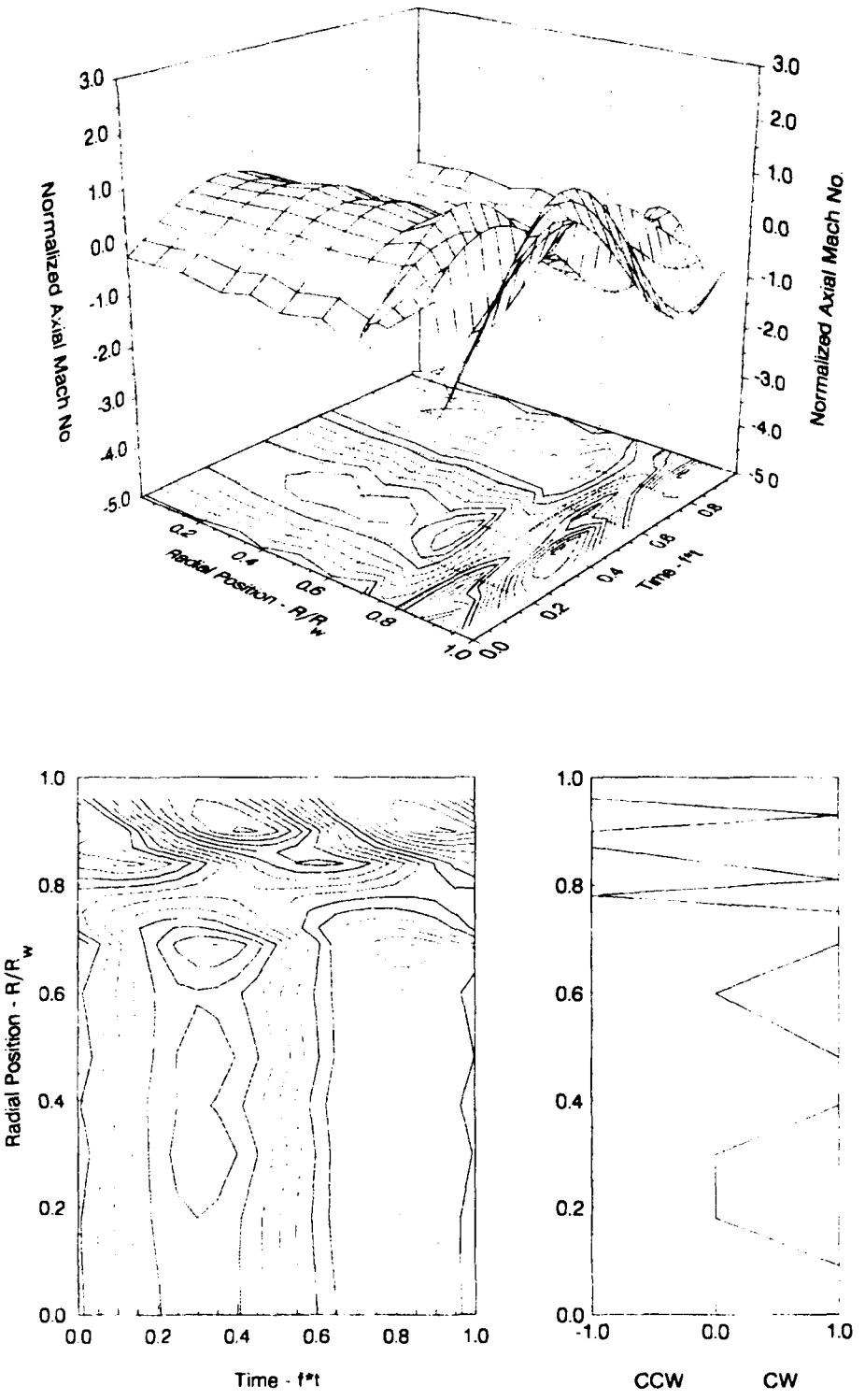

Figure 3-31. Axial Oscillatory Velocity at L/D = 4.22 (30 psia, M_s = 0.00327)

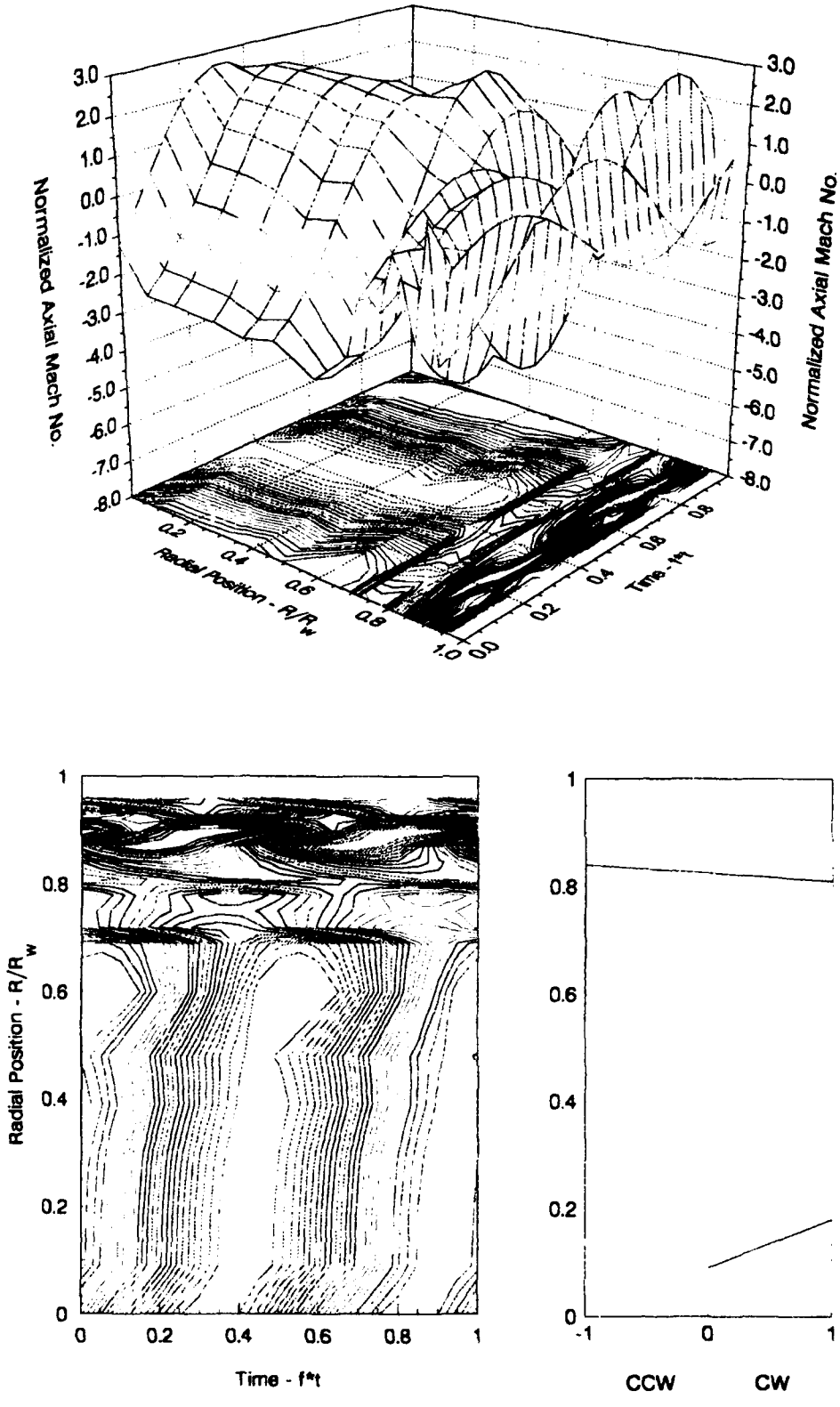

Figure 3-32. Axial Oscillatory Velocity at L/D = 5.46 (30 psia, M_s = 0.00197)

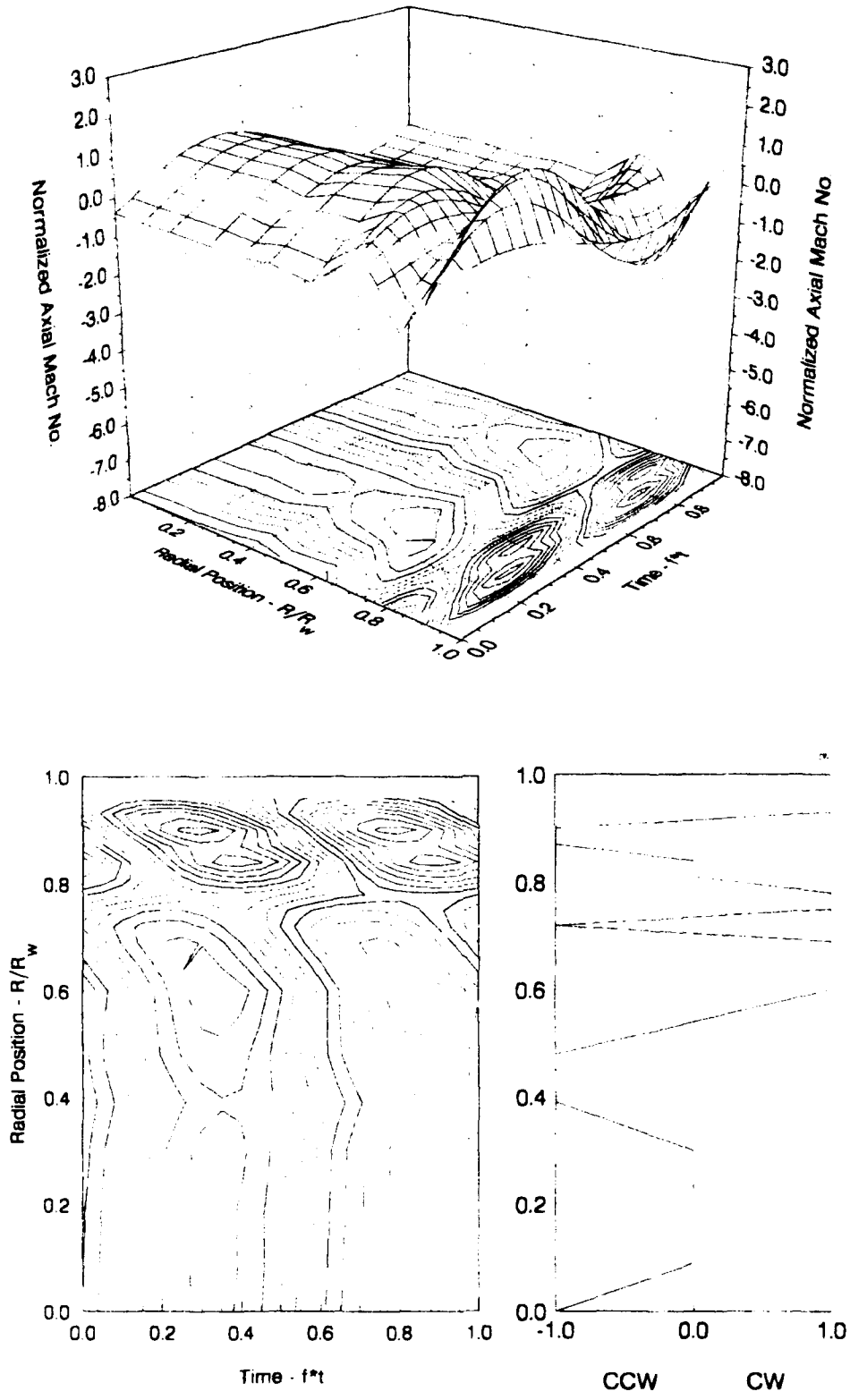

Figure 3-33. Axial Oscillatory Velocity at L/D = 5.46 (30 psia, M_s = 0.00327)

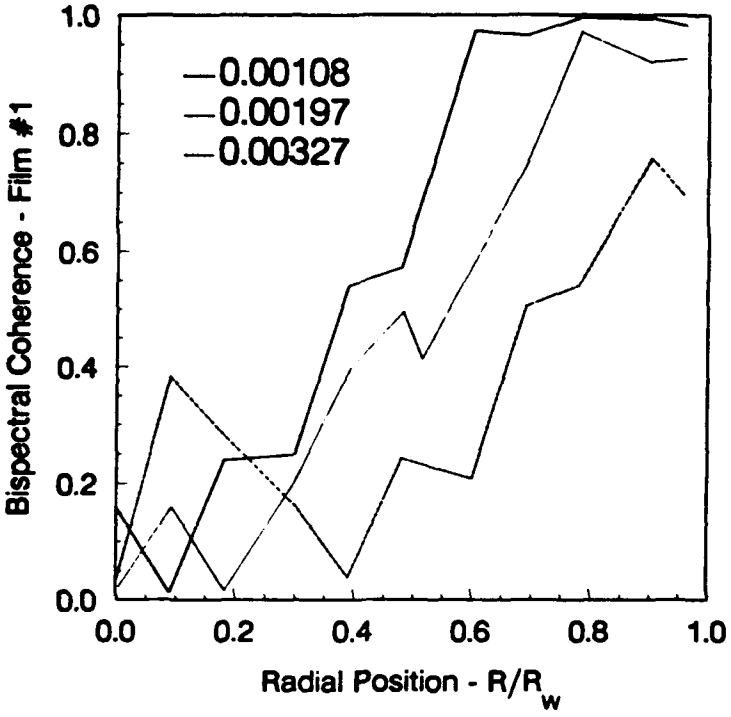

Figure 3-34. Bispectral Coherence of Film No. 1 at L/D = 3.04 (30 psia, Frequency = 92 Hz)

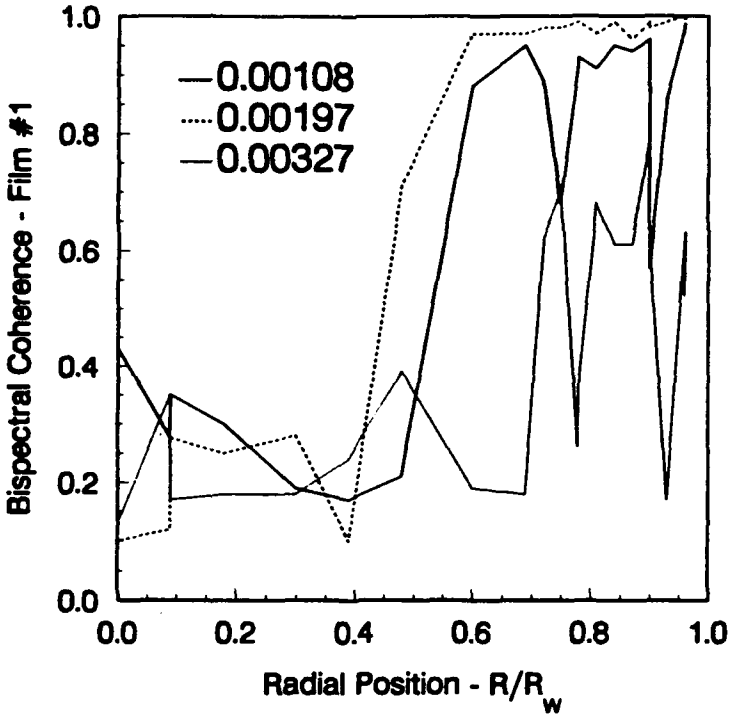

Figure 3-35. Bispectral Coherence of Film No. 1 at L/D = 4.22 (30 psia, Frequency = 92 Hz)

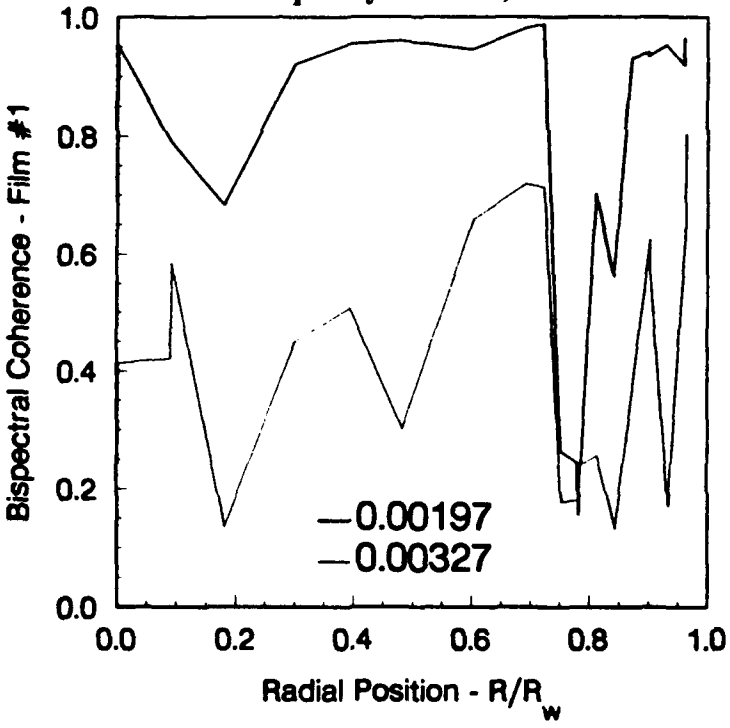

Figure 3-36. Bispectral Coherence of Film No. 1 at L/D = 5.46 (30 psia, Frequency = 92 Hz)

Generation of nonlinear behavior is surprising at these low oscillatory pressures, and hence low oscillatory velocities. In linearizing the momentum equations, the oscillatory components are assumed to be small compared to their mean values. Even though the wall response functions are reasonably high, relatively high oscillatory radial components are not expected because oscillatory pressures (and hence the maximum oscillatory Mach numbers) are of the order 0.05% of the mean pressure. Thus, under the worst case, the radial oscillatory velocity would be less than 2% of the mean radial velocity.

It is also interesting to note the changing behavior of the bispectral behavior with axial position and surface Mach number.

At an L/D of 3.04 (i.e., figure 3-34), the nonlinear behavior occurs near the wall. Furthermore, the bispectral coherence decreases with increasing surface Mach number. Because the surface response decreases with increasing surface Mach number, the oscillatory radial velocities would also decrease correspondingly. Hence, one might expect the flow behavior to become more linear and the bispectral coherence to decrease with increasing surface Mach number. Note also the the region of nonlinear behavior occurs at radial positions where r/r_w exceeds 0.5, which is the same region where significant deviations from potential wave behavior are also observed. Similar, though less dramatic behavior is also observed at an L/D of 4.22, as shown in figure 3-35.

At an L/D of 5.46, however, figure 3-36 shows the nonlinear behavior extends across the entire chamber at the intermediate surface Mach number, but is still relatively low across the chamber at the higher surface Mach number. Thus, these data show some consistency with the hypothesis that these nonlinearities are related to the magnitudes of both the oscillatory and mean flows.

All the mean and oscillatory flow data are summarized in Appendix B.

4.0 CONCLUSIONS

Results from these experimental studies have demonstrated the extensive rotational behavior of the oscillatory flows associated with combustion instabilities in solid propellant rocket motors. These rotational effects extend over significant portions of the chamber volume, both axially and radially. The amplitude of the axial component of the oscillatory velocity varies with the radius between near zero near the wall to levels well in excess of the centerline levels in an oscillatory manner over roughly the outer third of the chamber. Thus these deviations from the classical potential wave motions occupy nearly half the chamber volume. Therefore substantial changes are required in the acoustic energy balance associated with combustion stability predictions, as suggested in earlier studies by Brown et al.[19]

The radial variations in the amplitude of the axial oscillatory velocity appear to be related to radial momentum effects. The distance between the peaks correlates with distances predicted by approximate solutions of the radial momentum equation, assuming the oscillatory pressure does not vary with the radius. The agreement is best near the head end of the chamber. Further downstream, convection effects from the mean flow distorts these radial variations at low (compared to typical solid propellant values) surface Mach numbers. At higher surface Mach numbers, these radial momentum effects are maintained downstream at least 5.46 diameters.

Measured levels of the axial oscillatory velocity at the centerline agree reasonably well with potential wave behavior at 30 psia, but are somewhat higher at 90 psia. Insufficient data were obtained to differential between kinematic viscosity effects and surface response function effects since both possible contributions are a function of the mean pressure level.

Similarly, a small mean pressure effect was observed on the oscillatory motions near the wall where the rotational behavior was observed. The phase angle of these motions (with respect to the head-end oscillatory pressure) correlates with the phase angle of the surface response functions.

Significant nonlinear behavior was observed near the wall at three axial stations. At the lower surface Mach numbers, this behavior even extended all the way across the chamber at the downstream location (5.46 diameters). This nonlinear behavior occurred at much lower oscillatory pressure (and hence oscillatory velocity levels) than previously expected. From the observed effect of surface Mach number, it appears the nonlinearities are associated with interactions between the mean and oscillatory flows.

Finally, there is some evidence in the mean flow profiles that natural convection effects may be significant near the head end. More detailed studies are required to define these effects.

REFERENCES

1. Hart, R. W., Bird, J. F., and McClure, F. T., "The Influence of Erosive Burning on Acoustic Instability in Solid Propellant Rocket Motors," Solid Propellant Rocket Research, M. Summerfield, Ed., Academic Press, 1960, pp. 423-451.

2. Culick, F. E. C., "Stability of Three-Dimensional Motions in a Combustion Chamber," Combustion Science and Technology, Vol. 10, 1974, pp. 109-124.

3. Culick, F. E. C, "Stability of Longitudinal Oscillations with Pressure and Velocity Coupling in a Solid Propellant Rocket," Combustion Science and Technology, Vol. 2, 1970, pp. 179-201.

4. Lovine, R. L.. Dudley, D. P., and Waugh, R. C., "Standardized Stability Prediction Method for Solid Rocket Motors," AFRPL-TR-76-32, Aerojet Solid Propulsion Co., 1976.

5. Brown, R. S., "Progress on Improved Combustion Stability Evaluation Methods," Paper presented at the 25th JANNAF Combustion Meeting, Huntsville, AL, October 1988.

6. Flandro, G. A., "Solid Propellant Admittance Corrections," Journal of Vibration and Sound, Vol. 36, No. 3, 1974, pp. 297- 312.

7. Flandro, G. A., "Nonlinear Time-Dependent Combustion of a Solid Propellant Rocket," CPIA Publication No. 366, Vol. 2, 1982, pp. 111-122.

8. Flandro, G. A., "Analysis of Oscillatory Vorticity," CSD IR&D Report 86-6.4, December 1986.

9. Flandro, G. A., Finlayson, P. A., and Brown, R. S., "A Rational Model for Velocity Coupled Combustion Response," Paper resented at the 26th JANNAF Combustion Meeting, Pasadena, CA, October 1989.

10. Flandro, G. A., "Effects of Vorticity on Axial Waves in a Porous Tube with Blowing," IR&D Report 89-6.4 to CSD, January 1989.

11. de Jong, F. J., and Baum, J. D., "Numerical Study of Acoustic Energy Exchange Mechanisms in a Solid Rocket Motor," AIAA Paper No. 91-1864, June 1991.

12. Vuillot, F., and Avalon, G., "Acoustic Boundary Layers in Solid Propellant Motors using Navier-Stokes Equations," Journal of Prop. and Power, Vol. 7, 1991, pp. 231-239.

13. Avalon, G., and Comas, P., "Simulative Study of the Unsteady Flow Inside a Solid Rocket Motor," AIAA Paper No. 91-1865, June 1991.

14. Dunlap, R., Willoughby, P. G., and Hermsen, R. W., "Flow Field in the Combustion Chamber of a Solid Propellant Rocket Motor," AIAA Journal, Vol. 12, 1974, pp. 1440-1442.

15. Yogodkin, I., "Use of Channels with Porous Walls for Studying Flows Which Occur During Combustion of Solid Propellants," Proceedings of the 18th Astronautics Conference, Vol. 3, 1967, pp. 69-79.

16. Dunlap, R. et al., "Internal Flow Field Investigation," AFRPL TR-86-104, Chemical Systems Division/UTC, November 1985.

17. Taylor, Sir Geoffrey, "Fluid Flow in Regions Bounded by Porous Surfaces," Proceedings of the Royal Society, London, Vol. 234A, 1956, pp. 456-475.

18. Culick, F. E. C., "Rotational Axisymmetric Mean Flow and Damping of Acoustic Waves in Solid Propellant Motors," AIAA Journal, Vol. 4, 1966, pp. 1462-1464.

19. Beddini, R. A., "Analysis of Injection-Induced Flows in Porous Walled Ducts with Application to the Aerothermochemistry of Erosive Burning," PhD Thesis, Rutgers Univ., New Brunswick, N.J, October 1981.

20. Brown, R. S., Blackner, A. M., Willoughby, P. G., and Dunlap, R., "Coupling Between Velocity Oscillations and Solid Propellant Combustion," Journal of Propulsion and Power, Vol. 2, 1986, pp. 428-437.

21. Brown, R. S., Blackner, A. M., Willoughby, P. G., and Dunlap, R., "Coupling Between Velocity Oscillations and Solid Propellant Combustion," Final Report on Contracts F49620-81-C-0027 and F49620-84-C-0082, Chemicals Systems Div., August 1986.

22. Ma, Y., Van Moorhem, W. K., and Shorthill, R. W., "An Experimental Investigation of Velocity Coupling in Combustion Instability," AIAA Paper No. 90-0038, January 1990.

23. Ben Reuven, M., "The Viscous Wall-Layer Effect in Injected Porous Pipe Flow," AIAA Journal, Vol. 24, 1986, pp. 284-292.

24. Hegde, U. G., Chen, F. L., and Zinn, B. T., "Investigation of the Acoustic Boundary Layer in Porous Walled Ducts with Flow," AIAA Journal, Vol. 24, 1986, pp. 1474-1482.

25. Brown R. S., Dunlap, R., Young, S. W., and Waugh, R. C, "Vortex Shedding as a Source of Acoustic Energy in Segmented Solid Rockets," Journal of Spacecraft and Rockets, Vol. 18, 1981, pp. 312-319.

26. Brown, R. S., Erickson, J. E., and Babcock, W. R., "Combustion Response Function Measurements by the Rotating Valve Method," AIAA Journal, Vol. 12, 1974, pp. 1502-1510.

27. Brown, R. S., Dunlap, R., Young, S. W., and Waugh, R. C., "Vortex Shedding as a Source of Acoustic Energy in Segmented Solid Rockets," Journal of Spacecraft and Rockets, Vol. 18. 1981, pp. 312-319.

28. Brown, R. S., Erickson, J. E., and Babcock, W. R., "Combustion Response Function Measurements by the Rotating Valve Method," AIAA Journal, Vol. 12, 1974, pp. 1502-1510.

29. Bendat, J. S., and Piersol, A. C., "Random Data: Analysis and Measurement Procedures," Wiley-Interscience, pp. 199-203, 1971.

Appendix A

ERROR ANALYSIS EFFECT ON MEAN VOLTAGE ERRORS IN OSCILLATORY COMPONENTS

Reduction Sensitivity Study

Test 091691-1

Source	R/Rw	Normalized Amp. Axial	Normalized Amp. Radial	Phase Axial	Phase Radial	Coherence Axial	Coherence Radial
E1,E2	.00	.383	.107	-124	-66	.80	.31
E1+.01,E2-.01	.00	.382	.110	-125	-68	.80	.31
E1+.1,E2-.1	.00	.365	.164	-127	-82	.81	.38
E1,E2	.09	.373	.174	-124	-95	.87	.41
E1+.01,E2-.01	.09	.371	.179	-124	-95	.87	.42
E1+.1,E2-.1	.09	.340	.258	-126	-100	.88	.49
E1,E2	.18	.371	.095	-122	-111	.89	.23
E1+.01,E2-.01	.18	.370	.101	-122	-111	.89	.25
E1+.1,E2-.1	.18	.353	.247	-122	-115	.90	.43
E1,E2	.30	.361	.053	-118	-97	.96	.33
E1+.01,E2-.01	.30	.360	.058	-118	-99	.96	.36
E1+.1,E2+.1	.30	.350	.150	-119	-109	.96	.64
E1,E2	.39	.373	.02	-124	-49	.99	.23
E1+.01,E2-.01	.39	.373	.022	-124	-62	.99	.27
E1+.1,E2-.1	.39	.369	.10	-124	-109	.99	.79
E1,E2	.48	.404	.054	-123	-80	1.00	.86
E1+.01,E2-.01	.48	.404	.059	-123	-84	1.00	.88
E1+.1,E2-.1	.48	.398	.165	-123	-105	1.00	.96
E1,E2	.60	.390	.064	-132	-77	1.00	.97
E1+.01,E2-.01	.60	.389	.068	-132	-81	1.00	.98
E1+.1,E2-.1	.60	.390	.183	-133	-109	1.00	.99
E1,E2	.69	.318	.124	-128	39	1.00	1.00
E1+.01,E2-.01	.69	.322	.112	-128	38	1.00	1.00
E1+.1,E2-.1	.69	.347	.032	-128	-60	1.00	.97
E1,E2	.78	.249	.073	-116	52	1.00	1.00
E1+.01,E2-.01	.78	.249	.071	-116	52	1.00	1.00
E1+.1,E2-.1	.78	.253	.055	-117	51	1.00	1.00
E1,E2	.90	.654	.099	-146	-167	1.00	1.00
E1+.01,E2-.01	.90	.618	.057	-146	178	1.00	1.00
E1+.1,E2-.1	.90	.597	.192	-145	-157	1.00	1.00

Reduction Sensitivity Study

Test 091791-2

Source	R/Rw	Normalized Amp. Axial	Normalized Amp. Radial	Phase Axial	Phase Radial	Coherence Axial	Coherence Radial
E1,E2	.00	.470	.070	-123	-50	.78	.05
E1+.01,E2-.01	.00	.484	.071	-123	-50	.78	.05
E1+.1,E2-.1	.00	.482	.090	-124	-70	.78	.07
E1,E2	.09	.473	.251	-121	-107	.92	.39
E1+.01,E2-.01	.09	.471	.256	-121	-107	.92	.40
E1+.1,E2-.1	.09	.458	.301	-122	-108	.91	.44
E1,E2	.18	.518	.173	-113	-105	.92	.24
E1+.01,E2-.01	.18	.516	.179	-113	-105	.92	.25
E1+.1,E2-.1	.18	.513	.223	-114	-106	.92	.30
E1,E2	.30	.488	.049	-118	-114	.98	.20
E1+.01,E2-.01	.30	.487	.053	-118	-114	.98	.23
E1+.1,E2-.1	.30	.496	.087	-118	-115	.98	.40
E1,E2	.39	.476	.048	-122	-154	.99	.25
E1+.01,E2-.01	.39	.475	.051	-122	-153	.99	.28
E1+.1,E2-.1	.39	.484	.083	-122	-142	.99	.46
E1,E2	.48	.499	.013	-114	-59	.99	.10
E1+.01,E2-.01	.48	.503	.036	-114	-94	.99	.39
E1+.1,E2-.1	.48	.513	.071	-114	-103	.99	.69
E1,E2	.60	.466	.066	-133	98	.99	.83
E1+.01,E2-.01	.60	.466	.063	-133	102	.99	.82
E1+.1,E2-.1	.60	.471	.064	-132	155	.99	.80
E1,E2	.69	.475	.016	-132	133	.99	.15
E1+.01,E2-.01	.69	.475	.016	-132	141	.99	.15
E1+.1,E2-.1	.69	.474	.035	-131	-158	.99	.48
E1,E2	.78	.288	.174	-128	59	.99	.97
E1+.01,E2-.01	.78	.288	.176	-128	58	1.00	.98
E1+.1,E2-.1	.78	.304	.174	-127	59	1.00	.97
E1,E2	.90	.287	.128	-149	-61	.99	.99
E1+.01,E2-.01	.90	.288	.129	-149	-64	.99	.99
E1+.1,E2-.1	.90	.304	.205	-151	-87	.99	.99
E1,E2	.96	.608	.086	-92	-63	1.00	.99
E1+.01,E2-.01	.96	.605	.098	-92	-67	1.00	.99
E1+.1,E2-.1	.96	.537	.055	-93	-56	1.00	.98

Reduction Sensitivity Study

TEST 092391-4

Source	R/Rw	Normalized Amp. Axial	Normalized Amp. Radial	Phase Axial	Phase Radial	Coherence Axial	Coherence Radial
E1,E2	.00	.613	.120	-118	-117	.54	.03
E1+.01,E2-.01	.00	.612	.123	-118	-117	.53	.03
E1+.1,E2-.1	.00	.608	.067	-118	62	.51	.04
E1,E2	.09	.566	.033	-121	-75	.66	.00
E1+.01,E2-.01	.09	.566	.035	-121	-78	.67	.00
E1+.1,E2-.1	.09	.567	.089	-121	53	.68	.12
E1,E2	.18	.464	.069	-130	-109	.70	.01
E1+.01,E2-.01	.18	.464	.071	-130	-110	.70	.01
E1+.1,E2-.1	.18	.460	.063	-130	42	.72	.07
E1,E2	.30	.475	.087	-119	-124	.83	.06
E1+.01,E2-.01	.30	.474	.090	-119	-124	.83	.06
E1+.1,E2-.1	.30	.483	.108	-119	-123	.84	.07
E1,E2	.39	.459	.020	-116	138	.92	.01
E1+.01,E2-.01	.39	.459	.020	-116	145	.92	.00
E1+.1,E2-.1	.39	.475	.023	-116	178	.93	.01
E1,E2	.48	.438	.056	-117	164	.95	.08
E1+.01,E2-.01	.48	.438	.057	-117	167	.95	.08
E1+.1,E2-.1	.48	.451	.066	-117	179	.95	.10

Reduction Sensitivity Study

Test 092591-1

Source	R/Rw	Normalized Amp. Axial	Normalized Amp. Radial	Phase Axial	Phase Radial	Coherence Axial	Coherence Radial
E1,E2	.00	.450	.197	-120	19	.59	.07
E1+.01,E2-.01	.00	.470	.204	-120	19	.59	.07
E1+.1,E2-.1	.00	.487	.153	-122	17	.59	.07
E1,E2	.09	.300	.105	-148	-168	.36	.02
E1+.01,E2-.01	.09	.312	.105	-148	-169	.36	.02
E1+.1,E2-.1	.09	.302	.115	-147	-164	.30	.03
E1,E2	.18	.316	.101	-119	-22	.52	.03
E1+.01,E2-.01	.18	.317	.101	-120	-24	.52	.03
E1+.1,E2-.1	.18	.332	.089	-121	-35	.53	.03
E1,E2	.30	.352	.132	-129	49	.76	.08
E1+.01,E2-.01	.30	.353	.132	-129	49	.76	.08
E1+.1,E2-.1	.30	.382	.115	-129	49	.78	.05
E1,E2	.39	.329	.060	-122	29	.82	.04
E1+.01,E2-.01	.39	.330	.059	-123	28	.82	.04
E1+.1,E2-.1	.39	.351	.039	-123	-14	.83	.01
E1,E2	.48	.345	.069	-125	97	.91	.07
E1+.01,E2-.01	.48	.345	.068	-125	97	.91	.07
E1+.1,E2-.1	.48	.366	.060	-124	133	.92	.03
E1,E2	.60	.327	.045	-109	49	.97	.28
E1+.01,E2-.01	.60	.327	.044	-109	48	.97	.27
E1+.1,E2-.1	.60	.346	.024	-109	4	.97	.07
E1,E2	.69	.425	.065	-124	-20	.98	.67
E1+.01,E2-.01	.69	.425	.065	-124	-22	.98	.66
E1+.1,E2-.1	.69	.425	.068	-125	-38	.98	.67
E1,E2	.78	.432	.130	-111	32	.99	.88
E1+.01,E2-.01	.78	.432	.128	-111	32	.99	.88
E1+.1,E2-.1	.78	.439	.119	-112	25	.99	.85
E1,E2	.90	.204	.090	-141	-12	.96	.92
E1+.01,E2-.01	.90	.226	.071	-141	-35	.96	.89
E1+.1,E2-.1	.90	.226	.073	-143	-50	.96	.88
E1,E2	.96	.623	.037	-174	144	.99	.44
E1+.01,E2-.01	.96	.623	.044	-174	151	.99	.52
E1+.1,E2-.1	.96	.670	.122	-174	171	1.00	.82

Appendix B

SUMMARY OF MEAN AND OSCILLATORY FLOW DATA

Compilation of Tests 061292-1 and 062592-1

L/D = 5.46 Pc = 30 Ms = .001977

R/Rw	Mz	Mr	Mz/Ms	Mr/Ms	M	Angle	Mz/Mcl	Cosine
0.00	0.058918	0.001045	29.802	0.528	29.81	-1.0	1.000	1.000
0.00	0.059162	-0.000634	29.925	-0.321	29.93	0.6	1.000	1.000
0.09	0.059861	-0.001944	30.279	-0.983	30.29	1.9	1.012	1.000
0.18	0.060279	-0.002594	30.490	-1.312	30.52	2.5	1.019	0.999
0.30	0.060423	-0.003210	30.563	-1.624	30.61	3.0	1.021	0.990
0.39	0.059879	-0.003386	30.288	-1.712	30.34	3.2	1.012	0.972
0.48	0.057293	-0.003604	28.980	-1.823	29.04	3.6	0.968	0.935
0.60	0.052145	-0.003567	26.376	-1.804	26.44	3.9	0.881	0.844
0.69	0.046416	-0.004154	23.478	-2.101	23.57	5.1	0.785	0.733
0.72	0.040611	-0.001904	20.542	-0.963	20.56	2.7	0.689	0.686
0.75	0.037596	-0.001657	19.017	-0.838	19.04	2.5	0.638	0.634
0.78	0.033642	-0.001105	17.017	-0.559	17.03	1.9	0.571	0.577
0.78	0.037359	-0.003642	18.897	-1.842	18.99	5.6	0.631	0.577
0.81	0.029929	-0.000876	15.139	-0.443	15.15	1.7	0.508	0.514
0.84	0.025884	-0.001533	13.093	-0.776	13.12	3.4	0.439	0.446
0.87	0.021085	-0.002176	10.665	-1.101	10.72	5.9	0.358	0.373
0.90	0.016304	-0.000762	8.247	-0.386	8.26	2.7	0.277	0.294
0.90	0.020339	-0.003909	10.288	-1.977	10.48	10.9	0.344	0.294
0.93	0.010680	-0.001754	5.402	-0.887	5.47	9.3	0.181	0.211
0.96	0.005944	-0.000988	3.007	-0.500	3.05	9.4	0.101	0.123
0.96	0.008869	-0.002685	4.486	-1.358	4.69	16.8	0.150	0.123

Compilation of Tests 062592-2 and 062592-3

L/D = 5.46 Pc = 30 Ms = .003265

R/Rw	Mz	Mr	Mz/Ms	Mr/Ms	M	Angle	Mz/Mcl	Cosine
0.00	0.093310	0.001903	28.579	0.583	28.58	-1.2	1.000	1.000
0.00	0.098424	-0.005196	30.145	-1.591	30.19	3.0	1.000	1.000
0.09	0.093647	0.000713	28.682	0.218	28.68	-0.4	1.004	1.000
0.09	0.098745	-0.006223	30.243	-1.906	30.30	3.6	1.003	1.000
0.18	0.093498	0.000077	28.636	0.023	28.64	-0.0	1.002	0.999
0.30	0.092565	0.001850	28.351	0.567	28.36	-1.1	0.992	0.990
0.39	0.090627	0.001826	27.757	0.559	27.76	-1.2	0.971	0.972
0.48	0.086291	0.001947	26.429	0.596	26.44	-1.3	0.925	0.935
0.60	0.076430	-0.000132	23.409	-0.040	23.41	0.1	0.819	0.844
0.69	0.069883	-0.000106	21.404	-0.033	21.40	0.1	0.749	0.733
0.72	0.069253	-0.003664	21.211	-1.122	21.24	3.0	0.704	0.686
0.75	0.062605	-0.004854	19.174	-1.487	19.23	4.4	0.636	0.634
0.78	0.054161	0.001070	16.588	0.328	16.59	-1.1	0.580	0.577
0.78	0.056533	-0.004778	17.315	-1.463	17.38	4.8	0.574	0.577
0.81	0.048764	-0.005036	14.935	-1.542	15.01	5.9	0.495	0.514
0.84	0.042072	-0.005217	12.886	-1.598	12.98	7.1	0.427	0.446
0.87	0.035614	-0.003964	10.908	-1.214	10.98	6.4	0.362	0.373
0.90	0.026745	0.000539	8.191	0.165	8.19	-1.2	0.287	0.294
0.90	0.027782	-0.004191	8.509	-1.284	8.61	8.6	0.282	0.294
0.93	0.018185	-0.003745	5.570	-1.147	5.69	11.6	0.185	0.211
0.96	0.009785	-0.002183	2.997	-0.669	3.07	12.6	0.105	0.123
0.96	0.010057	-0.004538	3.080	-1.390	3.38	24.3	0.102	0.123

Compilation of Tests 091691-1 and 091691-2

L/D = 1.8 Pc = 30 Ms = .00108

R/Rw	Mz	Mr	Mz/Ms	Mr/Ms	M	Angle	Mz/Mcl	Cosine
0.00	0.012770	-0.002420	11.824	-2.241	12.03	10.7	0.996	1.000
0.00	0.012871	-0.002512	11.918	-2.326	12.14	11.0	1.004	1.000
0.09	0.012902	-0.002653	11.946	-2.456	12.20	11.6	1.006	1.000
0.18	0.012840	-0.002940	11.889	-2.722	12.20	12.9	1.002	0.999
0.30	0.012681	-0.003174	11.741	-2.939	12.10	14.1	0.989	0.990
0.39	0.012424	-0.003309	11.504	-3.064	11.90	14.9	0.969	0.972
0.48	0.012042	-0.003348	11.150	-3.100	11.57	15.5	0.939	0.935
0.60	0.010947	-0.003477	10.136	-3.220	10.64	17.6	0.854	0.844
0.69	0.009733	-0.002728	9.012	-2.526	9.36	15.7	0.759	0.733
0.69	0.009658	-0.002959	8.942	-2.740	9.35	17.0	0.753	0.733
0.72	0.009360	-0.002453	8.667	-2.271	8.96	14.7	0.730	0.686
0.75	0.008790	-0.002156	8.139	-1.997	8.38	13.8	0.686	0.634
0.78	0.008295	-0.001948	7.681	-1.804	7.89	13.2	0.647	0.577
0.78	0.008092	-0.002210	7.493	-2.046	7.77	15.3	0.631	0.577
0.81	0.007553	-0.001981	6.994	-1.834	7.23	14.7	0.589	0.514
0.84	0.006663	-0.002068	6.170	-1.915	6.46	17.2	0.520	0.446
0.87	0.005979	-0.002128	5.536	-1.970	5.88	19.6	0.466	0.373
0.90	0.005003	-0.002221	4.633	-2.057	5.07	23.9	0.390	0.294
0.90	0.004593	-0.002432	4.253	-2.252	4.81	27.9	0.358	0.294
0.93	0.003919	-0.002382	3.629	-2.205	4.25	31.3	0.306	0.211
0.96	0.003001	-0.001746	2.778	-1.617	3.21	30.2	0.234	0.123

Combination of tests 091791-1 and 091791-2

L/D = 1.8 Pc = 90 Ms = .001080

R/Rw	Mz	Mr	Mz/Ms	Mr/Ms	M	Angle	Mz/Mcl	Cosine
0.00	0.013171	-0.001331	12.195	-1.233	12.26	5.8	0.986	1.000
0.00	0.013538	-0.001405	12.535	-1.301	12.60	5.9	1.014	1.000
0.09	0.013208	-0.001421	12.230	-1.316	12.30	6.1	0.989	1.000
0.18	0.013205	-0.001856	12.226	-1.718	12.35	8.0	0.989	0.999
0.30	0.013079	-0.002112	12.110	-1.956	12.27	9.2	0.979	0.990
0.39	0.012818	-0.002413	11.869	-2.234	12.08	10.7	0.960	0.972
0.48	0.012432	-0.002484	11.511	-2.300	11.74	11.3	0.931	0.935
0.60	0.011527	-0.002625	10.673	-2.431	10.95	12.8	0.863	0.844
0.69	0.010436	-0.002774	9.663	-2.569	10.00	14.9	0.781	0.733
0.69	0.010168	-0.002619	9.415	-2.425	9.72	14.4	0.761	0.733
0.72	0.010119	-0.002516	9.369	-2.330	9.65	14.0	0.758	0.686
0.75	0.009423	-0.002357	8.725	-2.182	8.99	14.0	0.706	0.634
0.78	0.008797	-0.002145	8.146	-1.986	8.38	13.7	0.659	0.577
0.78	0.008883	-0.002338	8.225	-2.165	8.51	14.7	0.665	0.577
0.81	0.008234	-0.002267	7.624	-2.099	7.91	15.4	0.617	0.514
0.84	0.007316	-0.002279	6.774	-2.110	7.09	17.3	0.548	0.446
0.87	0.006478	-0.002056	5.998	-1.903	6.29	17.6	0.485	0.373
0.90	0.005640	-0.001854	5.222	-1.716	5.50	18.2	0.422	0.294
0.90	0.005328	-0.002027	4.933	-1.877	5.28	20.8	0.399	0.294
0.93	0.004300	-0.002080	3.982	-1.926	4.42	25.8	0.322	0.211
0.96	0.003546	-0.001842	3.284	-1.706	3.70	27.4	0.266	0.123
0.96	0.003241	-0.001980	3.001	-1.833	3.52	31.4	0.243	0.123

Combination of tests 091991-1 and 091991-2

L/D = 1.8 Pc = 30 Ms = .001977

R/Rw	Mz	Mr	Mz/Ms	Mr/Ms	M	Angle	Mz/Mcl	Cosine
0.00	0.021164	-0.002559	10.705	-1.294	10.78	6.9	0.979	1.000
0.00	0.022073	-0.001704	11.165	-0.862	11.20	4.4	1.021	1.000
0.09	0.022555	-0.002313	11.409	-1.170	11.47	5.9	1.043	1.000
0.18	0.022706	-0.003081	11.485	-1.558	11.59	7.7	1.050	0.999
0.30	0.022411	-0.003906	11.336	-1.976	11.51	9.9	1.037	0.990
0.39	0.021953	-0.004468	11.104	-2.260	11.33	11.5	1.015	0.972
0.48	0.021310	-0.004716	10.779	-2.385	11.04	12.5	0.986	0.935
0.60	0.019829	-0.004978	10.030	-2.518	10.34	14.1	0.917	0.844
0.69	0.016300	-0.004998	8.245	-2.528	8.62	17.0	0.754	0.733
0.69	0.017620	-0.005099	8.912	-2.579	9.28	16.1	0.815	0.733
0.72	0.016423	-0.005035	8.307	-2.547	8.69	17.0	0.760	0.686
0.75	0.015600	-0.004932	7.891	-2.494	8.28	17.5	0.722	0.634
0.78	0.013897	-0.004618	7.029	-2.336	7.41	18.4	0.643	0.577
0.78	0.014809	-0.004630	7.491	-2.342	7.85	17.4	0.685	0.577
0.81	0.012650	-0.004573	6.399	-2.313	6.80	19.9	0.585	0.514
0.84	0.011355	-0.004504	5.744	-2.278	6.18	21.6	0.525	0.446
0.87	0.010403	-0.004410	5.262	-2.231	5.72	23.0	0.481	0.373
0.90	0.009183	-0.003569	4.645	-1.805	4.98	21.2	0.425	0.294
0.90	0.009439	-0.003551	4.774	-1.796	5.10	20.6	0.437	0.294
0.93	0.007458	-0.003601	3.773	-1.822	4.19	25.8	0.345	0.211
0.96	0.005921	-0.003555	2.995	-1.798	3.49	31.0	0.274	0.123
0.96	0.006011	-0.003481	3.040	-1.761	3.51	30.1	0.278	0.123

Compilation of tests 092091-1, 092091-2, 092391-4 and 092491-1

L/D = 1.8 Pc = 90 Ms = .001977

R/Rw	Mz	Mr	Mz/Ms	Mr/Ms	M	Angle	Mz/Mcl	Cosine
0.00	0.023321	-0.001716	11.796	-0.868	11.83	4.2	1.000	1.000
0.00	0.023305	-0.000762	11.788	-0.386	11.79	1.9	1.000	1.000
0.09	0.023755	-0.001698	12.015	-0.859	12.05	4.1	1.019	1.000
0.18	0.023272	-0.002132	11.771	-1.078	11.82	5.2	0.998	0.999
0.30	0.022603	-0.002718	11.433	-1.375	11.52	6.9	0.970	0.990
0.39	0.022562	-0.003328	11.412	-1.683	11.54	8.4	0.968	0.972
0.48	0.021200	-0.002744	10.723	-1.388	10.81	7.4	0.909	0.935
0.48	0.021227	-0.003550	10.737	-1.796	10.89	9.5	0.911	0.935
0.60	0.020227	-0.003213	10.231	-1.625	10.36	9.0	0.868	0.844
0.69	0.018059	-0.004239	9.134	-2.144	9.38	13.2	0.775	0.733
0.69	0.018448	-0.003484	9.331	-1.762	9.50	10.7	0.791	0.733
0.72	0.017822	-0.004216	9.015	-2.132	9.26	13.3	0.764	0.686
0.75	0.016854	-0.004065	8.525	-2.056	8.77	13.6	0.723	0.634
0.78	0.015458	-0.004298	7.819	-2.174	8.12	15.5	0.663	0.577
0.78	0.016509	-0.003940	8.350	-1.993	8.58	13.4	0.708	0.577
0.81	0.013209	-0.004532	6.681	-2.292	7.06	18.9	0.567	0.514
0.84	0.011875	-0.004255	6.007	-2.152	6.38	19.7	0.509	0.446
0.87	0.010639	-0.004162	5.381	-2.105	5.78	21.4	0.456	0.373
0.90	0.011043	-0.003717	5.586	-1.880	5.89	18.6	0.474	0.294
0.90	0.009501	-0.003889	4.806	-1.967	5.19	22.3	0.408	0.294
0.93	0.007687	-0.003853	3.888	-1.949	4.35	26.6	0.330	0.211
0.96	0.008353	-0.003282	4.225	-1.660	4.54	21.5	0.358	0.123
0.96	0.005876	-0.003670	2.972	-1.856	3.50	32.0	0.252	0.123

Compilation of tests 092591-1 and 092591-2

L/D = 1.8 Pc = 30 Ms = .003259

R/Rw	Mz	Mr	Mz/Ms	Mr/Ms	M	Angle	Mz/Mcl	Cosine
0.00	0.033467	-0.003525	10.250	-1.080	10.31	6.0	0.984	1.000
0.00	0.034549	-0.003545	10.582	-1.086	10.64	5.9	1.016	1.000
0.09	0.035596	-0.003612	10.902	-1.106	10.96	5.8	1.047	1.000
0.18	0.035757	-0.004126	10.952	-1.264	11.02	6.6	1.051	0.999
0.30	0.035461	-0.005244	10.861	-1.606	10.98	8.4	1.043	0.990
0.39	0.035024	-0.005685	10.727	-1.741	10.87	9.2	1.030	0.972
0.48	0.034315	-0.006260	10.510	-1.917	10.68	10.3	1.009	0.935
0.60	0.032841	-0.006283	10.058	-1.924	10.24	10.8	0.966	0.844
0.69	0.030224	-0.006484	9.257	-1.986	9.47	12.1	0.889	0.733
0.69	0.030551	-0.006444	9.357	-1.974	9.56	11.9	0.898	0.733
0.72	0.028639	-0.006242	8.771	-1.912	8.98	12.3	0.842	0.686
0.75	0.027351	-0.007240	8.377	-2.217	8.67	14.8	0.804	0.634
0.78	0.026760	-0.006350	8.196	-1.945	8.42	13.3	0.787	0.577
0.78	0.027204	-0.006310	8.332	-1.933	8.55	13.1	0.800	0.577
0.81	0.025347	-0.006142	7.763	-1.881	7.99	13.6	0.745	0.514
0.84	0.023085	-0.006304	7.070	-1.931	7.33	15.3	0.679	0.446
0.87	0.021634	-0.006437	6.626	-1.972	6.91	16.6	0.636	0.373
0.90	0.018391	-0.005530	5.633	-1.694	5.88	16.7	0.541	0.294
0.90	0.018854	-0.005702	5.775	-1.746	6.03	16.8	0.554	0.294
0.93	0.017125	-0.005439	5.245	-1.666	5.50	17.6	0.504	0.211
0.96	0.014800	-0.004896	4.533	-1.500	4.77	18.3	0.435	0.123
0.96	0.014572	-0.004824	4.463	-1.478	4.70	18.3	0.428	0.123

Combination of tests 091691-1 and 091691-2

L/D=1.8 P = 30 psi Ms = 0.00108 f = 92 hz

	Normalized Amplitude		Phase Angle		Coherence	
R/Rw	Axial	Radial	Axial	Radial	Axial	Radial
0.00	0.375	0.095	-124	-62	0.780	0.132
0.00	0.383	0.107	-124	-66	0.797	0.307
0.09	0.373	0.174	-124	-95	0.872	0.412
0.18	0.371	0.095	-122	-111	0.889	0.230
0.30	0.361	0.053	-118	-97	0.958	0.328
0.39	0.373	0.020	-124	-49	0.988	0.234
0.48	0.404	0.054	-123	-80	0.996	0.861
0.60	0.390	0.064	-132	-77	0.997	0.974
0.69	0.318	0.041	-121	63	0.999	0.968
0.69	0.318	0.124	-128	39	0.999	0.998
0.72	0.328	0.098	-122	43	0.999	0.997
0.75	0.446	0.106	-98	72	0.999	0.999
0.78	0.237	0.051	-90	25	0.997	0.993
0.78	0.249	0.073	-116	52	0.996	0.996
0.81	0.408	0.021	-135	86	0.999	0.950
0.84	0.571	0.174	-121	-136	0.999	0.999
0.87	0.353	0.070	-101	-124	0.999	0.997
0.90	0.398	0.047	-157	174	0.998	0.997
0.90	0.654	0.099	-146	-167	0.998	0.997
0.93	0.761	0.117	-126	-153	0.999	0.999
0.96	0.302	0.044	-91	110	0.998	0.966

Combination of tests 091791-1 and 091791-2

L/D=1.8 P = 90 psi Ms = 0.00108 f = 92 hz

	Normalized Amplitude		Phase Angle		Coherence	
R/Rw	Axial	Radial	Axial	Radial	Axial	Radial
0.00	0.470	0.070	-123	-50	0.782	0.051
0.00	0.497	0.091	-130	-51	0.852	0.079
0.09	0.473	0.251	-121	-107	0.922	0.388
0.18	0.518	0.173	-113	-105	0.915	0.240
0.30	0.488	0.049	-118	-114	0.982	0.201
0.39	0.476	0.048	-122	-154	0.988	0.249
0.48	0.499	0.013	-114	-59	0.990	0.104
0.60	0.466	0.066	-133	98	0.994	0.829
0.69	0.470	0.099	-131	73	0.996	0.808
0.69	0.475	0.016	-132	133	0.994	0.153
0.72	0.356	0.198	-120	55	0.991	0.973
0.75	0.438	0.220	-79	30	0.992	0.977
0.78	0.288	0.174	-128	59	0.994	0.971
0.78	0.425	0.174	-131	54	0.997	0.971
0.81	0.532	0.121	-123	17	0.999	0.970
0.84	0.550	0.113	-113	33	0.999	0.978
0.87	0.470	0.123	-112	-59	0.999	0.974
0.90	0.287	0.128	-149	-61	0.987	0.988
0.90	0.538	0.061	-166	-136	0.993	0.889
0.93	0.766	0.195	-118	-101	0.998	0.997
0.96	0.608	0.086	-92	-63	0.999	0.989
0.96	0.411	0.128	-91	-90	0.991	0.986

Combination of tests 091991-1 and 091991-2

L/D=1.8 P = 30 psi Ms = 0.001977 f = 92 hz

	Normalized Amplitude		Phase Angle		Coherence	
R/Rw	Axial	Radial	Axial	Radial	Axial	Radial
0.00	0.413	0.211	-135	-103	0.731	0.240
0.00	0.389	0.176	-133	-55	0.707	0.136
0.09	0.353	0.095	-128	-124	0.622	0.046
0.18	0.333	0.157	-128	-129	0.686	0.188
0.30	0.403	0.135	-108	-104	0.855	0.306
0.39	0.378	0.067	-126	179	0.932	0.157
0.48	0.336	0.003	-122	32	0.952	0.001
0.60	0.469	0.097	-121	78	0.994	0.906
0.69	0.367	0.072	-116	139	0.993	0.780
0.69	0.365	0.116	-116	131	0.993	0.888
0.72	0.350	0.111	-99	91	0.992	0.957
0.75	0.206	0.025	-99	180	0.984	0.646
0.78	0.326	0.077	-158	47	0.997	0.950
0.78	0.436	0.108	-158	-75	0.997	0.982
0.81	0.412	0.023	-142	25	0.998	0.808
0.84	0.604	0.057	-134	-113	0.999	0.945
0.87	0.372	0.269	-109	73	0.999	0.996
0.90	0.286	0.068	-88	98	0.998	0.987
0.90	0.249	0.113	-81	114	0.996	0.985
0.93	0.226	0.051	-133	-54	0.997	0.983
0.96	0.473	0.114	-154	47	0.998	0.995
0.96	0.611	0.113	-164	31	0.997	0.990

Combination of tests 092091-1, 092091-2, 092391-4 and 092491-1

L/D=1.8 P = 90 psi Ms = 0.001977 f = 92 hz

	Normalized Amplitude		Phase Angle		Coherence	
R/Rw	Axial	Radial	Axial	Radial	Axial	Radial
0.00	0.613	0.120	-118	-117	0.536	0.026
0.00	0.486	0.065	-103	-120	0.649	0.009
0.09	0.566	0.033	-121	-75	0.663	0.002
0.18	0.464	0.069	-130	-109	0.695	0.011
0.30	0.475	0.087	-119	-124	0.825	0.055
0.39	0.459	0.020	-116	138	0.922	0.005
0.48	0.511	0.058	-123	-147	0.988	0.310
0.48	0.438	0.056	-117	164	0.950	0.080
0.60	0.435	0.086	-117	-146	0.980	0.489
0.69	0.463	0.124	-111	-121	0.981	0.631
0.69	0.559	0.125	-116	-146	0.983	0.847
0.72	0.481	0.024	-114	-161	0.980	0.100
0.75	0.452	0.134	-141	-153	0.976	0.755
0.78	0.470	0.017	-150	140	0.985	0.069
0.78	0.744	0.047	-116	150	0.994	0.507
0.81	0.657	0.109	-130	104	0.997	0.860
0.84	0.609	0.087	-116	83	0.997	0.861
0.87	0.589	0.158	-81	55	0.993	0.965
0.90	0.353	0.173	-92	45	0.969	0.947
0.90	0.266	0.130	-121	49	0.974	0.940
0.93	0.782	0.200	-154	-26	0.998	0.970
0.96	0.135	0.059	150	70	0.072	0.016
0.96	0.092	0.106	15	50	0.123	0.804

Combination of tests 092591-1 and 092591-2

L/D=1.8 P = 30 psi Ms = 0.00327 f = 92 hz

	Normalized Amplitude		Phase Angle		Coherence	
R/Rw	Axial	Radial	Axial	Radial	Axial	Radial
0.00	0.208	0.061	-128	-74	0.199	0.011
0.00	0.450	0.197	-120	19	0.594	0.070
0.09	0.300	0.105	-148	-168	0.361	0.016
0.18	0.316	0.101	-119	-22	0.515	0.029
0.30	0.352	0.132	-129	49	0.757	0.077
0.39	0.330	0.060	-123	29	0.815	0.041
0.48	0.346	0.069	-125	97	0.909	0.074
0.60	0.327	0.045	-109	48	0.974	0.280
0.69	0.414	0.074	-120	-44	0.983	0.638
0.69	0.425	0.065	-124	-21	0.986	0.665
0.72	0.553	0.016	-126	-76	0.974	0.056
0.75	0.439	0.052	-137	-170	0.984	0.461
0.78	0.447	0.097	-110	69	0.990	0.909
0.78	0.432	0.130	-111	32	0.989	0.883
0.81	0.565	0.045	-77	-111	0.980	0.695
0.84	0.122	0.020	-65	-53	0.894	0.331
0.87	0.157	0.073	-125	-120	0.957	0.902
0.90	0.236	0.142	-124	26	0.976	0.953
0.90	0.204	0.090	-141	-12	0.962	0.923
0.93	0.251	0.110	-143	18	0.900	0.963
0.96	0.438	0.120	-162	57	0.991	0.958
0.96	0.623	0.037	-174	144	0.994	0.443

Compilation of Tests 030992-1 and 030992-2 and 033092-1

L/D = 3.04 Pc = 30 Ms = .00108

R/Rw	Mz	Mr	Mz/Ms	Mr/Ms	M	Angle	Mz/Mcl	Cosine
-0.002	0.019726	-0.001154	18.265	-1.069	18.30	3.3	0.997	1.000
0.00	0.019799	-0.001775	18.332	-1.643	18.41	5.1	1.001	1.000
0.00	0.019833	-0.001170	18.364	-1.083	18.40	3.4	1.002	1.000
0.09	0.019895	-0.001636	18.421	-1.515	18.48	4.7	1.006	1.000
0.09	0.019743	-0.002039	18.280	-1.888	18.38	5.9	0.998	1.000
0.18	0.019776	-0.001796	18.311	-1.663	18.39	5.2	0.999	0.999
0.30	0.019656	-0.001927	18.200	-1.784	18.29	5.6	0.993	0.990
0.39	0.019395	-0.001911	17.959	-1.769	18.05	5.6	0.980	0.972
0.48	0.018675	-0.001848	17.291	-1.711	17.38	5.7	0.944	0.935
0.60	0.017424	-0.001445	16.133	-1.338	16.19	4.7	0.881	0.844
0.69	0.015415	-0.001443	14.274	-1.336	14.34	5.3	0.779	0.733
0.695	0.015397	-0.001383	14.256	-1.281	14.31	5.1	0.778	0.726
0.710	0.014963	-0.001335	13.855	-1.236	13.91	5.1	0.756	0.703
0.72	0.014436	-0.002175	13.367	-2.014	13.52	8.6	0.730	0.686
0.723	0.014599	-0.001406	13.517	-1.301	13.58	5.5	0.738	0.681
0.737	0.014159	-0.001477	13.110	-1.367	13.18	6.0	0.716	0.658
0.756	0.013430	-0.001589	12.435	-1.471	12.52	6.7	0.679	0.623
0.769	0.012982	-0.001707	12.021	-1.581	12.12	7.5	0.656	0.599
0.78	0.012422	-0.002483	11.502	-2.299	11.73	11.3	0.628	0.577
0.78	0.012641	-0.001920	11.704	-1.778	11.84	8.6	0.639	0.577
0.785	0.012574	-0.001824	11.643	-1.689	11.76	8.3	0.636	0.567
0.799	0.011891	-0.002000	11.010	-1.852	11.16	9.5	0.601	0.538
0.81	0.010794	-0.002429	9.994	-2.249	10.24	12.7	0.546	0.514
0.813	0.011117	-0.002049	10.293	-1.897	10.47	10.4	0.562	0.508
0.829	0.010183	-0.001953	9.429	-1.808	9.60	10.9	0.515	0.472
0.84	0.009442	-0.002146	8.743	-1.987	8.97	12.8	0.477	0.446
0.843	0.009610	-0.001885	8.898	-1.745	9.07	11.1	0.486	0.439
0.858	0.009104	-0.001803	8.429	-1.669	8.59	11.2	0.460	0.403
0.87	0.008533	-0.001800	7.901	-1.667	8.08	11.9	0.431	0.373
0.870	0.008758	-0.001717	8.109	-1.590	8.26	11.1	0.443	0.373
0.888	0.008012	-0.001386	7.418	-1.283	7.53	9.8	0.405	0.326
0.894	0.007775	-0.001265	7.199	-1.172	7.29	9.2	0.393	0.310
0.90	0.007211	-0.000839	6.677	-0.777	6.72	6.6	0.364	0.294
0.90	0.007110	-0.000911	6.583	-0.844	6.64	7.3	0.359	0.294
0.902	0.007359	-0.001017	6.814	-0.942	6.88	7.9	0.372	0.289
0.916	0.006576	-0.000563	6.089	-0.522	6.11	4.9	0.332	0.250
0.922	0.006271	-0.000707	5.806	-0.655	5.84	6.4	0.317	0.233
0.93	0.005472	-0.001428	5.067	-1.322	5.24	14.6	0.277	0.211
0.931	0.005785	-0.000951	5.356	-0.881	5.43	9.3	0.292	0.208
0.944	0.005084	-0.001235	4.707	-1.144	4.84	13.7	0.257	0.170
0.953	0.004571	-0.001578	4.233	-1.461	4.48	19.0	0.231	0.144
0.96	0.003776	-0.001654	3.496	-1.532	3.82	23.7	0.191	0.123
0.96	0.003680	-0.001761	3.407	-1.631	3.78	25.6	0.186	0.123

Compilation of Tests 031092-1 and 031092-2

L/D = 3.04 Pc = 90 Ms = .00108

R/Rw	Mz	Mr	Mz/Ms	Mr/Ms	M	Angle	Mz/Mcl	Cosine
0.00	0.020610	0.000130	19.083	0.120	19.08	-0.4	0.994	1.000
0.00	0.020862	0.000032	19.317	0.030	19.32	-0.1	1.006	1.000
0.09	0.020688	-0.000018	19.156	-0.016	19.16	0.0	0.998	1.000
0.09	0.021027	-0.000100	19.470	-0.093	19.47	0.3	1.014	1.000
0.18	0.020662	-0.000122	19.131	-0.113	19.13	0.3	0.996	0.999
0.30	0.020488	-0.000211	18.971	-0.195	18.97	0.6	0.988	0.990
0.39	0.020222	-0.000174	18.724	-0.161	18.73	0.5	0.975	0.972
0.48	0.019521	-0.000109	18.075	-0.101	18.07	0.3	0.941	0.935
0.60	0.018072	-0.000284	16.734	-0.263	16.74	0.9	0.872	0.844
0.69	0.016059	-0.000723	14.869	-0.669	14.88	2.6	0.774	0.733
0.72	0.015231	-0.000934	14.103	-0.865	14.13	3.5	0.735	0.686
0.75	0.014217	-0.001142	13.164	-1.058	13.21	4.6	0.686	0.634
0.78	0.012879	-0.001199	11.925	-1.110	11.98	5.3	0.621	0.577
0.78	0.012957	-0.001236	11.997	-1.144	12.05	5.4	0.625	0.577
0.81	0.011310	-0.001616	10.473	-1.497	10.58	8.1	0.545	0.514
0.84	0.010019	-0.001623	9.277	-1.503	9.40	9.2	0.483	0.446
0.87	0.008923	-0.001385	8.262	-1.282	8.36	8.8	0.430	0.373
0.90	0.007537	-0.000797	6.979	-0.738	7.02	6.0	0.363	0.294
0.90	0.007517	-0.000826	6.960	-0.765	7.00	6.3	0.363	0.294
0.93	0.005705	-0.001125	5.282	-1.042	5.38	11.2	0.275	0.211
0.96	0.004309	-0.001346	3.990	-1.247	4.18	17.4	0.208	0.123
0.96	0.004266	-0.001572	3.950	-1.455	4.21	20.2	0.206	0.123

Compilation of tests 030192-3 and 030392-1 and 033092-2

L/D = 3.04 Pc = 30 Ms = .001977

R/Rw	Mz	Mr	Mz/Ms	Mr/Ms	M	Angle	Mz/Mcl	Cosine
0.00	0.034753	-0.000846	17.579	-0.428	17.58	1.4	0.998	1.000
0.00	0.034925	-0.001724	17.666	-0.872	17.69	2.8	1.003	1.000
0.001	0.034756	0.000836	17.580	0.423	17.59	-1.4	0.998	1.000
0.09	0.034973	-0.001554	17.690	-0.786	17.71	2.5	1.005	1.000
0.09	0.035365	-0.002568	17.888	-1.299	17.94	4.2	1.016	1.000
0.18	0.035419	-0.003098	17.915	-1.567	17.98	5.0	1.017	0.999
0.30	0.034800	-0.003821	17.602	-1.933	17.71	6.3	1.000	0.990
0.39	0.034414	-0.003988	17.407	-2.017	17.52	6.6	0.989	0.972
0.48	0.033153	-0.004540	16.769	-2.296	16.93	7.8	0.952	0.935
0.515	0.032837	-0.000100	16.609	-0.051	16.61	0.2	0.943	0.914
0.547	0.032338	-0.000044	16.357	-0.022	16.36	0.1	0.929	0.892
0.577	0.031724	0.000029	16.046	0.014	16.05	-0.1	0.911	0.866
0.60	0.030457	-0.003013	15.406	-1.524	15.48	5.6	0.875	0.844
0.606	0.030988	0.000110	15.674	0.056	15.67	-0.2	0.890	0.838
0.637	0.030062	0.000271	15.206	0.137	15.21	-0.5	0.864	0.804
0.668	0.026895	0.000047	14.616	0.024	14.62	-0.1	0.830	0.764
0.69	0.027411	-0.005105	13.865	-2.582	14.10	10.6	0.787	0.733
0.698	0.027585	-0.000283	13.953	-0.143	13.95	0.6	0.792	0.721
0.726	0.026082	-0.000829	13.193	-0.419	13.20	1.8	0.749	0.676
0.75	0.024086	-0.003910	12.183	-1.978	12.34	9.2	0.692	0.634
0.757	0.024700	-0.001511	12.494	-0.764	12.52	3.5	0.710	0.621
0.78	0.022409	-0.005261	11.335	-2.661	11.64	13.2	0.644	0.577
0.78	0.022124	-0.004062	11.191	-2.055	11.38	10.4	0.636	0.577
0.787	0.022712	-0.001698	11.488	-0.859	11.52	4.3	0.652	0.563
0.81	0.019979	-0.003700	10.106	-1.871	10.28	10.5	0.574	0.514
0.816	0.020536	-0.001935	10.388	-0.979	10.43	5.4	0.590	0.501
0.84	0.017382	-0.002895	8.792	-1.464	8.91	9.5	0.499	0.446
0.847	0.017889	-0.001815	9.049	-0.918	9.10	5.8	0.514	0.429
0.87	0.015385	-0.002869	7.782	-1.451	7.92	10.6	0.442	0.373
0.878	0.015932	-0.001284	8.058	-0.650	8.08	4.6	0.458	0.352
0.90	0.012941	-0.003018	6.546	-1.527	6.72	13.1	0.372	0.294
0.90	0.012976	-0.003753	6.564	-1.898	6.83	16.1	0.373	0.294
0.907	0.013632	-0.001236	6.895	-0.625	6.92	5.2	0.392	0.275
0.911	0.013219	-0.001328	6.687	-0.672	6.72	5.7	0.380	0.264
0.922	0.012029	-0.001203	6.084	-0.608	6.11	5.7	0.346	0.233
0.93	0.009967	-0.002989	5.042	-1.512	5.26	16.7	0.286	0.211
0.933	0.010921	-0.002226	5.524	-1.126	5.64	11.5	0.314	0.202
0.941	0.010269	-0.002172	5.194	-1.099	5.31	11.9	0.295	0.179
0.953	0.009416	-0.002120	4.763	-1.072	4.88	12.7	0.270	0.144
0.96	0.007419	-0.002289	3.752	-1.158	3.93	17.1	0.213	0.123
0.96	0.007467	-0.001776	3.777	-0.898	3.88	13.4	0.215	0.123
0.962	0.008476	-0.001905	4.287	-0.964	4.39	12.7	0.243	0.117

Compilation of tests 030492-1, 030492-3 and 030592-1

L/D = 3.04 Pc = 90 Ms = .001977

R/Rw	Mz	Mr	Mz/Ms	Mr/Ms	M	Angle	Mz/Mcl	Cosine
0.00	0.035023	-0.000538	17.715	-0.272	17.72	0.9	0.996	1.000
0.00	0.035291	-0.001790	17.851	-0.905	17.87	2.9	1.004	1.000
0.09	0.035174	-0.001104	17.792	-0.558	17.80	1.8	1.000	1.000
0.09	0.035596	-0.002496	18.005	-1.263	18.05	4.0	1.012	1.000
0.18	0.035210	-0.001557	17.810	-0.788	17.83	2.5	1.002	0.999
0.30	0.035076	-0.002018	17.742	-1.021	17.77	3.3	0.998	0.990
0.39	0.034721	-0.002332	17.562	-1.180	17.60	3.8	0.988	0.972
0.48	0.034048	-0.002784	17.222	-1.408	17.28	4.7	0.968	0.935
0.60	0.031589	-0.002983	15.978	-1.509	16.05	5.4	0.899	0.844
0.60	0.031465	-0.003914	15.915	-1.980	16.04	7.1	0.895	0.844
0.69	0.028556	-0.002751	14.444	-1.391	14.51	5.5	0.812	0.733
0.75	0.025384	-0.002696	12.840	-1.364	12.91	6.1	0.722	0.634
0.78	0.023697	-0.002164	11.986	-1.094	12.04	5.2	0.674	0.577
0.81	0.021382	-0.001908	10.815	-0.965	10.86	5.1	0.608	0.514
0.84	0.018782	-0.002401	9.500	-1.214	9.58	7.3	0.534	0.446
0.84	0.019334	-0.001935	9.780	-0.979	9.83	5.7	0.550	0.446
0.87	0.017009	-0.002409	8.603	-1.219	8.69	8.1	0.484	0.373
0.90	0.014848	-0.002695	7.510	-1.363	7.63	10.3	0.422	0.294
0.93	0.011438	-0.003081	5.786	-1.558	5.99	15.1	0.325	0.211
0.96	0.009074	-0.002390	4.590	-1.209	4.75	14.8	0.258	0.123

Compilation of Tests 031392-1 and 031392-2

L/D = 3.04 Pc = 30 Ms = .003265

R/Rw	Mz	Mr	Mz/Ms	Mr/Ms	M	Angle	Mz/Mcl	Cosine
0.00	0.055799	-0.000139	17.090	-0.043	17.09	0.1	1.002	1.000
0.00	0.055579	-0.000171	17.023	-0.052	17.02	0.2	0.998	1.000
0.09	0.056077	-0.001239	17.175	-0.380	17.18	1.3	1.007	1.000
0.09	0.055853	-0.001113	17.107	-0.341	17.11	1.1	1.003	1.000
0.18	0.055931	-0.001965	17.130	-0.602	17.14	2.0	1.004	0.999
0.30	0.055616	-0.002780	17.034	-0.851	17.06	2.9	0.999	0.990
0.39	0.054983	-0.003024	16.840	-0.926	16.87	3.1	0.987	0.972
0.48	0.053139	-0.003684	16.275	-1.128	16.31	4.0	0.954	0.935
0.60	0.049132	-0.004115	15.048	-1.260	15.10	4.8	0.882	0.844
0.69	0.043846	-0.004029	13.429	-1.234	13.49	5.3	0.787	0.733
0.72	0.040222	-0.004089	12.319	-1.252	12.38	5.8	0.722	0.686
0.75	0.038296	-0.004143	11.729	-1.269	11.80	6.2	0.688	0.634
0.78	0.036103	-0.003248	11.057	-0.995	11.10	5.1	0.648	0.577
0.78	0.035366	-0.003734	10.832	-1.144	10.89	6.0	0.635	0.577
0.81	0.032444	-0.003174	9.937	-0.972	9.98	5.6	0.583	0.514
0.84	0.028089	-0.004077	8.603	-1.249	8.69	8.3	0.504	0.446
0.87	0.024733	-0.004587	7.575	-1.405	7.70	10.5	0.444	0.373
0.90	0.021090	-0.004601	6.459	-1.409	6.61	12.3	0.379	0.294
0.90	0.020926	-0.004546	6.409	-1.392	6.56	12.3	0.376	0.294
0.93	0.016191	-0.003192	4.959	-0.978	5.05	11.2	0.291	0.211
0.96	0.011867	-0.004187	3.634	-1.282	3.85	19.4	0.213	0.123
0.96	0.011577	-0.004183	3.546	-1.281	3.77	19.9	0.208	0.123

Compilation of Tests 030992-1 and 030992-2
L/D = 3.04 Pc = 30 Ms = 0.00108 f = 92 hz

	Normalized Amplitude		Phase Angle		Coherence	
R/Rw	Axial	Radial	Axial	Radial	Axial	Radial
-0.002	0.614	0.226	-134	-37	0.921	0.521
0	0.5805	0.1255	-126.5	-17	0.9235	0.282
0.09	0.524	0.108	-120	26	0.9565	0.352
0.18	0.538	0.105	-119	19	0.971	0.410
0.30	0.591	0.132	-122	34	0.995	0.867
0.39	0.599	0.151	-123	52	0.994	0.934
0.48	0.504	0.224	-120	60	0.995	0.981
0.60	0.587	0.075	-123	70	0.999	0.906
0.69	0.305	0.141	-111	135	0.996	0.991
0.695	0.471	0.057	-127	-56	0.909	0.066
0.710	0.206	0.245	-153	154	0.983	0.992
0.72	0.078	0.241	96	114	0.943	0.996
0.723	0.199	0.261	-176	152	0.967	0.992
0.737	0.160	0.316	-177	141	0.990	0.994
0.756	0.276	0.392	-171	136	0.995	0.998
0.769	0.344	0.401	-145	144	0.993	0.989
0.78	0.3445	0.3375	-107.5	127	0.998	0.9955
0.785	0.312	0.424	-131	151	0.996	0.997
0.799	0.432	0.333	-100	156	0.997	0.988
0.81	0.565	0.432	-90	106	0.998	0.996
0.813	0.460	0.330	-93	135	0.995	0.994
0.829	0.486	0.410	-93	128	0.997	0.992
0.84	0.724	0.568	-100	93	0.999	0.998
0.843	0.583	0.450	-96	115	0.999	0.996
0.858	0.748	0.461	-101	108	0.999	0.995
0.87	0.815	0.493	-118	91	0.9995	0.9985
0.888	0.821	0.443	-130	103	0.999	0.997
0.894	0.795	0.444	-130	104	0.999	0.997
0.901	0.677	0.4405	-123	101	0.9995	0.998
0.902	0.721	0.434	-127	106	0.998	0.994
0.916	0.627	0.427	-120	147	0.999	0.991
0.922	0.587	0.449	-128	153	0.999	0.993
0.9305	0.649	0.3895	-152	148.5	0.998	0.9935
0.944	0.876	0.456	-167	151	0.999	0.998
0.953	1.413	0.564	-171	152	0.999	0.998
0.96	1.3445	1.203	-154	38	0.9995	0.9995

Compilation of Tests 031092-1 and 031092-2
L/D = 3.04 Pc = 90 Ms = 0.00108 f = 92 hz

	Normalized Amplitude		Phase Angle		Coherence	
R/Rw	Axial	Radial	Axial	Radial	Axial	Radial
0	0.728	0.148	-122.5	47	0.92	0.6435
0.09	0.668	0.138	-118	67.5	0.9625	0.682
0.18	0.709	0.169	-118	62	0.979	0.844
0.30	0.771	0.169	-116	67	0.994	0.956
0.39	0.768	0.176	-116	67	0.993	0.976
0.48	0.699	0.164	-115	68	0.992	0.970
0.60	0.678	0.130	-112	-132	0.993	0.906
0.69	0.514	0.334	-126	141	0.988	0.973
0.72	0.473	0.453	-158	143	0.981	0.979
0.75	0.229	0.495	-117	113	0.868	0.982
0.78	0.647	0.315	-67	98.5	0.972	0.9365
0.81	0.954	0.341	-87	81	0.994	0.952
0.84	0.752	0.645	-112	90	0.996	0.978
0.87	1.137	0.395	-119	79	0.998	0.981
0.9	0.852	0.247	-119.5	133.5	0.9955	0.951
0.93	0.984	0.293	-133	-133	0.997	0.984
0.96	1.694	0.6945	-156.5	4.5	0.993	0.9865

Compilation of tests 030192-3 and 030392-1

L/D = 3.04 Pc = 30 Ms = 0.001977 f = 92 hz

	Normalized Amplitude		Phase Angle		Coherence	
R/Rw	Axial	Radial	Axial	Radial	Axial	Radial
0.0005	0.6225	0.055	-119.5	-20.5	0.8955	0.05
0.09	0.6635	0.16	-119	-19	0.926	0.233
0.18	0.721	0.125	-117	-164	0.967	0.093
0.30	0.754	0.082	-123	-34	0.986	0.116
0.39	0.746	0.150	-124	-28	0.992	0.689
0.48	0.861	0.212	-125	-61	0.993	0.860
0.515	0.742	0.151	-121	26	0.939	0.584
0.547	0.988	0.193	-112	37	0.995	0.972
0.577	1.026	0.231	-112	30	0.996	0.978
0.60	1.007	0.439	-102	-53	0.997	0.992
0.606	1.011	0.240	-104	42	0.995	0.976
0.637	0.858	0.274	-115	35	0.995	0.982
0.668	1.011	0.341	-133	-83	0.996	0.975
0.69	0.966	0.243	-119	-26	0.998	0.992
0.698	1.069	0.407	-122	-57	0.995	0.998
0.726	1.161	0.776	-105	-57	0.998	0.995
0.75	0.881	0.333	-92	-30	0.996	0.994
0.757	1.034	0.699	-96	-47	0.997	0.994
0.78	0.709	0.2455	-113.5	-40	0.9965	0.992
0.787	0.710	0.280	-99	-55	0.995	0.986
0.81	0.624	0.451	-111	36	0.996	0.996
0.816	0.722	0.417	-103	-43	0.995	0.993
0.84	0.242	0.240	-92	-4	0.991	0.992
0.847	0.303	0.373	-91	-21	0.994	0.996
0.87	0.140	0.229	119	143	0.984	0.997
0.878	0.075	0.326	82	131	0.901	0.998
0.9	0.7945	0.1795	126	8	0.9985	0.997
0.907	0.675	0.171	123	23	0.997	0.991
0.911	0.801	0.258	127	71	0.998	0.993
0.922	0.789	0.349	171	135	0.999	0.996
0.93	0.718	0.304	-155	46	0.999	0.999
0.933	0.746	0.118	-178	35	0.999	0.997
0.941	0.741	0.126	-143	69	0.999	0.999
0.953	0.887	0.154	160	63	0.999	0.999
0.961	0.93575	0.16125	-138.75	115	0.999	0.99825

Compilation of tests 030492-1, 030492-3 and 030592-1

L/D = 3.04 Pc = 90 Ms = 0.001977 f = 92 hz

	Normalized Amplitude		Phase Angle		Coherence	
R/Rw	Axial	Radial	Axial	Radial	Axial	Radial
0	0.865	0.127	-117	-128.5	0.8905	0.05
0.09	0.8575	0.295	-115	-94.5	0.892	0.0146
0.18	0.779	0.198	-122	-163	0.945	0.209
0.30	0.862	0.063	-119	-64	0.968	0.058
0.39	0.796	0.181	-122	-70	0.978	0.555
0.48	0.843	0.215	-118	-82	0.981	0.722
0.6	1.1273	0.3115	-115.5	-1	0.9925	0.938
0.69	1.304	0.270	-115	18	0.994	0.942
0.75	1.016	0.272	-95	47	0.990	0.951
0.78	0.972	0.369	-114	38	0.978	0.941
0.81	0.630	0.567	-94	-10	0.969	0.965
0.84	0.5835	0.515	-81.5	-23.5	0.985	0.978
0.87	0.180	0.437	74	20	0.835	0.986
0.90	0.627	0.127	158	16	0.990	0.866
0.93	1.398	0.228	180	117	0.995	0.948
0.96	1.283	0.192	-153	26	0.999	0.938

Combination of Tests 031392-1 and 031392-2

L/D = 3.04 Pc = 30 Ms = 0.003265 f = 92 hz

	Normalized Amplitude		Phase Angle		Coherence	
R/Rw	Axial	Radial	Axial	Radial	Axial	Radial
0	0.7005	0.1255	-117.5	22.5	0.865	0.0505
0.09	0.68	0.1505	-122	-138.5	0.879	0.081
0.18	0.643	0.128	-121	-146	0.947	0.105
0.30	0.616	0.097	-123	-104	0.973	0.137
0.39	0.537	0.059	-128	109	0.962	0.123
0.48	0.670	0.077	-127	-60	0.975	0.244
0.60	0.534	0.107	-128	-53	0.975	0.622
0.69	0.609	0.057	-135	-179	0.979	0.346
0.72	0.899	0.175	-119	-119	0.987	0.835
0.75	0.551	0.125	-128	102	0.976	0.784
0.78	0.487	0.029	-136	33	0.9545	0.1035
0.81	0.251	0.240	-148	-75	0.897	0.875
0.84	0.617	0.242	-146	160	0.988	0.947
0.87	0.906	0.048	-139	-168	0.993	0.408
0.9	0.731	0.0585	-123.5	106.5	0.9935	0.6975
0.93	0.864	0.109	-111	26	0.998	0.962
0.96	0.8975	0.198	-88	-99	0.998	0.9875

Compilation of Tests 041392-2, 041492-1, and 052892-1

L/D = 4.22 Pc = 30 Ms = .00108

R/Rw	Mz	Mr	Mz/Ms	Mr/Ms	M	Angle	Mz/Mcl	Cosine
0.000	0.027761	0.001126	25.705	1.043	25.73	-2.3	1.000	1.000
0.00	0.027985	-0.000595	25.912	-0.551	25.92	1.2	1.000	1.000
0.00	0.027542	0.001660	25.502	1.537	25.55	-3.4	0.984	1.000
0.09	0.027898	-0.001196	25.831	-1.107	25.86	2.5	0.997	1.000
0.09	0.027524	0.001436	25.485	1.330	25.52	-3.0	0.984	1.000
0.18	0.027882	-0.001604	25.817	-1.485	25.86	3.3	0.996	0.999
0.30	0.027745	-0.001777	25.690	-1.645	25.74	3.7	0.991	0.990
0.39	0.027288	-0.002066	25.267	-1.913	25.34	4.3	0.975	0.972
0.48	0.026487	-0.002237	24.525	-2.072	24.61	4.8	0.946	0.935
0.60	0.023795	-0.002441	22.032	-2.260	22.15	5.9	0.850	0.844
0.602	0.024628	-0.001226	22.804	-1.135	22.83	2.8	0.887	0.842
0.69	0.020890	-0.002720	19.343	-2.519	19.51	7.4	0.746	0.733
0.704	0.021301	-0.001679	19.723	-1.555	19.78	4.5	0.767	0.712
0.716	0.021027	-0.001691	19.469	-1.565	19.53	4.6	0.757	0.693
0.72	0.020027	-0.001256	18.544	-1.163	18.58	3.6	0.716	0.686
0.730	0.020671	-0.001713	19.140	-1.586	19.21	4.7	0.745	0.670
0.746	0.020182	-0.001743	18.687	-1.614	18.76	4.9	0.727	0.642
0.75	0.018650	-0.001256	17.269	-1.163	17.31	3.9	0.666	0.634
0.760	0.019565	-0.001721	18.116	-1.593	18.19	5.0	0.705	0.616
0.775	0.018662	-0.001550	17.280	-1.435	17.34	4.7	0.672	0.587
0.78	0.018911	-0.000855	15.658	-0.792	15.68	2.9	0.604	0.577
0.78	0.016633	-0.001754	15.401	-1.624	15.49	6.0	0.594	0.577
0.791	0.017567	-0.001214	16.266	-1.124	16.30	4.0	0.633	0.555
0.806	0.016513	-0.000794	15.290	-0.735	15.31	2.8	0.595	0.523
0.81	0.016142	-0.000652	14.946	-0.604	14.96	2.3	0.577	0.514
0.820	0.015507	-0.000930	14.358	-0.861	14.38	3.4	0.559	0.492
0.835	0.014837	-0.001069	13.738	-0.990	13.77	4.1	0.534	0.458
0.84	0.013961	-0.000815	12.927	-0.754	12.95	3.3	0.499	0.446
0.851	0.014169	-0.001181	13.119	-1.094	13.16	4.8	0.510	0.420
0.866	0.013493	-0.001244	12.494	-1.152	12.55	5.3	0.486	0.383
0.87	0.012430	-0.000942	11.509	-0.872	11.54	4.3	0.444	0.373
0.882	0.012845	-0.001354	11.894	-1.254	11.96	6.0	0.463	0.342
0.893	0.012265	-0.001459	11.356	-1.351	11.44	6.8	0.442	0.313
0.90	0.010560	-0.001422	9.778	-1.316	9.87	7.7	0.377	0.294
0.90	0.010343	-0.002167	9.577	-2.007	9.78	11.8	0.370	0.294
0.901	0.011805	-0.001540	10.931	-1.426	11.02	7.4	0.425	0.291
0.911	0.011239	-0.001639	10.406	-1.518	10.52	8.3	0.405	0.264
0.923	0.010448	-0.001620	9.674	-1.500	9.79	8.8	0.376	0.230
0.93	0.008973	-0.001401	8.308	-1.297	8.41	8.9	0.321	0.211
0.932	0.009829	-0.001519	9.101	-1.407	9.21	8.8	0.354	0.205
0.941	0.009203	-0.001442	8.521	-1.335	8.63	8.9	0.332	0.179
0.954	0.008506	-0.001307	7.876	-1.210	7.97	8.7	0.306	0.141
0.96	0.006819	-0.000587	6.314	-0.543	6.34	4.9	0.244	0.123
0.96	0.006785	-0.000535	6.282	-0.495	6.30	4.5	0.242	0.123
0.962	0.008139	-0.001212	7.536	-1.122	7.62	8.5	0.293	0.117

Compilation of Tests 041492-2 and 041592-1

L/D = 4.22 Pc = 90 Ms = .00108

R/Rw	Mz	Mr	Mz/Ms	Mr/Ms	M	Angle	Mz/Mcl	Cosine
0.00	0.028509	-0.002378	26.397	-2.201	26.49	4.8	1.000	1.000
0.00	0.028869	-0.001578	26.730	-1.461	26.77	3.1	1.000	1.000
0.09	0.028434	-0.002438	26.328	-2.257	26.42	4.9	0.997	1.000
0.09	0.028727	-0.001668	26.599	-1.545	26.64	3.3	0.995	1.000
0.18	0.028401	-0.002497	26.298	-2.312	26.40	5.0	0.996	0.999
0.30	0.028134	-0.002723	26.050	-2.522	26.17	5.5	0.987	0.990
0.39	0.027878	-0.002854	25.813	-2.642	25.95	5.8	0.978	0.972
0.48	0.027170	-0.002823	25.157	-2.614	25.29	5.9	0.953	0.935
0.60	0.025035	-0.002371	23.181	-2.195	23.28	5.4	0.878	0.844
0.69	0.022825	-0.001731	21.134	-1.603	21.19	4.3	0.801	0.733
0.72	0.021867	-0.000595	20.247	-0.551	20.25	1.6	0.757	0.686
0.75	0.020656	-0.000393	19.126	-0.364	19.13	1.1	0.716	0.634
0.78	0.018800	-0.002065	17.407	-1.912	17.51	6.3	0.659	0.577
0.78	0.018976	-0.000758	17.572	-0.702	17.59	2.3	0.657	0.577
0.81	0.016726	-0.001214	15.487	-1.124	15.53	4.2	0.579	0.514
0.84	0.014718	-0.001697	13.628	-1.571	13.72	6.6	0.510	0.446
0.87	0.013458	-0.001981	12.461	-1.834	12.60	8.4	0.466	0.373
0.90	0.011338	-0.002877	10.498	-2.664	10.83	14.2	0.398	0.294
0.90	0.011529	-0.002116	10.675	-1.959	10.85	10.4	0.399	0.294
0.93	0.009397	-0.001703	8.701	-1.577	8.84	10.3	0.326	0.211
0.96	0.007365	-0.001989	6.838	-1.841	7.08	15.1	0.259	0.123
0.96	0.007202	-0.001304	6.668	-1.208	6.78	10.3	0.249	0.123

Compilation of Tests 040892-1 and 040892-2 and 052892-3

L/D = 4.22 Pc = 30 Ms = .001977

R/Rw	Mz	Mr	Mz/Ms	Mr/Ms	M	Angle	Mz/Mcl	Cosine
0.000	0.045738	0.000070	23.135	0.035	23.14	-0.1	0.968	1.000
0.00	0.047446	-0.003222	23.999	-1.630	24.05	3.9	1.004	1.000
0.00	0.048591	-0.001200	24.578	-0.607	24.59	1.4	1.028	1.000
0.09	0.047648	-0.004311	24.101	-2.181	24.20	5.2	1.008	1.000
0.09	0.048857	-0.002321	24.713	-1.174	24.74	2.7	1.034	1.000
0.18	0.047211	-0.004833	23.880	-2.445	24.01	5.8	0.999	0.999
0.30	0.046921	-0.005134	23.733	-2.597	23.88	6.2	0.993	0.990
0.39	0.045976	-0.005320	23.255	-2.691	23.41	6.6	0.973	0.972
0.48	0.044524	-0.005445	22.521	-2.754	22.69	7.0	0.942	0.935
0.516	0.043801	-0.002356	22.155	-1.192	22.19	3.1	0.927	0.914
0.545	0.042950	-0.002434	21.725	-1.231	21.76	3.2	0.909	0.893
0.576	0.041861	-0.002494	21.174	-1.262	21.21	3.4	0.886	0.867
0.60	0.039919	-0.005468	20.192	-2.766	20.38	7.8	0.845	0.844
0.606	0.040852	-0.002480	20.663	-1.254	20.70	3.5	0.864	0.838
0.636	0.039522	-0.002512	19.991	-1.271	20.03	3.6	0.836	0.805
0.667	0.038163	-0.002353	19.303	-1.190	19.34	3.5	0.808	0.766
0.69	0.035527	-0.005987	17.970	-3.028	18.22	9.6	0.752	0.733
0.696	0.036584	-0.002102	18.505	-1.063	18.54	3.3	0.774	0.724
0.72	0.034518	-0.002645	17.460	-1.338	17.51	4.4	0.730	0.686
0.726	0.034990	-0.001883	17.699	-0.952	17.72	3.1	0.740	0.676
0.75	0.030983	-0.003631	15.672	-1.837	15.78	6.7	0.656	0.634
0.756	0.032172	-0.001787	16.273	-0.904	16.30	3.2	0.681	0.623
0.78	0.028741	-0.005987	14.538	-3.028	14.85	11.8	0.608	0.577
0.78	0.029659	-0.003756	15.002	-1.900	15.12	7.2	0.628	0.577
0.785	0.028879	-0.002863	14.607	-1.448	14.68	5.7	0.611	0.567
0.81	0.027410	-0.003431	13.864	-1.736	13.97	7.1	0.580	0.514
0.815	0.027840	-0.003112	14.082	-1.574	14.17	6.4	0.589	0.503
0.84	0.023961	-0.003662	12.120	-1.852	12.26	8.7	0.507	0.446
0.844	0.025964	-0.002754	13.133	-1.393	13.21	6.1	0.549	0.437
0.87	0.020531	-0.003732	10.385	-1.888	10.56	10.3	0.434	0.373
0.875	0.022657	-0.002977	11.460	-1.506	11.56	7.5	0.479	0.360
0.90	0.017154	-0.004575	8.677	-2.314	8.98	14.9	0.363	0.294
0.90	0.017655	-0.002902	8.930	-1.468	9.05	9.3	0.374	0.294
0.920	0.017576	-0.002029	8.890	-1.026	8.95	6.6	0.372	0.239
0.929	0.016802	-0.001894	8.499	-0.958	8.55	6.4	0.356	0.213
0.93	0.013228	-0.002918	6.691	-1.476	6.85	12.4	0.280	0.211
0.937	0.015963	-0.001672	8.074	-0.846	8.12	6.0	0.338	0.191
0.951	0.014241	-0.001513	7.203	-0.765	7.24	6.1	0.301	0.150
0.959	0.012931	-0.001755	6.541	-0.888	6.60	7.7	0.274	0.126
0.96	0.009258	-0.002658	4.683	-1.344	4.87	16.0	0.196	0.123
0.96	0.009263	-0.003673	4.686	-1.858	5.04	21.6	0.196	0.123

Compilation of Tests 041092-1, 041092-2 and 041092-3

L/D = 4.22 Pc = 90 Ms = .001977

R/Rw	Mz	Mr	Mz/Ms	Mr/Ms	M	Angle	Mz/Mcl	Cosine
0.00	0.046903	0.001566	23.724	0.792	23.74	-1.9	0.987	1.000
0.00	0.048135	0.000609	24.347	0.308	24.35	-0.7	1.013	1.000
0.09	0.046834	0.001129	23.689	0.571	23.70	-1.4	0.986	1.000
0.09	0.047679	0.000287	24.117	0.145	24.12	-0.3	1.003	1.000
0.18	0.047170	0.000375	23.859	0.190	23.86	-0.5	0.993	0.999
0.30	0.047378	-0.000040	23.965	-0.020	23.96	0.0	0.997	0.990
0.39	0.046729	-0.000369	23.636	-0.187	23.64	0.5	0.983	0.972
0.48	0.045480	-0.001307	23.005	-0.661	23.01	1.6	0.957	0.935
0.60	0.041598	-0.002894	21.041	-1.464	21.09	4.0	0.875	0.844
0.69	0.036893	-0.003645	18.661	-1.844	18.75	5.6	0.776	0.733
0.72	0.034287	-0.003063	17.343	-1.549	17.41	5.1	0.722	0.686
0.75	0.031751	-0.003353	16.060	-1.696	16.15	6.0	0.668	0.634
0.78	0.030531	-0.003629	15.443	-1.836	15.55	6.8	0.642	0.577
0.84	0.024626	-0.001666	12.456	-0.843	12.48	3.9	0.518	0.446
0.87	0.021543	-0.000979	10.897	-0.495	10.91	2.6	0.453	0.373
0.90	0.018308	-0.001687	9.260	-0.853	9.30	5.3	0.385	0.294
0.93	0.014259	-0.002088	7.212	-1.056	7.29	8.3	0.300	0.211
0.96	0.009647	-0.002303	4.981	-1.165	5.12	13.2	0.207	0.123

Compilation of Tests 041692-1 and 041692-2

L/D = 4.22 Pc = 30 Ms = .003265

R/Rw	Mz	Mr	Mz/Ms	Mr/Ms	M	Angle	Mz/Mcl	Cosine
0.00	0.079489	-0.003566	24.346	-1.092	24.37	2.6	1.006	1.000
0.00	0.078590	-0.003007	24.070	-0.921	24.09	2.2	0.994	1.000
0.09	0.079652	-0.004566	24.396	-1.398	24.44	3.3	1.008	1.000
0.09	0.078824	-0.003789	24.142	-1.161	24.17	2.8	0.997	1.000
0.18	0.079731	-0.005076	24.420	-1.555	24.47	3.6	1.009	0.999
0.30	0.079565	-0.005506	24.369	-1.686	24.43	4.0	1.007	0.990
0.39	0.078970	-0.005744	24.187	-1.759	24.25	4.2	0.999	0.972
0.48	0.077224	-0.005727	23.652	-1.754	23.72	4.2	0.977	0.935
0.60	0.071118	-0.004421	21.782	-1.354	21.82	3.6	0.900	0.844
0.69	0.063850	-0.002674	19.556	-0.819	19.57	2.4	0.808	0.733
0.72	0.060286	-0.000795	18.464	-0.244	18.47	0.8	0.763	0.686
0.75	0.056524	-0.001633	17.312	-0.500	17.32	1.7	0.715	0.634
0.78	0.050787	-0.005064	15.555	-1.551	15.63	5.7	0.643	0.577
0.78	0.050544	-0.003356	15.481	-1.028	15.51	3.8	0.639	0.577
0.81	0.048193	-0.003935	14.760	-1.205	14.81	4.7	0.610	0.514
0.84	0.044752	-0.003731	13.706	-1.143	13.75	4.8	0.566	0.446
0.87	0.037298	-0.004919	11.423	-1.507	11.52	7.5	0.472	0.373
0.90	0.031129	-0.006708	9.534	-2.055	9.75	12.2	0.394	0.294
0.90	0.031359	-0.005424	9.605	-1.661	9.75	9.8	0.397	0.294
0.93	0.027260	-0.004476	8.349	-1.371	8.46	9.3	0.345	0.211
0.96	0.019894	-0.004370	6.093	-1.338	6.24	12.4	0.252	0.123
0.96	0.020208	-0.003656	6.189	-1.120	6.29	10.3	0.256	0.123

Compilation of Tests 041392-2 and 041492-1 and 052892-1
L/D = 4.22 Pc = 30 Ms = .00108 f = 92 hz

	Normalized Amplitude		Phase Angle		Coherence	
r/Rw	Axial	Radial	Axial	Radial	Axial	Radial
0.000	0.788	0.529	-123	-153	0.967	0.778
0.00	0.744	0.210	-126	88	0.962	0.867
0.00	0.768	0.547	-128	-174	0.970	0.735
0.09	0.808	0.394	-122	-177	0.968	0.641
0.09	0.860	0.460	-123	-164	0.972	0.636
0.18	0.815	0.348	-120	-150	0.991	0.831
0.30	0.794	0.221	-119	-129	0.991	0.778
0.39	0.827	0.211	-120	-134	0.995	0.863
0.48	0.904	0.107	-119	-150	0.996	0.883
0.60	0.979	0.065	-120	16	0.997	0.782
0.602	0.962	0.161	-122	92	0.995	0.883
0.69	0.847	0.507	-128	44	0.998	0.989
0.704	0.833	0.497	-124	97	0.997	0.980
0.716	0.737	0.534	-125	108	0.995	0.978
0.72	0.657	0.445	-119	-3	0.997	0.981
0.730	0.659	0.509	-121	101	0.991	0.977
0.746	0.585	0.484	-116	96	0.939	0.882
0.75	1.229	0.670	-109	-18	0.998	0.990
0.760	0.572	0.578	-115	103	0.990	0.983
0.775	0.716	0.657	-106	100	0.988	0.970
0.78	1.803	0.771	-121	7	0.998	0.986
0.78	1.915	0.777	-132	-38	0.998	0.986
0.791	1.053	0.758	-101	92	0.975	0.959
0.806	1.369	0.795	-104	81	0.975	0.940
0.81	2.143	0.947	-152	-81	0.996	0.997
0.820	1.550	0.683	-106	75	0.992	0.983
0.835	1.642	0.661	-107	69	0.970	0.937
0.84	1.276	0.852	-144	-91	0.997	0.994
0.851	1.593	0.577	-110	59	0.943	0.779
0.866	1.505	0.498	-119	35	0.995	0.865
0.87	1.117	1.152	-114	-63	0.999	0.993
0.882	1.228	0.444	-120	53	0.989	0.816
0.893	0.928	0.546	-122	38	0.994	0.859
0.90	0.895	0.834	-61	6	0.990	0.991
0.90	1.288	1.108	-90	-53	0.999	0.994
0.901	0.691	0.672	-116	37	0.981	0.920
0.911	0.530	0.798	-106	43	0.905	0.900
0.923	0.380	0.817	-57	43	0.824	0.957
0.93	0.847	0.749	-43	-49	0.985	0.986
0.932	0.292	0.900	-27	41	0.725	0.954
0.941	0.234	0.906	-31	25	0.708	0.947
0.954	0.272	0.807	125	38	0.830	0.965
0.96	0.405	0.465	-9	-27	0.934	0.988
0.96	1.005	0.552	113	24	0.986	0.996
0.962	0.584	0.733	120	38	0.929	0.968

Compilation of Tests 041492-2 and 041592-1
L/D = 4.22 Pc = 90 Ms = .00108 f = 92 hz

	Normalized Amplitude		Phase Angle		Coherence	
R/Rw	Axial	Radial	Axial	Radial	Axial	Radial
0	0.9549	0.1015	-116.5	99	0.9695	0.271
0.09	0.98	0.1385	-116	89	0.984	0.477
0.18	0.978	0.183	-118	76	0.988	0.613
0.30	0.879	0.227	-118	73	0.979	0.763
0.39	0.922	0.186	-117	65	0.985	0.704
0.48	0.977	0.228	-118	69	0.985	0.909
0.60	1.176	0.356	-120	55	0.996	0.984
0.69	0.958	0.421	-128	47	0.992	0.981
0.72	0.531	0.258	-131	115	0.883	0.919
0.75	0.517	0.810	-56	144	0.904	0.961
0.78	1.694	0.811	-80.5	55	0.984	0.961
0.81	1.425	1.086	-70	134	0.969	0.965
0.84	1.830	0.925	-84	133	0.984	0.970
0.87	1.663	1.051	-117	142	0.994	0.953
0.9	1.3905	1.073	-118	59.5	0.977	0.967
0.93	1.809	0.867	-174	115	0.974	0.972
0.96	1.855	0.834	-58.5	72.5	0.9625	0.978

Compilation of Tests 040892-1 and 040892-2 and 052892-3

L/D = 4.22 Pc = 30 Ms = .001977 F = 92 hz.

	Normalized Amplitude		Phase Angle		Coherence	
R/Rw	Axial	Radial	Axial	Radial	Axial	Radial
0.00	1.945	0.046	-128	-106	0.988	0.020
0.002	1.818	0.261	-128	179	0.992	0.357
0.09	1.908	0.101	-134	-16	0.991	0.110
0.09	1.886	0.119	-141	21	0.988	0.216
0.18	1.847	0.281	-144	-50	0.994	0.698
0.30	1.938	0.350	-146	-59	0.993	0.879
0.39	1.958	0.488	-143	-61	0.993	0.940
0.48	1.795	0.523	-139	-51	0.994	0.955
0.516	1.725	0.230	-130	-50	0.994	0.340
0.545	1.842	0.407	-129	-61	0.988	0.987
0.576	2.010	0.439	-130	-59	0.996	0.985
0.60	1.630	0.463	-136	-67	0.993	0.965
0.606	1.675	0.427	-133	-50	0.998	0.989
0.636	1.530	0.335	-126	-40	0.997	0.984
0.667	1.676	0.372	-121	-22	0.997	0.984
0.69	0.813	1.023	-158	-64	0.987	0.989
0.696	1.318	0.609	-133	-32	0.996	0.989
0.72	1.021	1.165	-76	-47	0.993	0.995
0.726	0.889	0.723	-147	-37	0.994	0.992
0.75	0.732	1.289	-110	-41	0.991	0.995
0.756	1.170	1.152	-67	-40	0.994	0.992
0.78	1.434	0.438	172	-26	0.992	0.984
0.78	1.105	0.632	150	-38	0.990	0.992
0.785	0.692	1.330	-117	-40	0.988	0.994
0.81	1.771	0.632	-76	-52	0.998	0.994
0.815	1.531	0.374	170	-25	0.993	0.982
0.84	1.351	0.652	-31	-34	0.997	0.996
0.844	1.644	0.493	-70	-58	0.997	0.992
0.87	1.016	0.286	7	-63	0.995	0.989
0.875	1.299	0.577	-26	-39	0.991	0.993
0.90	0.599	0.129	43	-68	0.980	0.970
0.90	0.478	0.221	50	-34	0.960	0.986
0.920	0.539	0.547	63	-27	0.975	0.996
0.929	0.538	0.259	72	-26	0.983	0.996
0.93	0.254	0.284	109	47	0.934	0.985
0.937	0.414	0.292	89	-9	0.972	0.996
0.951	0.489	0.359	102	4	0.941	0.992
0.959	0.527	0.264	-129	56	0.877	0.912
0.96	0.206	0.119	-78	58	0.906	0.971
0.96	0.276	0.214	-43	114	0.967	0.959

Compilation of Tests 041092-1, 041092-2 and 041092-3

L/D = 4.22 Pc = 90 Ms = .001977 f = 92 hz

	Normalized Amplitude		Phase Angle		Coherence	
R/Rw	Axial	Radial	Axial	Radial	Axial	Radial
0	1.54125	0.3505	-156.5	-100.5	0.9545	0.321
0.09	1.4355	0.4355	-157.5	-118	0.97	0.4175
0.18	1.725	0.507	-144	-116	0.985	0.478
0.30	1.839	0.698	-147	-114	0.991	0.734
0.39	1.763	0.725	-149	-99	0.980	0.674
0.48	1.763	0.818	-145	-88	0.977	0.910
0.60	1.802	0.822	-134	-79	0.987	0.971
0.69	0.921	0.863	-164	-65	0.980	0.976
0.72	0.658	0.810	-107	-120	0.953	0.977
0.75	1.492	0.879	-114	-124	0.987	0.979
0.78	0.809	0.802	-107	-42	0.965	0.981
0.84	1.165	0.035	-39	81	0.957	0.368
0.87	1.340	1.003	14	-9	0.988	0.989
0.90	0.469	0.546	57	-15	0.880	0.964
0.93	0.592	0.304	131	57	0.871	0.887
0.96	0.141	0.157	-81	-26	0.492	0.925

Compilation of Tests 041592-1 and 041692-2

L/D = 4.22 Pc = 30 Ms = .003265 f=92 hz

	Normalized Amplitude		Phase Angle		Coherence	
R/Rw	Axial	Radial	Axial	Radial	Axial	Radial
0	0.7455	0.3945	-110.5	-89	0.8625	0.412
0.09	0.7565	0.2885	-109	-68.5	0.924	0.309
0.18	0.801	0.081	-107	-107	0.980	0.034
0.30	0.934	0.106	-113	17	0.980	0.186
0.39	0.833	0.079	-106	26	0.980	0.291
0.48	0.898	0.147	-116	62	0.984	0.641
0.60	0.779	0.025	-109	15	0.975	0.083
0.69	1.211	0.115	-120	-11	0.992	0.578
0.72	0.829	0.074	-99	-4	0.985	0.498
0.75	0.471	0.176	-94	26	0.957	0.777
0.78	0.1775	0.2545	-114.5	65.5	0.5885	0.844
0.81	1.092	0.117	-103	-39	0.984	0.498
0.84	0.866	0.026	140	-97	0.971	0.137
0.87	0.900	0.321	-166	26	0.988	0.869
0.9	1.642	0.5285	-151	167	0.995	0.9705
0.93	1.579	0.213	-130	-24	0.996	0.930
0.96	1.3995	0.171	-111.5	77.5	0.998	0.957

Compilation of Tests 061292-1 and 062592-1

L/D = 5.46 Pc = 30 Ms = .001977

R/Rw	Mz	Mr	Mz/Ms	Mr/Ms	M	Angle	Mz/Mcl	Cosine
0.00	0.058918	0.001045	29.802	0.528	29.81	-1.0	1.000	1.000
0.00	0.059162	-0.000634	29.925	-0.321	29.93	0.6	1.000	1.000
0.09	0.059861	-0.001944	30.279	-0.983	30.29	1.9	1.012	1.000
0.18	0.060279	-0.002594	30.490	-1.312	30.52	2.5	1.019	0.999
0.30	0.060423	-0.003210	30.563	-1.624	30.61	3.0	1.021	0.990
0.39	0.059879	-0.003386	30.288	-1.712	30.34	3.2	1.012	0.972
0.48	0.057293	-0.003604	28.980	-1.823	29.04	3.6	0.968	0.935
0.60	0.052145	-0.003567	26.376	-1.804	26.44	3.9	0.881	0.844
0.69	0.046416	-0.004154	23.478	-2.101	23.57	5.1	0.785	0.733
0.72	0.040611	-0.001904	20.542	-0.963	20.56	2.7	0.689	0.686
0.75	0.037596	-0.001657	19.017	-0.838	19.04	2.5	0.638	0.634
0.78	0.033642	-0.001105	17.017	-0.559	17.03	1.9	0.571	0.577
0.78	0.037359	-0.003642	18.897	-1.842	18.99	5.6	0.631	0.577
0.81	0.029929	-0.000876	15.139	-0.443	15.15	1.7	0.508	0.514
0.84	0.025884	-0.001533	13.093	-0.776	13.12	3.4	0.439	0.446
0.87	0.021085	-0.002176	10.665	-1.101	10.72	5.9	0.358	0.373
0.90	0.016304	-0.000762	8.247	-0.386	8.26	2.7	0.277	0.294
0.90	0.020339	-0.003909	10.288	-1.977	10.48	10.9	0.344	0.294
0.93	0.010680	-0.001754	5.402	-0.887	5.47	9.3	0.181	0.211
0.96	0.005944	-0.000988	3.007	-0.500	3.05	9.4	0.101	0.123
0.96	0.008869	-0.002685	4.486	-1.358	4.69	16.8	0.150	0.123

Compilation of Tests 062592-2 and 062592-3

L/D = 5.46 Pc = 30 Ms = .003265

R/Rw	Mz	Mr	Mz/Ms	Mr/Ms	M	Angle	Mz/Mcl	Cosine
0.00	0.093310	0.001903	28.579	0.583	28.58	-1.2	1.000	1.000
0.00	0.098424	-0.005196	30.145	-1.591	30.19	3.0	1.000	1.000
0.09	0.093647	0.000713	28.682	0.218	28.68	-0.4	1.004	1.000
0.09	0.098745	-0.006223	30.243	-1.906	30.30	3.6	1.003	1.000
0.18	0.093498	0.000077	28.636	0.023	28.64	-0.0	1.002	0.999
0.30	0.092565	0.001850	28.351	0.567	28.36	-1.1	0.992	0.990
0.39	0.090627	0.001826	27.757	0.559	27.76	-1.2	0.971	0.972
0.48	0.086291	0.001947	26.429	0.596	26.44	-1.3	0.925	0.935
0.60	0.076430	-0.000132	23.409	-0.040	23.41	0.1	0.819	0.844
0.69	0.069883	-0.000106	21.404	-0.033	21.40	0.1	0.749	0.733
0.72	0.069253	-0.003664	21.211	-1.122	21.24	3.0	0.704	0.686
0.75	0.062605	-0.004854	19.174	-1.487	19.23	4.4	0.636	0.634
0.78	0.054161	0.001070	16.588	0.328	16.59	-1.1	0.580	0.577
0.78	0.056533	-0.004778	17.315	-1.463	17.38	4.8	0.574	0.577
0.81	0.048764	-0.005036	14.935	-1.542	15.01	5.9	0.495	0.514
0.84	0.042072	-0.005217	12.886	-1.598	12.98	7.1	0.427	0.446
0.87	0.035614	-0.003964	10.908	-1.214	10.98	6.4	0.362	0.373
0.90	0.026745	0.000539	8.191	0.165	8.19	-1.2	0.287	0.294
0.90	0.027782	-0.004191	8.509	-1.284	8.61	8.6	0.282	0.294
0.93	0.018185	-0.003745	5.570	-1.147	5.69	11.6	0.185	0.211
0.96	0.009785	-0.002183	2.997	-0.669	3.07	12.6	0.105	0.123
0.96	0.010057	-0.004538	3.080	-1.390	3.38	24.3	0.102	0.123

Compilation of Tests 061292-1 and 062592-1

L/D = 5.46 Pc = 30 Ms = .001977

	Normalized Amplitude		Phase Angle		Coherence	
R/Rw	Axial	Radial	Axial	Radial	Axial	Radial
0.00	2.735	0.060	-147	-148	0.994	0.027
0.00	2.643	0.283	-88	172	0.990	0.439
0.09	2.662	0.040	-150	-109	0.994	0.017
0.18	2.669	0.349	-151	-96	0.983	0.671
0.30	2.652	0.469	-155	-97	0.947	0.847
0.39	2.650	0.592	-166	-94	0.993	0.964
0.48	2.488	0.978	-162	-102	0.990	0.976
0.60	3.079	1.121	165	-92	0.988	0.985
0.69	2.249	0.935	163	-84	0.995	0.988
0.72	1.327	0.595	-124	19	0.995	0.977
0.75	0.918	0.605	-130	3	0.986	0.964
0.78	0.487	0.509	-167	8	0.888	0.982
0.78	1.865	1.130	-110	-67	0.992	0.982
0.81	0.563	0.898	10	20	0.944	0.980
0.84	1.110	0.949	89	25	0.974	0.987
0.87	2.804	0.508	119	77	0.971	0.967
0.90	3.229	0.904	-22	-178	0.989	0.986
0.90	2.638	0.529	139	-12	0.978	0.977
0.93	1.693	0.224	-174	154	0.989	0.954
0.96	1.650	0.893	11	-159	0.960	0.952
0.96	0.790	0.321	-138	-155	0.983	0.975

Compilation of Tests 062592-2 and 062592-3

L/D = 5.46 Pc = 30 Ms = .003265

	Normalized Amplitude		Phase Angle		Coherence	
R/Rw	Axial	Radial	Axial	Radial	Axial	Radial
0.00	0.789	0.502	-115	-138	0.911	0.400
0.00	0.932	0.460	-118	-157	0.948	0.386
0.09	0.846	0.306	-120	-157	0.928	0.220
0.09	0.890	0.246	-118	-156	0.951	0.178
0.18	0.852	0.223	-120	-148	0.964	0.200
0.30	0.895	0.143	-123	-106	0.980	0.274
0.39	0.789	0.163	-133	-139	0.965	0.548
0.48	0.943	0.250	-120	-125	0.968	0.709
0.60	1.153	0.362	-123	-111	0.984	0.897
0.69	1.049	0.139	-89	-65	0.988	0.717
0.72	0.934	0.072	-77	-114	0.983	0.399
0.75	0.623	0.129	-77	-57	0.937	0.592
0.78	0.387	0.107	-126	-28	0.873	0.521
0.78	0.290	0.105	-134	-24	0.691	0.518
0.81	0.941	0.038	-145	-134	0.967	0.080
0.84	1.535	0.035	-140	120	0.981	0.110
0.87	1.317	0.155	-119	151	0.989	0.607
0.90	1.597	0.637	-103	-116	0.983	0.926
0.90	1.816	0.242	-105	-123	0.989	0.856
0.93	1.340	0.295	-80	90	0.995	0.969
0.96	0.561	0.053	-61	-52	0.989	0.624
0.96	0.423	0.350	-59	122	0.995	0.996